Detection, Localization, and Recognition of Faults in Transmission Networks Using Transient Currents

By

Nuwan Dileepa Perera

A thesis submitted to the Faculty of Graduate Studies of
The University of Manitoba
in partial fulfilment of
the requirements for the degree of

Doctor of Philosophy

Department of Electrical and Computer Engineering
Faculty of Engineering
University of Manitoba
Winnipeg, Manitoba

Abstract

The fast clearing of faults is essential for preventing equipment damage and preserving the stability of the power transmission systems with smaller operating margins. This thesis examined the application of fault generated transients for fast detection and isolation of faults in a transmission system. The basis of the transient based protection scheme developed and implemented in this thesis is the fault current directions identified by a set of relays located at different nodes of the system. The direction of the fault currents relative to a relay location is determined by comparing the signs of the wavelet coefficients of the currents measured in all branches connected to the node. The faulted segment can be identified by combining the fault directions identified at different locations in the system. In order to facilitate this, each relay is linked with the relays located at the adjacent nodes through a telecommunication network.

In order to prevent possible malfunctioning of relays due to transients originating from non-fault related events, a transient recognition system to supervise the relays is proposed. The applicability of different classification methods to develop a reliable transient recognition system was examined. A Hidden Markov Model classifier that utilizes the energies associated with the wavelet coefficients of the measured currents as input features was selected as the most suitable solution.

Performance of the protection scheme was evaluated using a high voltage transmission system simulated in PSCAD/EMTDC simulation software. The custom models required

to simulate the complete protection scheme were implemented in PSCAD/EMTDC. The effects of various factors such as fault impedance, signal noise, fault inception angle and current transformer saturation were investigated. The performance of the protection scheme was also tested with the field recorded signals.

Hardware prototypes of the fault direction identification scheme and the transient classification system were implemented and tested under different practical scenarios using input signals generated with a real-time waveform playback instrument. The test results presented in this thesis successfully demonstrate the potential of using transient signals embedded in currents for detection, localization and recognition of faults in transmission networks in a fast and reliable manner.

Acknowledgments

I would like to express my sincere thanks to Dr. Athula Rajapakse for his continuous advice, guidance and encouragement throughout the course of this work. I consider myself privileged to have had the opportunity to work under his guidance. I would also like to thank the advisory committee members for their comments and feedbacks to improve the quality of the thesis.

The financial support received from the Natural Science and Engineering Research Council, the University of Manitoba, the MITACS Accelerate Canada, the Manitoba Hydro and the Manitoba HVDC Research Center is greatly appreciated.

The technical support received form the technical staff of the University of Manitoba, the Manitoba HVDC Research Centre, and the Texas Instruments is highly appreciated.

I would like to thank the staff and all of my friends in the Department of Electrical and Computer Engineering for their continuous encouragement and for making my years at the University of Manitoba a pleasant experience.

This acknowledgement will not be complete without thanking my family. I extend my heartfelt gratitude to my parents, wife and brother.

Nuwan Dileepa Perera

May 2012

Dedication

To my parents and late grand parents.

Contents

List of Tables

List of Figures

List of Symbols

I_a	Current in Phase-A
I_b	Current in Phase-B
I_c	Current in Phase-C
I_0	Ground mode current
I_α	Aerial mode-1 current
I_β	Aerial mode-2 current
f_s	Sampling frequency
r	Correlation of coefficient
D_i	Directional information on the i^{th} branch
S_i	Sign information of the i^{th} branch
CAi_j	j^{th} sample of level i approximation wavelet coefficient
CDi_j	j^{th} sample of level i detail wavelet coefficient
EAi	Energy of level i approximation wavelet coefficients
EDi	Energy of level i detail wavelet coefficients
R_f	Fault impendence
σ	Smoothing parameter
A	State transition probability distribution
B	Observation symbol probability distribution

π	Initial state distribution
λ	Hidden Markov Model
W	Feature set
$H(n)$	High pass filter
$L(n)$	Low pass filter
$H'(n)$	Inverse high pass filter
$L'(n)$	Inverse low pass filter
Z_c	Characteristic impedance
f_1, f_2	Backward and forward travelling waves
ω	Angular frequency
$[Z_M]$	Modal transformation matrix

List of Acronyms

HV	High Voltage
FIR	Finite Impulse Response
DWT	Discrete Wavelet Transform
CWT	Continuous Wavelet Transform
WTC	Wavelet Transform Coefficients
CT	Current Transformer
DSP	Digital Signal Processors
HIF	High Impedance Fault
CVT	Capacitive Voltage Transformer
FPGA	Field Programmable Gate Array
DT	Decision Tree
HMM	Hidden Markov Model
PNN	Probabilistic Neural Network
RTP	Real Time Playback
RTDS	Real Time Digital Simulator
EMTDC™	Electromagnetic Transient including DC; a registered trademark of Manitoba Hydro

PSCAD^{TM}	Power Systems CAD (Computer Aided Design); a registered trademark of Manitoba HVDC Research Centre Inc
EMT	Electromagnetic Transient
SIR	Source to Line Impedance Ratio

List of Appendices

Chapter 1

Introduction

1.1 Background

A reliable supply of electricity is essential for the proper functioning of modern society. Electricity is delivered from the generating stations to urban load centers using high voltage power transmission systems that are designed to be highly reliable [1]. However, faults occur in transmission systems due to multitude of reasons that are unavoidable. If not removed promptly, faults can result in system instability, equipment damage, and compromised public safety. Therefore, it is extremely important to identify and remove the faults as soon as possible [2]-[3]. A fault must be cleared within the 'critical clearing time' to preserve the system stability and prevent the fault event evolving into a system wide blackout. Due to economic reasons, competitive industry structures, and environmental constrains that restrict the building of new transmission facilities, power systems are now operated with increasingly smaller transmission capacity margins. Integration of large scale non-dispatchable, intermittent power from renewable sources increases the uncertainties. These factors make the critical clearing times shorter, and thus demanding faster response from protection relays.

Transmission systems are principally protected using distance relays. Although they are successfully used in almost all transmission systems, there are certain limiting factors that prevent further improvement in their speed of operation without compromising the accuracy [3]. The operation of distance relay is based on the apparent impedance calculated using the voltage and current phasors estimated at the relay location. The process of estimating fundamental frequency phasors in a digital relay incorporates an inherent delay. The change of apparent impedance from a load condition to a fault condition is not instantaneously visible on phasor quantities. This directly affects the fault detection time and, hence, the total fault clearing time [3]. Furthermore, operation of these relays can be affected by fault levels, power swings, current transformer saturation and fault impedance [3]-[4]. Apart from the distance relays, line phase differential and line current differential are two common methods used in transmission line protection. These methods require interchange of multiple signals between end-to-end relays. Therefore, the communication methods associated with these protection schemes involve the use of multiplexing devices. Use of multiplexing devices can introduce additional delays on communication which will ultimately affect the response time of the relay. In addition to that, threshold levels used in line current differential should be high enough to prevent malfunctions due to charging currents especially in the case of long transmission lines [5]-[6].

On the other hand, transient based protection techniques that use high frequency components of the signals can be used to develop faster protection systems that can overcome some of the above drawbacks of phasor based relays. They are immune to power swings and current transformer saturation. Their performance is generally less affected by the fault impedance and fault level. They can be successfully applied for mutually coupled tower geometries as well as for series capacitor compensated lines [7].

During the last few decades a considerable amount of research has been carried out to investigate applicability of transient based protection methods. The protection techniques presented in [4], [8]-[14] are the earliest transient based techniques proposed for transmission systems. These methods are based on one of the two general principles; (i) fault distance estimation using travelling waves and (ii) fault direction identification using transients.

Travelling wave based methods use the time difference between the arrivals of transients originated from the fault to estimate the distance to the fault from the relay location. These schemes could be based on double ended measurements or single ended measurements. Different methods to locate the faults using travelling waves detected at the two ends of the lines have been proposed in [10]-[11]. In [13]-[14] the single ended schemes have been discussed and different techniques have been proposed to detect the forward and reflected wave fronts in order to estimate the time difference between the waves.

Transient directional methods involve the use of transient signals to find the fault direction. In the method proposed in [9], transient changes in both the voltage and current signals are analyzed to determine the direction of a fault with respect to the point of measurement. This has been practically implemented and successfully field tested on a transmission system [9]. The protection scheme proposed in [12] uses forward and reflected traveling waves to determine the fault direction. The transient directional protection scheme proposed in [15] uses only the current signals, avoiding the need for voltage measurements. The method utilises band pass filters to isolate the high frequency signal components, however the selection of the frequency bands of the filters and their design is not straightforward.

In recent research, the robustness of the transient based protection concepts has been improved using new techniques. Application of new signal processing techniques such as wavelet transform has contributed to improve the effectiveness and robustness of both transient based distance and directional protection methods. In [7], wavelet transform has been used to detect the wave fronts. Changes in wavelet coefficients help accurate estimation of the timing data required to accurately determine the distance to the fault. The potential for locating the faults in mutually coupled transmission lines as well as in the transmission lines with series compensation using wavelet based travelling wave relays has been demonstrated in [16]. A wavelet transform based transient directional protection scheme for distribution system with distributed generation has been proposed in [17]. This method uses the signs of wavelet coefficients of the branch currents to determine the fault direction with respect to the relay. In addition, different pattern classification methods such as Artificial Neural Networks, Decision Trees, etc. have also been used to analyze the high frequency transients [18]-[19]. Results of these recent studies indicate the potential for developing fast transmission system protection schemes using transient based methods.

1.2 Challenges for Transient Based Protection

Although the transient based protection methods have several benefits and the operation of these methods has been demonstrated using simulation studies, there are number of challenges that limit the practical implementation of these methods.

One of the primary concerns in transient based protection is the capability of capturing high frequency transients using the existing transducers. Conventionally, the current measurements are obtained using current transformers (CTs) whereas the voltage measurements are obtained through potential transforms (PTs) or capacitive voltage transformers (CVTs). Although the conventional CTs and PTs have a sufficient bandwidth to capture the fault generated transients, the capability of CVTs is limited to 1-3 kHz due to the interaction of the capacitors [3]. This has come to the attention of recent researchers in implementing the transient based protection methodologies for high voltage transmission systems where the voltage measurements are obtained through CVTs. Another related problem is that on the rare occasion when a single phase to ground fault occurs near the zero voltage level (small fault inception angle), the fault generated transient waves will not contain any steep wave-fronts. The wave-fronts are not distinct and difficult to isolate for measurement purposes and hence a travelling wave based distance protection scheme may fail to detect such a fault [3].

Another major issue that prevents the wider acceptance of transient based protection methodologies is the possibility of relay malfunction due to non-fault related transients [20]. This is because, the normal switching events such as switching of capacitors, large loads, etc. also generate transients that appear similar to the fault transients. Although this has been identified as a major concern, solutions to this problem have not yet been properly investigated. The few investigations reported in literature are only based on simulations and limited to simple test systems [21]-[22].

Similar to the switching transients, high frequency noise and harmonics can also affect the performance of the transient based protection schemes. The voltage and current signals may contain high frequency noise and harmonics, which are generated by the equipment such as inverters and converters connected to the power network. The amount of the noise present in the system may vary depending on the location of the measurement [23]. In addition to the noise present in the signal itself, additional noise can also be generated from the transducers and other accessories [24]. If the noise level is high, it can significantly affect the performance of the transient based protection algorithms.

Hardware implementation and field testing are vital in establishing the confidence of new protection schemes. The requirement of a high frequency sampling rate is one of the main challenges in practical implementation of these protection schemes. In addition, the transient based protection methods require sophisticated signal processing tools to extract high frequency transients from the measured signals. Thus the computational burden on the signal processing hardware is very high and becomes a critical factor in the real-time implementation. Although these protection algorithms can be easily modeled in time domain simulation programs, it is challenging to implement them on a real-time hardware due to the requirement of a powerful signal processor. Furthermore, the hardware implementation needs to be achieved at a reasonable cost.

1.3 Motivation for the Research

The research presented in this thesis is essentially a step towards the development of practical transient based protection methodologies. The research investigates possible solutions to some of the issues stated in Section 1.2. Besides the primary motivation of developing a faster protection scheme for the transmission systems and other requirements already highlighted in the background, there are still other additional factors that have motivated this research.

Many of the challenges discussed in Section 1.2 are critical to the operation of travelling wave based distance protection schemes. However, as mentioned earlier, recent research [3] indicate the possibility of circumventing some inherent problems such as lack of bandwidth in CVT measurements or missing transients due to fault inception angle, by using transient directional type algorithms. Furthermore, with the advancement of computers and communication technologies, practical implementation of such transient directional type protection methods has become more feasible, and therefore warrants a fresh consideration.

The development of powerful signal processing algorithms such as wavelet transform, S-transform, etc., has enabled the development of robust methods for the extraction and the analysis of transient signals [25]. Some of these techniques are particularly suitable for processing non-stationary transient type signals, and can help reducing the influence of signal noise.

Powerful Digital Signal Processors (DSPs), microprocessors and Field Programmable Gate Arrays (FPGA) that can handle high sampling frequencies and complex protection algorithms are now available at affordable costs [26], [27]. The concepts such as parallel computing and distributed information processing are becoming integral in modern embedded system designs. Analog to digital converters capable of handing high sampling rates at high resolutions are becoming available at reasonable costs and the capability of integrating them with the signal processing hardware is becoming easier.

Furthermore, highly reliable and fast telecommunication facilities are becoming an integral part of the modern power transmission infrastructure. As a result, the use of telecommunication in power system protection and control is becoming more and more acceptable and affordable [28]. Introduction of IEC61850 substation communication protocols has widely increased the scope and the role of communication in power system protection [29]. Such developments make it easier to implement transient based protection methods that require information exchange between stations.

1.4 Research Objectives

The overall objective of this research is to investigate the high speed protection of transmission systems using the fault directions identified from high frequency transients. The protection scheme must be able to identify, locate and isolate faulty sections of the network faster than phasor based relays. Furthermore, the method should be reliable, economical to implement and easy to integrate with the existing protection and measurement devices.

The overall research goal is to be achieved by fulfilling the following specific objectives:

- Development of a practical transient directional protection scheme using the concepts proposed in [17] as a basis, to locate the faulty segments in a transmission network.

- Implementation of a time domain simulation model of the entire protection algorithm and the investigation of its dynamic behaviour under a variety of conditions.
- Development of a hardware platform that is suitable for implementing and testing of the above protection algorithms.
- Implementation, testing and verification of the protection algorithms using transients generated from the simulations.
- Development and implementation of a transient classification system to differentiate the fault generated transients from the switching generated transients to prevent malfunction of protection scheme.

1.5 Thesis Overview

The rest of the thesis is organized as follows. Chapter 2 includes a review of the theoretical and practical aspects related to the thesis. The proposed protection scheme and the simulation studies carried out using the power system simulation program PSCAD/EMTDC is presented in chapter 3. The main steps involved in laboratory prototype implementation and the test results are presented in chapter 4. Chapter 5 presents the development and prototype implementation of a transient recognition system used to discard the non-faulty disturbances. Finally, the conclusions and the recommendations for future research work are presented in chapter 6.

Chapter 2

Background Theory and Information

2.1 Introduction

This thesis investigates a transmission system protection scheme that uses high frequency current transients originating from faults as input signals to the protection scheme. The proposed method involves the use of (i) signal processing techniques to extract the high frequency transients and to determine the fault current directions, and (ii) communication facilities to exchange the fault direction information. The objective of this chapter is to briefly summarize the background theories used in the research. First, the transmission line theory is described followed by the theory of travelling waves. Next, the wavelet transform, the signal processing method used in this thesis is described. Finally, a short description of the communication methods used in protection applications is presented.

2.2 Transmission Line Theory

A system of conductors connected between two locations which can be used to deliver electromagnetic power from one location to the other is referred to as a transmission line

[30]. In transmission line analysis, different types of modeling methods are used. These methods include lumped parameter approach, distributed parameter approach, etc.. The lumped parameter approach is the simplest approach used for transmission line modelling. However this method doesn't give accurate results for wide range of frequencies. In such situations, the distributed parameter approach is applied [31]. In this thesis, distributed parameter approach was preferred to model transmission lines. This section describes the basics of transmission line theory.

2.2.1 Single Phase Transmission Line

Transmission lines can be either single phase or multi-phase. A single phase transmission line is considered first for understanding of the theory.

Characteristic Equation for Lossy Line

The distributed parameter model of the lossy transmission line is shown in Figure 2-1. The transmission line parameters such as inductance, capacitance, etc were assumed to be distributed along the transmission line. The resistance, inductance, capacitance and conductance per unit length are denoted by *R, L, C* and *G* respectively [3], [31],[32].

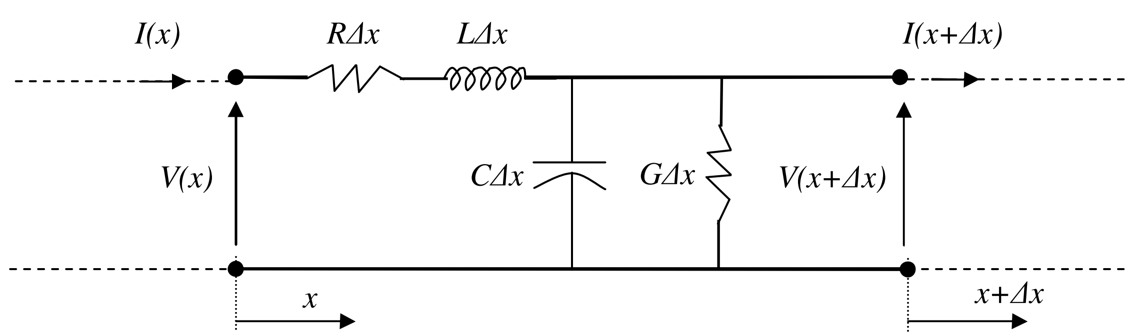

Figure 2-1 : Distributed parameter model of a single phase lossy transmission line [3]

The voltage and the current are functions of time (t) and distance (x) measured along the line given by (2.1) and (2.2).

$$v = V(x,t) \tag{2.1}$$

$$i = I(x,t) \tag{2.2}$$

Consider two points on the line x and $x+\Delta x$. The total voltage drop and capacitance current over the section Δx is given by (2.3) and (2.4) [31]-[32].

$$V(x,t) - V(x+\Delta x,t) = \int_{x}^{x+\Delta x} (Ri + L.\frac{\partial i}{\partial t})dx \tag{2.3}$$

$$I(x,t) - I(x+\Delta x,t) = \int_{x}^{x+\Delta x} (Gv + C.\frac{\partial v}{\partial t})dx \tag{2.4}$$

If, Δx is made to tend to zero, (2.3) becomes (2.5).

$$\frac{\partial v}{\partial x} = -\left(Ri + L.\frac{\partial i}{\partial t} \right) \tag{2.5}$$

Similarly, (2.4) becomes (2.6).

$$\frac{\partial i}{\partial x} = -\left(Gv + C.\frac{\partial v}{\partial t} \right) \tag{2.6}$$

Combining the differentiated equations (2.5) and (2.6), the wave equation corresponding to the lossy line can be determined using the steady state frequency domain analysis [31]-[32] as,

$$\frac{\partial v}{\partial x^2} = (R + j\omega L)(G + j\omega C).\frac{\partial^2 v}{\partial^2 t} \tag{2.7}$$

$$\frac{\partial i}{\partial x^2} = (R + j\omega L)(G + j\omega C).\frac{\partial^2 i}{\partial^2 t} \tag{2.8}$$

The solution to the wave equations can be found below in equations (2.9) and (2.10).

$$v_x = V^+ e^{-\gamma x} + V^- e^{\gamma x} \tag{2.9}$$

$$i_x = \frac{1}{Z_c} V^+ e^{-\gamma x} - \frac{1}{Z_c} V^- e^{\gamma x} \tag{2.10}$$

where, constant (γ) and impedance (Z_c) are given by equations (2.11) and (2.12).

$$\gamma = \frac{1}{\sqrt{(R + j\omega L)(G + j\omega C)}} \tag{2.11}$$

$$Z_c = \sqrt{\frac{(R + j\omega L)}{(G + j\omega C)}} \tag{2.12}$$

In the case of the lossless lines, the series resistance (R) and shunt conductance (G) can be neglected and therefore propagation constant (γ) and surge impedance (Z_c) given in (2.11) and (2.12) become (2.13) and (2.12) respectively.

$$\gamma = \frac{1}{\sqrt{LC}} \tag{2.13}$$

$$Z_c = \sqrt{\frac{L}{C}} \tag{2.14}$$

Travelling Wave Propagation, Reflection and Refraction

Consider a travelling wave that propagates along a transmission line. The relationship between the voltage and the current waves can be considered as fixed, and it is governed by the characteristic impedance Z_c of the transmission line. This relationship can change if the travelling wave reaches a discontinuity, such as a transmission line with different characteristic impedance. In such situations, a part of the energy associated with the wave is transmitted into the second transmission line and the rest of the energy is reflected back to the first transmission line [32]-[33]. In order to understand this phenomenon, consider a situation where a travelling wave propagating along one transmission line meets the second transmission line. Figure 2-2 shows the junction connecting two transmission lines. The characteristic impedances of the two lines are given to be Z_1 and Z_2. In Figure 2-2, $f_i(t)$, $f_t(t)$ and $f_r(t)$ are the incident, transmitted and reflected travelling waves respectively. Currents corresponding to each travelling wave are also shown in Figure 2-2.

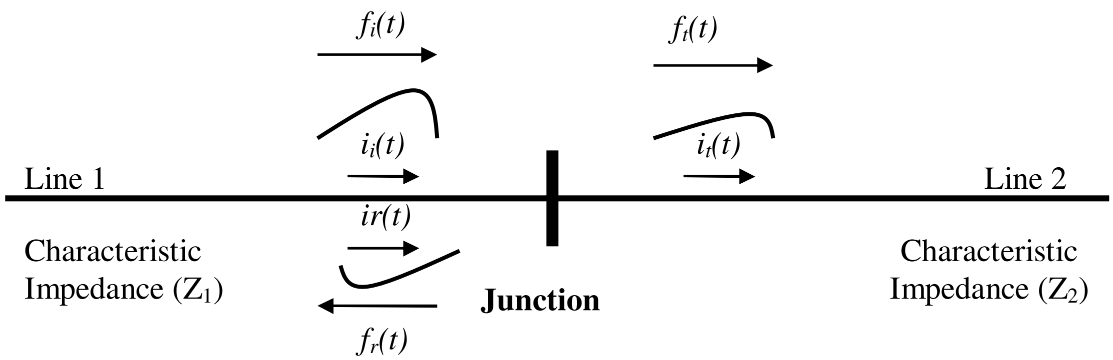

Figure 2-2 : Travelling waves at junction connecting two transmission lines

The relationship between the voltages and the currents of the travelling waves is given by [33],

$$i_i(t) = \frac{f_i(t)}{Z_1},\ i_r(t) = -\frac{f_r(t)}{Z_1} \text{ and } i_t(t) = \frac{f_t(t)}{Z_2} \tag{2.15}$$

As there are no discontinuities of potential and current at the junction, the voltages and currents satisfy the following equations.

$$f_t(t) = f_i(t) + f_r(t) \tag{2.16}$$

$$i_t(t) = i_i(t) + i_r(t) \tag{2.17}$$

After combining the equations (2.15), (2.16) and (2.17), the equations for $f_t(t)$ and $f_r(t)$ can be found as,

$$f_t(t) = \frac{2Z_2}{Z_1 + Z_2} f_i(t) \tag{2.18}$$

$$f_r(t) = \frac{Z_2 - Z_1}{Z_1 + Z_2} f_i(t) \tag{2.19}$$

The fraction of the transmitted wave and the fraction of the reflected waves are called the transmission (α) and the reflection (β) coefficients given by the equations below.

$$\alpha = \frac{f_t(t)}{f_i(t)} = \frac{2Z_2}{Z_1 + Z_2} \tag{2.20}$$

$$\beta = \frac{f_r(t)}{f_i(t)} = \frac{Z_2 - Z_1}{Z_1 + Z_2} \tag{2.21}$$

For practical High Voltage (HV) transmission lines, the imaginary part of the surge impedance is small and positive, and the surge impedance can therefore be approximated as a purely real number. Furthermore, depending on the values of Z_1 and Z_2, the reflection coefficient can be either negative or positive, while the transmission coefficient remains positive.

Figure 2-3 shows a junction with three branches. The characteristic impedances of the lines, the incident wave, transmitted waves and reflected wave are indicated in Figure 2-3.

Similar to the previous case, the voltages and currents at the junction satisfy the following equations.

$$f_t(t) = f_i(t) + f_r(t) \tag{2.22}$$

$$i_{t1}(t) + i_{t2}(t) = i_i(t) + i_r(t) \tag{2.23}$$

The transmission coefficient (α) and reflection coefficient (β) can be obtained [32] by the equations (2.24) and (2.25).

$$\alpha = \frac{f_t(t)}{f_i(t)} = \frac{2Z_2 // Z_3}{Z_1 + Z_2 // Z_3} \tag{2.24}$$

$$\beta = \frac{f_r(t)}{f_i(t)} = \frac{Z_2 // Z_3 - Z_1}{Z_1 + Z_2 // Z_3} \tag{2.25}$$

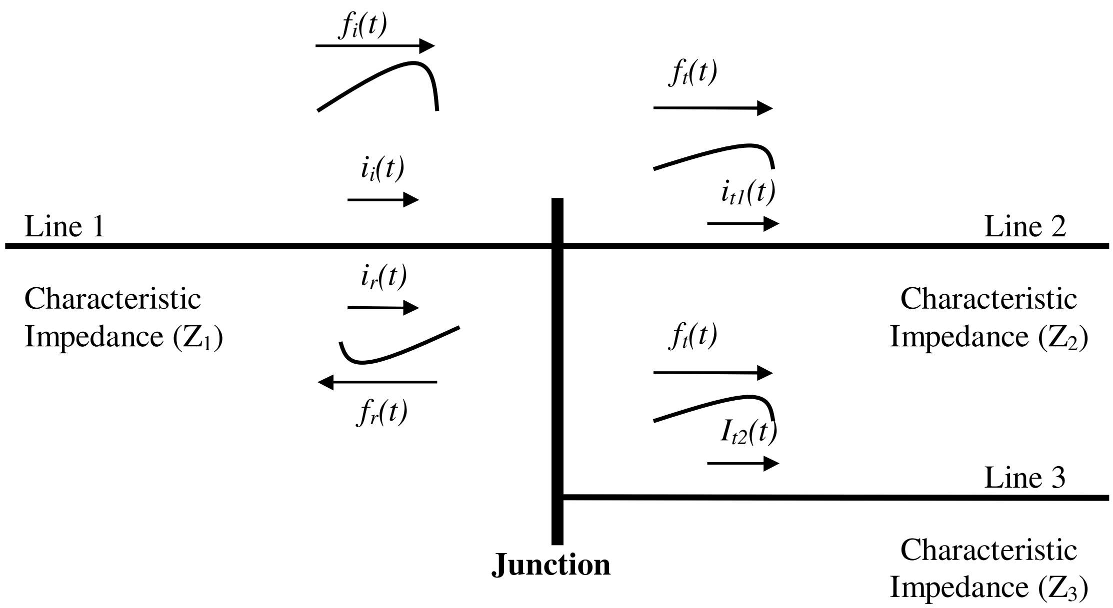

Figure 2-3 : Travelling waves at T-junction connecting three transmission lines

In this thesis, the fault directions are determined by considering the polarities of the incident, transmitted and reflected currents at each node.

2.2.2 Three Phase Transmission Line

Transmission lines that consist of three conductors running parallel to the ground are referred to as a three phase transmission system. Figure 2-4 shows the equivalent circuit of a three phase transmission line using uniform distributed parameters including the ground return path. In Figure 2-4, R_1, L_1 and C_1 are the positive sequence components and R_0, L_0 and C_0 are the zero sequence components [3], [31].

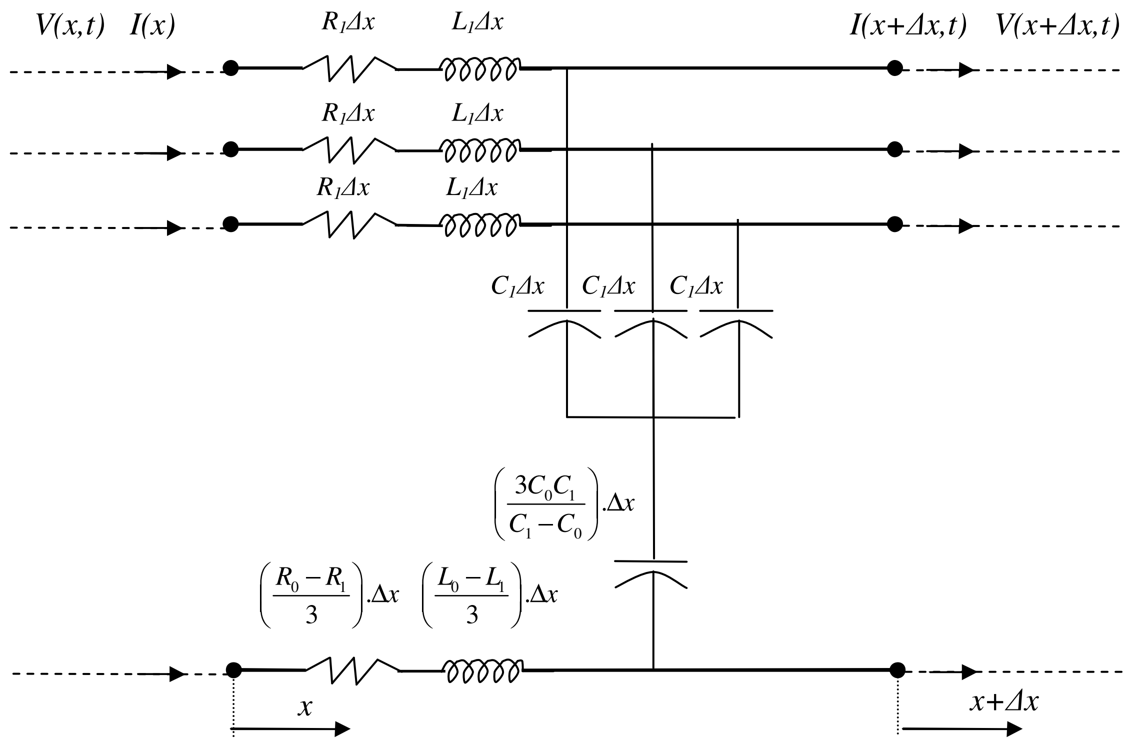

Figure 2-4 : Three phase transmission line model representation using uniform distributed parameters [3]

By applying the Kirchhoff's voltage law to the loops formed by each conductor pairs and the Kirchhoff's current law at the junction of each capacitor [3], [31] the following equations can be derived.

$$-\frac{\partial}{\partial x}\begin{bmatrix} V_a(x,t) \\ V_b(x,t) \\ V_c(x,t) \end{bmatrix} = \frac{1}{3}\begin{bmatrix} Zp_s & Zp_m & Zp_m \\ Zp_m & Zp_s & Zp_m \\ Zp_m & Zp_m & Zp_s \end{bmatrix}\begin{bmatrix} I_a(x,t) \\ I_b(x,t) \\ I_c(x,t) \end{bmatrix} \tag{2.26}$$

$$-\frac{\partial}{\partial t}\begin{bmatrix} V_a(x,t) \\ V_b(x,t) \\ V_c(x,t) \end{bmatrix} = \frac{1}{3}\begin{bmatrix} Zq_s & Zq_m & Zq_m \\ Zq_m & Zq_s & Zq_m \\ Zq_m & Zq_m & Zq_s \end{bmatrix}\frac{\partial}{\partial x}\begin{bmatrix} I_a(x,t) \\ I_b(x,t) \\ I_c(x,t) \end{bmatrix} \tag{2.27}$$

where,

$$Zp_s = (R_0 + 2R_1) + (L_0 + 2L_1)\frac{\partial}{\partial t} \tag{2.28}$$

$$Zp_m = (R_0 - R_1) + (L_0 - L_1)\frac{\partial}{\partial t} \tag{2.29}$$

$$Zq_s = \left(\frac{1}{C_0} + \frac{2}{C_1}\right) \tag{2.30}$$

$$Zq_m = \left(\frac{1}{C_0} - \frac{1}{C_1}\right) \tag{2.31}$$

Then by taking the Laplace Transform of equations above, the following equations can be derived.

$$-\frac{d}{dx}\begin{bmatrix} V_a(x,s) \\ V_b(x,s) \\ V_c(x,s) \end{bmatrix} = \frac{1}{3}\begin{bmatrix} Zp_0 + 2Zp_1 & Zp_0 - Zp_1 & Zp_0 - Zp_1 \\ Zp_0 - Zp_1 & Zp_0 + 2Zp_1 & Zp_0 - Zp_1 \\ Zp_0 - Zp_1 & Zp_0 - Zp_1 & Zp_0 + 2Zp_1 \end{bmatrix}\begin{bmatrix} I_a(x,s) \\ I_b(x,s) \\ I_c(x,s) \end{bmatrix} \tag{2.32}$$

$$-\begin{bmatrix} V_a(x,s) \\ V_b(x,s) \\ V_c(x,s) \end{bmatrix} = \frac{1}{3}\begin{bmatrix} Zq_0 + 2Zp_1 & Zq_0 - Zq_1 & Zq_0 - Zq_1 \\ Zq_0 - Zq_1 & Zq_0 + 2Zq_1 & Zq_0 - Zq_1 \\ Zq_0 - Zq_1 & Zq_0 - Zq_1 & Zq_0 + 2Zq_1 \end{bmatrix}\frac{d}{dx}\begin{bmatrix} I_a(x,s) \\ I_b(x,s) \\ I_c(x,s) \end{bmatrix} \tag{2.33}$$

where $Zp_0 = R_0 + sL_0$, $Zp_1 = R_1 + sL_1$, $Zq_0 = 1/sC_0$ and $Zq_1 = 1/sC_1$,

Equations (2.32) and (2.33) can be written in the general form as given below [30].

$$-\frac{d}{dx}[V] = \frac{1}{3}[Z_P][I] \tag{2.34}$$

$$-[V] = \frac{1}{3}\left[Z_Q\right]\frac{d}{dx}[I] \tag{2.35}$$

By eliminating the current matrix [*I*], voltage can be written as a second order differential equation given by the equation (2.37).

$$\frac{d^2}{dx^2}[V] - [Z][V] = 0 \tag{2.36}$$

where, $[Z] = [Z_P][Z_Q]^{-1}$.

As the conductors in the three phase system are mutually coupled, the impedance matrix $[Z]$ is not a diagonal matric. Therefore the equation (2.29) does not give a simple solution for the voltages. However by using a transformation matrix, the matrix [Z] can be diagonalized which results in an independent set of modes. This transform method is called modal transform [30], [31].

2.2.3 Modal Transform

Let the transformation matrix considered here be [T]. The new set of voltages [U] can be written as shown in equation (2.37).

$$[U] = [T]^{-1}[V] \tag{2.37}$$

Now, the differential equation for [V] can be rewritten as equation (2.38).

$$\frac{d^2}{dx^2}[U] - [Z_M][U] = 0 \tag{2.38}$$

where, $[Z_M]$ is given by equation (2.39).

$$[Z_M] = [T]^{-1}[Z][T] \tag{2.39}$$

By choosing the transformation matrix [T] appropriately, $[Z_M]$ can be made into a diagonal matrix. This results in three independent modal systems or modes. One of the most commonly used constant transformation matrix is the Clarke transformation [34].

Clarke Transformation matrix is given by,

$$[T] = \frac{1}{3}\begin{bmatrix} 1 & 1 & 1 \\ 2 & -1 & -1 \\ 0 & \sqrt{3} & -\sqrt{3} \end{bmatrix} \tag{2.40}$$

There are other types of constant transformation matrixes such as Wedepohl transformation and Karrenbauer transformation [35].

Although the modal transformation approach explained here is used for a three conductor system, it can be used to convert any dependent n-phase system into any independent n number of modes or systems.

This thesis uses the polarities of current transients (travelling waves) to identify the fault directions. The use of modal components helps to achieve better results by eliminating the effect of mutual coupling between conductors.

2.3 Wavelet Transform

This section explains the basics of the wavelet transform technique, which is used as the main signal processing method throughout this thesis. The wavelet transform is a signal processing technique that is well suited for decomposing an aperiodic signal into different frequency bands for time-frequency analysis [36]. The wavelet transform has been successfully used in several applications that required the analysis of high frequency transients.

The wavelet transform represents a time-limited signal as a weighted sum of orthogonal functions derived from a 'mother' wavelet. Each successive orthogonal function is obtained by suitably scaling and translating the original mother wavelet. This representation greatly reduces the amount of information required to represent a transient waveform, and also makes it possible to use a reduced number of weights (wavelet coefficients) to classify the disturbance types [36].

The mother wavelet function must satisfy several conditions: it should be short and oscillatory, i.e. it must have zero average and decay quickly at both ends [37], as in the examples shown in Figure 2-5.

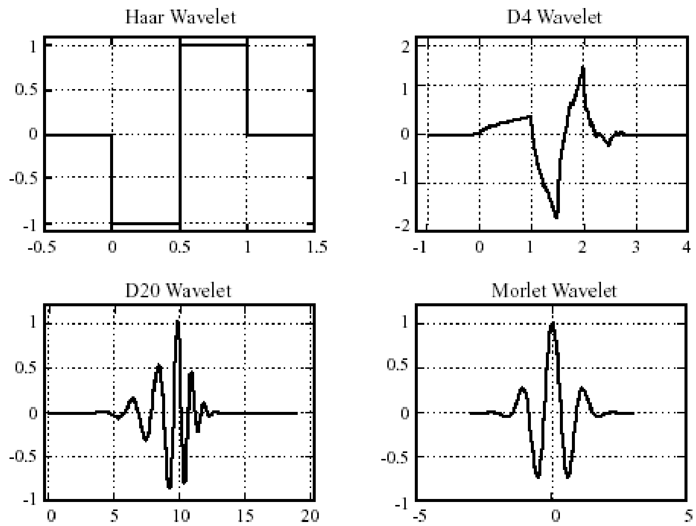

Figure 2-5 : Examples of Mother Wavelets [38]

Wavelet transforms can be continuous or discrete. The following two sections briefly describe the continuous wavelet transform (CWT) and the discrete wavelet transform (DWT).

2.3.1 Continuous Wavelet Transform

If *f(t)* is a signal with a finite energy, its CWT is defined as,

$$CWT_{\Psi} f(a,b) = \int_{-\infty}^{\infty} f(t) \Psi^{*}_{a,b}(t) dt \tag{2.41}$$

where,

$$\Psi_{a,b}(t) = |a|^{-1/2} \Psi\left(\tfrac{t-b}{a}\right) \tag{2.42}$$

The function $\Psi(t)$ is the basis function of the mother wavelet, the asterisk denotes a complex conjugate, and a ($\neq 0, \in \Re$) is the scale parameter and b ($\in \Re$) is the translation parameter [37].

2.3.2 Discrete Wavelet Transform

The discrete wavelet transformation of the discrete function $f(k)$ is defined as,

$$DWT_{\psi} f(m,n) = \sum_{k} f(k) \psi^{*}_{m,n}(k) \tag{2.43}$$

where, $\psi_{m,n}$ is the discretized mother wavelet given by,

$$\psi_{m,n}(k) = \frac{1}{\sqrt{a_0^m}} \psi\left(\frac{k - n b_0 a_0^m}{a_0^m} \right) \tag{2.44}$$

where a_o (>1) and b_o (>0) are fixed real values, and m and n are positive integers. Typically, the mother wavelet is dilated and translated discretely in dyadic blocks by selecting a_o =2 and b_o =1. This helps to remove highly redundant information and hence significantly reduce the computation time and resources. The parameter m is commonly referred to as the 'level' of details [37].

2.3.3 Implementation

The implementation of wavelet decomposition using the filter bank approach is shown in Figure 2-6. This implementation is commonly known as the 'Mallat tree algorithm', and consists of a series of high-pass filters and their dual low-pass filters [39]. H(n) denotes a high pass filter and L(n) denotes its dual low pass filter. The circle denotes down-sampling by a factor of 2. Outputs d_1, d_2, and d_3 are the detailed wavelet coefficients of level-1 to 3 respectively. The output of the last low pass filter, a_3 in Figure 2-6, is called the level-3 approximation coefficient.

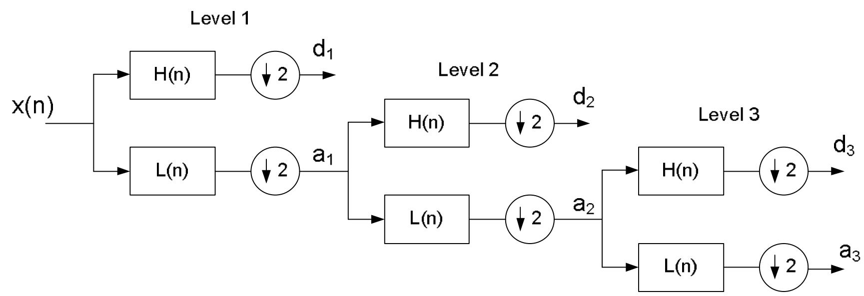

Figure 2-6 : Mallat tree algorithm for wavelet decomposition

The reconstruction of the original signal using wavelet decompositions is shown in Figure 2-7. This requires up-sampling by a factor of 2 at each level. H'(n) is the inverse high pass filter of H(n) and L'(n) is the dual low pass filter of H'(n).

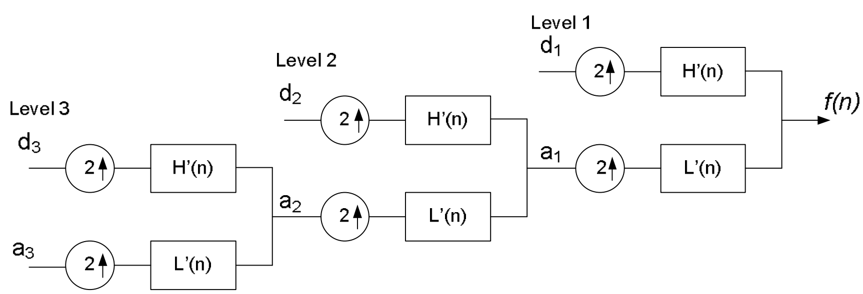

Figure 2-7 : Mallat tree algorithm for reconstruction

2.4 Communication used in Line Protection

Communication is used in transmission line protection, especially when high speed protection is desired. Examples include line differential protection and various transfer tripping schemes. The protection scheme proposed in this thesis also requires exchanging information between relays located at different locations. This section provides a brief overview of the telecommunication technologies currently used in line protection and their performance.

2.4.1 Communication Requirements for Different Communication Aided Protection Schemes

Communication aided protection schemes used in transmission line protection can be mainly categorized into three groups namely pilot protection, line current differential, and line phase comparison [40]-[42]. The communication requirements of these schemes differ from one scheme to the other.

Pilot Protection

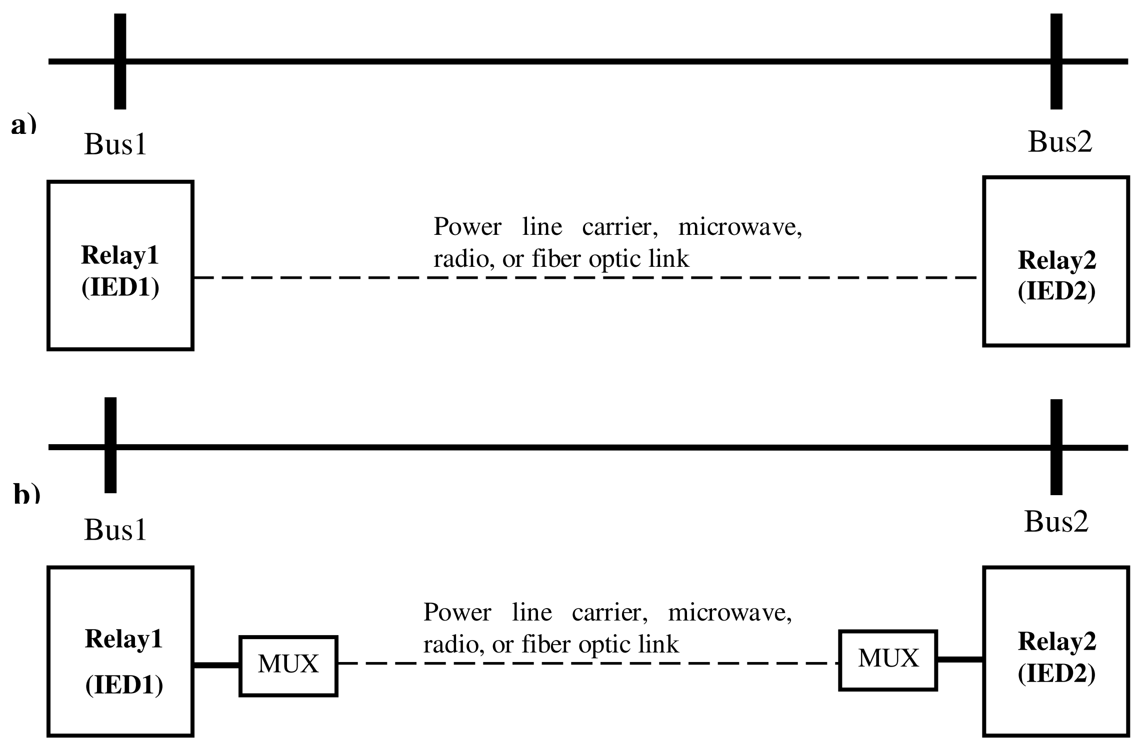

Figure 2-8: Process of Information exchange in a communication aided POTT protection scheme (a) relays connected directly (b) relays connected through multiplexers

The transfer tripping methods used in conjunction with distance relays such as directional comparison blocking and Permissive Overreach Transfer Trip (POTT) are two examples of pilot protection. Pilot protection does not require any synchronization between the sending and the receiving signals. Therefore, these methods can be easily implemented using simple binary communication methods such as power line carrier, microwave, radio, or fiber optic communications. The relay-to-relay communication for a pilot protection can be provided using a direct connection or standard multiplexing devices such as RS232, RS422, G.703, Institute of Electrical and Electronics Engineers (IEEE) C37.94 interfaces, etc. [40] as shown in Figure 2-8. If the transmission line is too long, repeaters must be used to amplify the transmitted signal. The time delays involved in sending the information from one end to the other can vary from 2 ms to several milliseconds depending on the type of the communication medium and the performance of the hardware devices involved [41].

Line Phase Comparison

Line phase comparison is one of the most popular methods used for line protection. In this method, a pulse signal is sent to the remote end when the phase angle of current is positive. For correct operation, the phase angle of the measured current at the local relay should be coordinated. Similar to the pilot protection schemes, a simple binary communication scheme such as power line carrier, microwave, radio, or fiber optic communications can be used to implement this protection scheme. Since the line phase comparison method requires the use of multiple signals, the involvement of a multiplexing device is necessary. The errors caused by the delays in the communication can be easily adjusted by delaying the local measurements according to the communication delays determined during commissioning. The same communication devices that are used in pilot protection can be used in line phase comparison schemes.

Line Current Differential

The line current differential protection scheme operates based on the principal of current differential. Therefore, it requires the interchange of analog information corresponding to each phase through a multiplexed channel with channel switching. For differential calculation to be accurate, precise time synchronization is required between the relays. Any errors in time synchronization will show up as a phase angle offset. For example, 2ms time difference between two ends will introduce a 45 degree phase shift. Although different compensation methods have been used to correct the phase shift error caused by the communication delays, application of such methods introduce a significant delay in overall operation of the scheme. Implementation of this method requires GPS synchronized communication and therefore the capital cost associated with the communication resources is high [40].

2.4.2 IEC61850 GOOSE Messaging Facility

The International Electrotechnical Commission's (IEC) 61850 is the latest international standard for communication that enables integration of all protection, control, measurement and monitoring functions. The protocol provides the means for high-speed substation protection applications, interlocking and inter-tripping [29], [43]. The main features of IEC 61850 architecture are given in Appendix-I.

The Generic Object Oriented Substation Event (GOOSE) and Generic Substation State Events (GSSE) are the two main control mechanisms available with the IEC 61850 framework. Using the GOOSE mechanism any format (status or value) information can be exchanged between the stations whereas the GSSE mechanism only supports the status information. These messaging facilities can be used to implement most of the communication aided protection schemes currently being used [29]. For example, the process of information exchange (published and subscribed) by relays using GOOSE messaging facility for a conventional POTT scheme protecting a simple radial transmission system is shown in Figure 2-9.

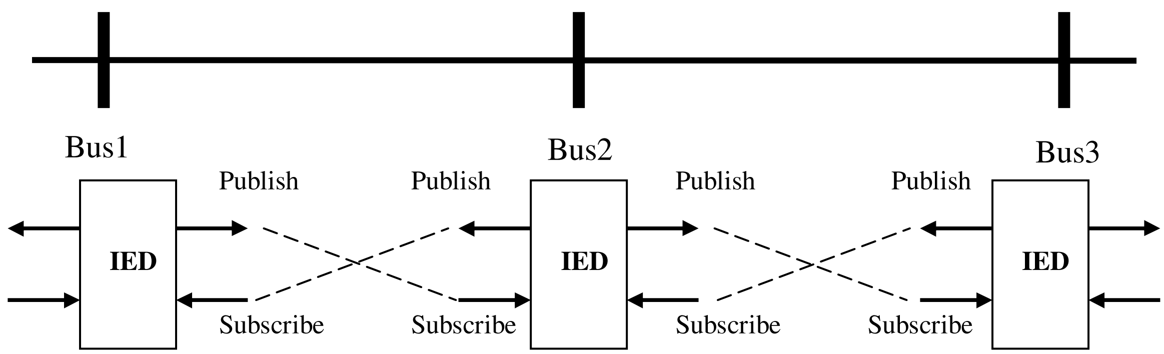

Figure 2-9: Process of Information exchange between Intelligent Electronic Devices (IEDs) (publish/subscribe) using IEC61850 based GOOSE messaging in a POTT scheme

2.5 Chapter Summary

The main theoretical aspects and background information related to the thesis were described in this chapter. This includes the transmission line theory, the theory of travelling waves, reflection and transmission of travelling waves, modal transform, wavelet transform and communication aided protection. The background knowledge provided in this chapter will be useful to understand the details of the proposed protection scheme described in the following chapters.

Chapter 3

Transient Directional Protection Scheme

3.1 Introduction

This chapter presents the transient based transmission network protection scheme developed in this thesis. The basis of the protection scheme is an algorithm which identifies the fault directions with respect to different nodes in the network. This is achieved by analysing the transient currents measured at the respective nodes. The transient signals considered here are in range of 5-10 kHz. The faulted network segment can then be pin-pointed using the fault directions identified at different nodes. This chapter introduces this fault direction identification method, which was first proposed in [17]. Then a number of areas that need to be improved for obtaining reliable performance and making the hardware implementation practicable are identified. Based on these factors, several modifications to the original fault direction algorithm are proposed. Additionally, a structure that facilitates modular implementation of the fault direction identification algorithm is also proposed. Finally, the faulted segment identification method using the determined fault directions is presented, including the results of detailed time domain simulation studies carried out using the power system simulation software PSCAD/EMTDC.

3.2 Fault Direction Identification Using Current Transients

In order to explain the fault direction identification method, consider the relay located at Bus-2 of the simple 3-bus power system shown in Figure 3-1. The busbar at the relay location interconnects three line segments. Three sets of CTs are used to measure the currents on the three branches at *X*, *Y*, and *Z*. The method requires categorization of the faults according to the location. A fault in the region between the CTs, such as fault *F1*, is known as an 'internal' fault, whereas a fault outside the region of the CTs, such as fault *F2*, is known as an 'external' fault [24].

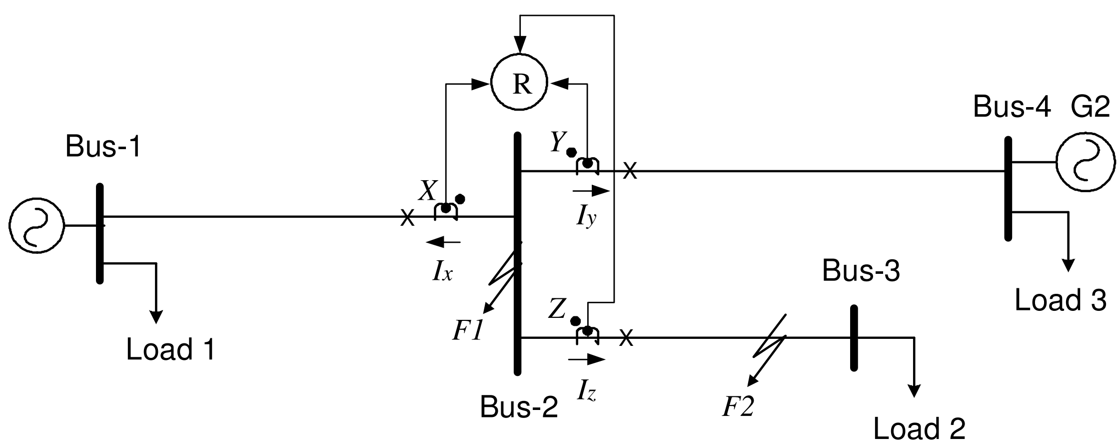

Figure 3-1 : Relay at a busbar interconnecting three lines

In the next step, the measured three-phase currents are transformed into Clarke components [34] using the constant transformation matrix given by (3.1).

$$\begin{pmatrix} I_0 \\ I_\alpha \\ I_\beta \end{pmatrix} = \frac{1}{3}\begin{pmatrix} 1 & 1 & 1 \\ 2 & -1 & -1 \\ 0 & \sqrt{3} & -\sqrt{3} \end{pmatrix}\begin{pmatrix} I_a \\ I_b \\ I_c \end{pmatrix} \tag{3.1}$$

Here, I_a, I_b, and I_c are the phase currents and I_α, I_β, and I_0 are the corresponding Clarke components. Only the transients due to faults involving ground will show up in the I_0 component. The I_α component can be used to analyze all types of faults except the faults between phases B and C where as the I_β component can be used to analyze the B-C faults. All ground faults can be analyzed using the I_0 component. A combination of I_α, I_β, and I_0 components can be used to analyze all types of faults.

In order to extract the travelling wave fronts generated due to faults, wavelet transformation can be used. In the examples presented below, the Level-1 discrete wavelet transform coefficients (WTCs) obtained with DB4 mother wavelet were used. Several other mother wavelets were tried, and *DB4* was found to give the most accurate results [17].

For example, consider the internal fault *F1* (ABC-G) in Figure 3-2. The three-phase current measurements, the corresponding α components and their WTCs at the CT locations X, Y and Z are shown in Figure 3-2. Since fault *F1* is inside the region of CTs, the WTCs have the same sign. Here the term "same sign" is used to describe the overall wave shape of the wavelets rather than the sample-by-sample basis. Whether the wavelet coefficients are of the same sign or not can be established by using a cross-correlation based method, described later in this section.

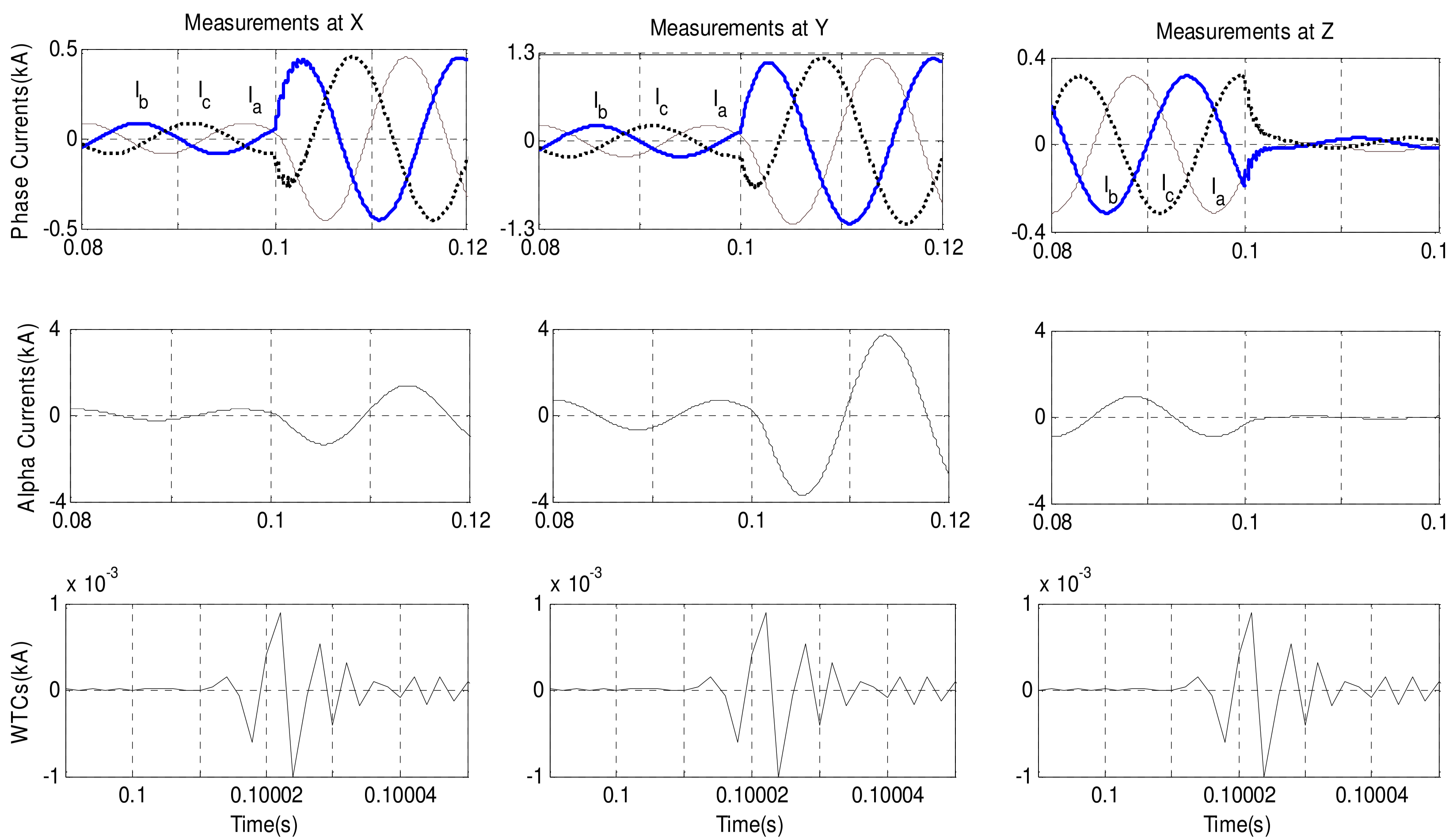

Figure 3-2 : Phase Current, corresponding Clarke components and their WTCs (DB4 level-1) following an internal ABC-G fault

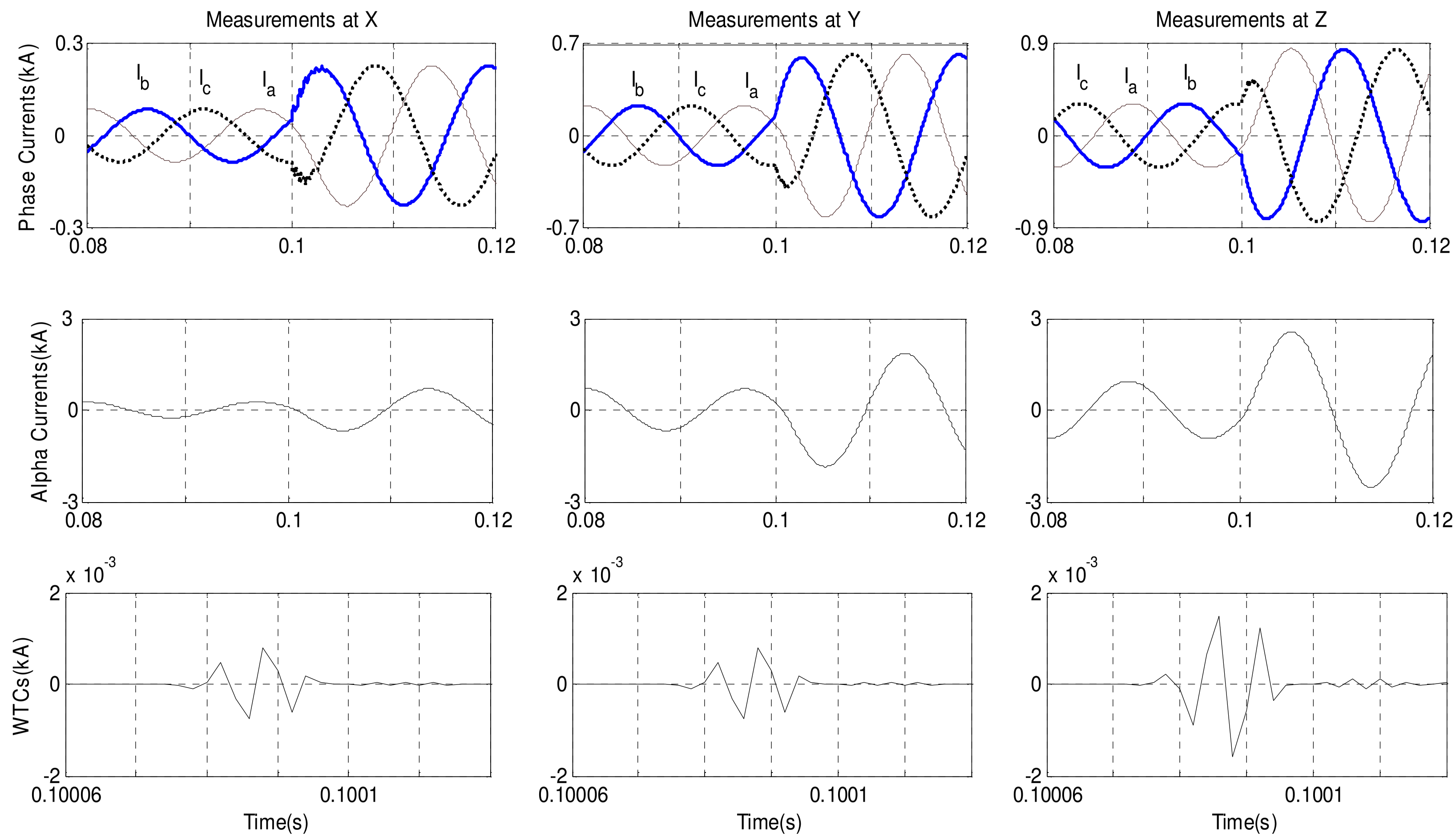

Figure 3-3 : Phase currents, corresponding Clarke components and their WTCs following an external ABC fault

For the external fault *F2* (ABC), three-phase current measurements, their alpha components and the corresponding WTCs are also shown in Figure 3-3. The CTs on the faulted branch measures the incident wave plus the reflection whereas the CTs on the non-faulted branches measure only the transmitted waves. As a result, the WTC of the faulted branch has a sign opposite to those of the non-faulted branches. This sign difference can be used to determine the fault direction. In addition, as pointed out in [17], the wavelet coefficient corresponding to the faulted branch has higher magnitude than the other branches. This can be used to confirm the direction results obtained with the sign.

Although this concept was proven [17], it requires real time wavelet analysis of three phase current signals on all branches connected to a busbar sampled at a high frequency. Thus, application of this algorithm for a busbar connecting many branches is challenging and requires a relay with a very high computational capability. Implementation of simultaneous sampling of a large number of inputs at a high sampling frequency and high resolution requires expensive hardware. In order to overcome this problem, a new simpler fault direction identification method that avoids the direct comparison of the wavelet coefficients of different branches is proposed. In the new method, signs of the wavelet coefficients are determined locally on each branch by comparing the respective wavelet coefficients with a 'reference wavelet'. Taking advantage of this new concept, a new modular architecture is then proposed for implementation of the protection scheme [44]. This new modular implementation not only eliminates the requirement for a powerful processor and simultaneous sampling of a larger number of input signals, but also facilitates a flexible, simple and economical hardware implementation that utilizes the resources better.

3.3 Modular Implementation of the Fault Direction Identification Method

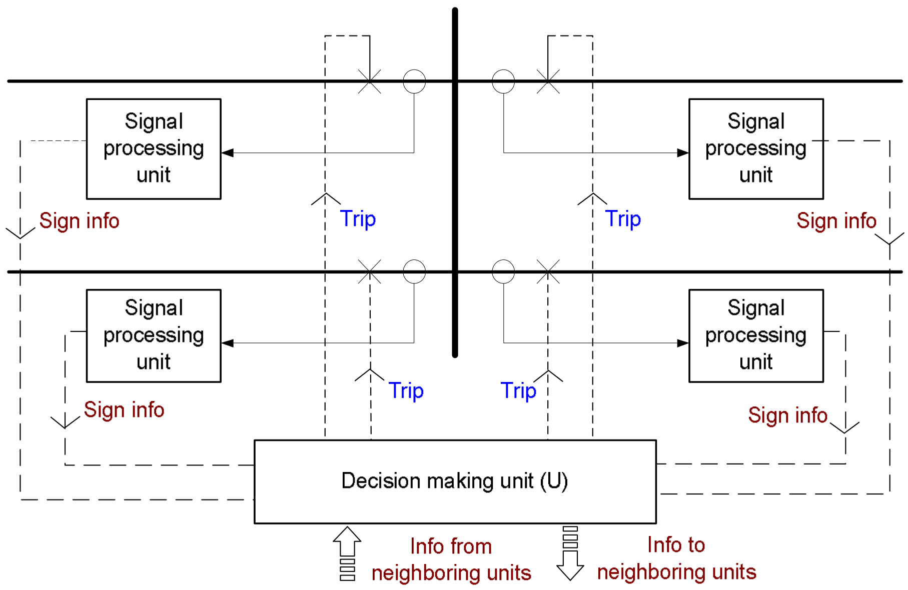

Figure 3-4: Modular arrangement of the fault direction identification units

In order to overcome some of the difficulties described above, a new modular structure for implementing the fault direction finding algorithm is proposed in this section. Figure 3-4 shows the arrangement of this new structure which includes different protection modules installed on a busbar interconnecting the four branches. Each branch can represent a line, transformer, load, reactor or a capacitor bank and is provided with a signal processing unit. The current transformers (CTs) supplying the signal processing units are connected in such a way that all CTs measure currents entering the bus as positive wave. The signal processing units determine the sign of the detected current transients by comparing its WTC coefficients to a reference wavelet. This sign information is sent to a decision making unit associated with the busbar, which analyses the information and identifies the direction of the fault with respect to the busbar. The fault directions determined by the decision making units installed at different stations on the transmission network can be combined to identify the faulted network segment.

3.3.1 Signal Processing Unit (SPU)

The inputs to the signal processing units (SPUs) are three-phase current measurements. The Clarke's transformation is applied to the sampled low-pass (anti-aliasing) filtered three-phase current signals to obtain the modal components. Then the wavelet transform coefficients (WTCs) of the modal components are obtained using the discrete wavelet transform (DWT). The WTCs of the modal current signal are compared with the shape of a reference mother wavelet. Only one modal current component, the component with the largest magnitude, is used to determine the sign. The cross correlation between the wavelet coefficient and the mother wavelet was used to ascertain whether the WTC is negative or positive. Figure 3-5 shows various stages in the signal processing unit.

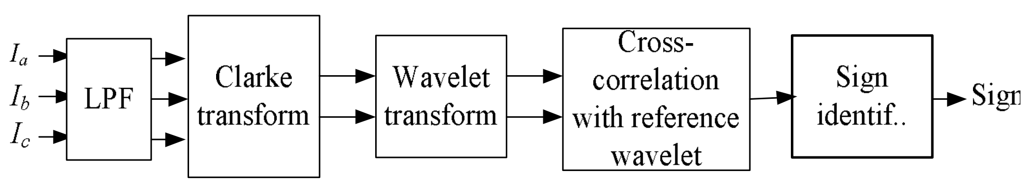

Figure 3-5: Algorithm for Signal Processing Unit

Figure 3-6 depicts an example of the processing done in the SPU. The graphs from the top to bottom show the variations of the measured three-phase current signals, the most significant Clarke component, its WTC and the cross-correlation between the reference mother wavelet and the WTC coefficient respectively. The reference mother wavelet (db4) which is also shown in Figure 3-6 was shifted along the time axis to determine cross-correlation coefficients at each sampling point, and the sign of the highest coefficient after the disturbance was taken as the sign of the WTC coefficient. In the example shown in Figure 3-6, the sign of WTC coefficient is positive. This sign information is communicated to the corresponding decision making unit to determine the fault category and direction.

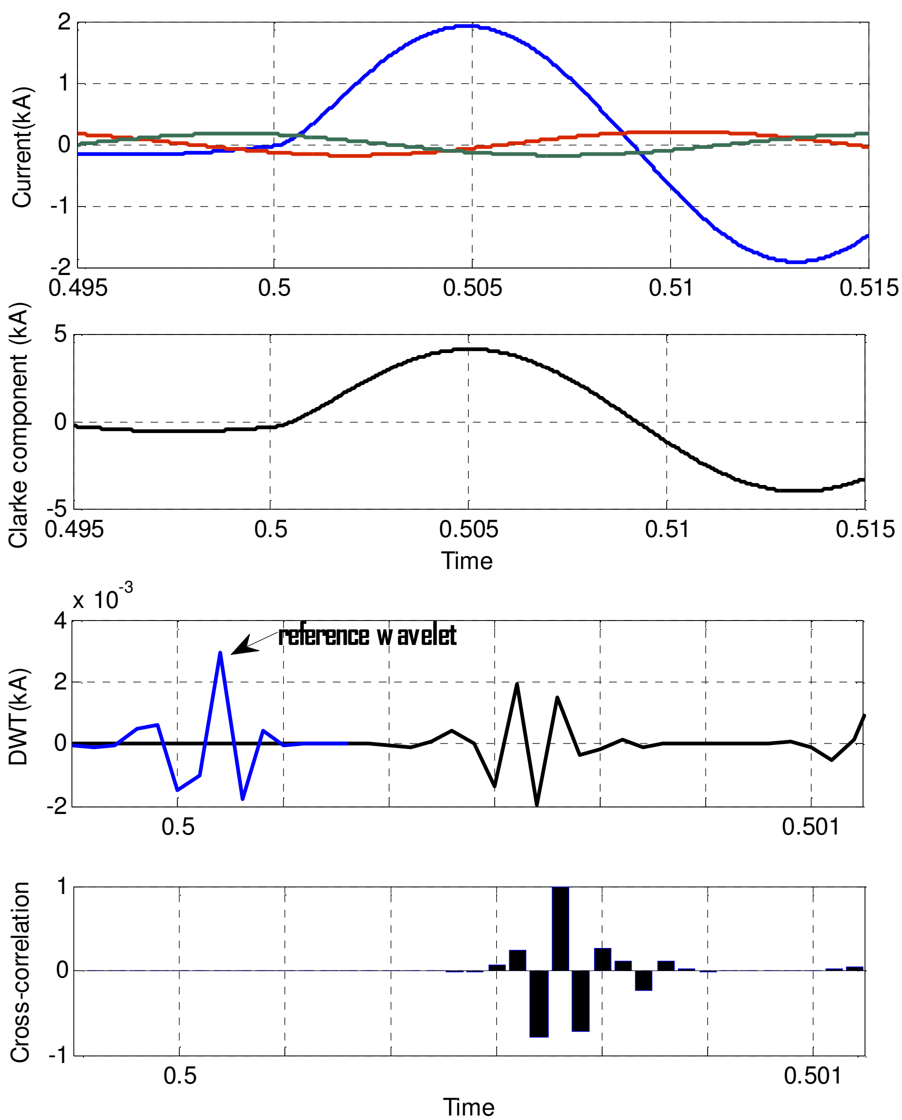

Figure 3-6: Three phase current signals, the Clarke component with the largest magnitude, DWT coefficient and coefficients of cross-correlation during a line-to-ground fault

3.3.2 Decision Making Unit (DMU)

The decision making unit (DMU) compares the signs of wavelet coefficients received from all the branches to determine the fault category and the fault direction. The rules used to determine the fault category and direction are as follows:

I. If the sign information received from all SPUs have the same sign, the fault is an internal (busbar zone) fault. Otherwise, it is an external fault with respect to the decision making unit concerned.

II. In case of an external fault, the sign information received from the SPU in the direction of the fault has a sign opposite to the others.

After determination of the fault category and direction, a decision making unit transmits that information to the neighbouring decision making units. It also receives the fault direction information from the other decision making units connected to it.

3.4 Faulty Segment Identification

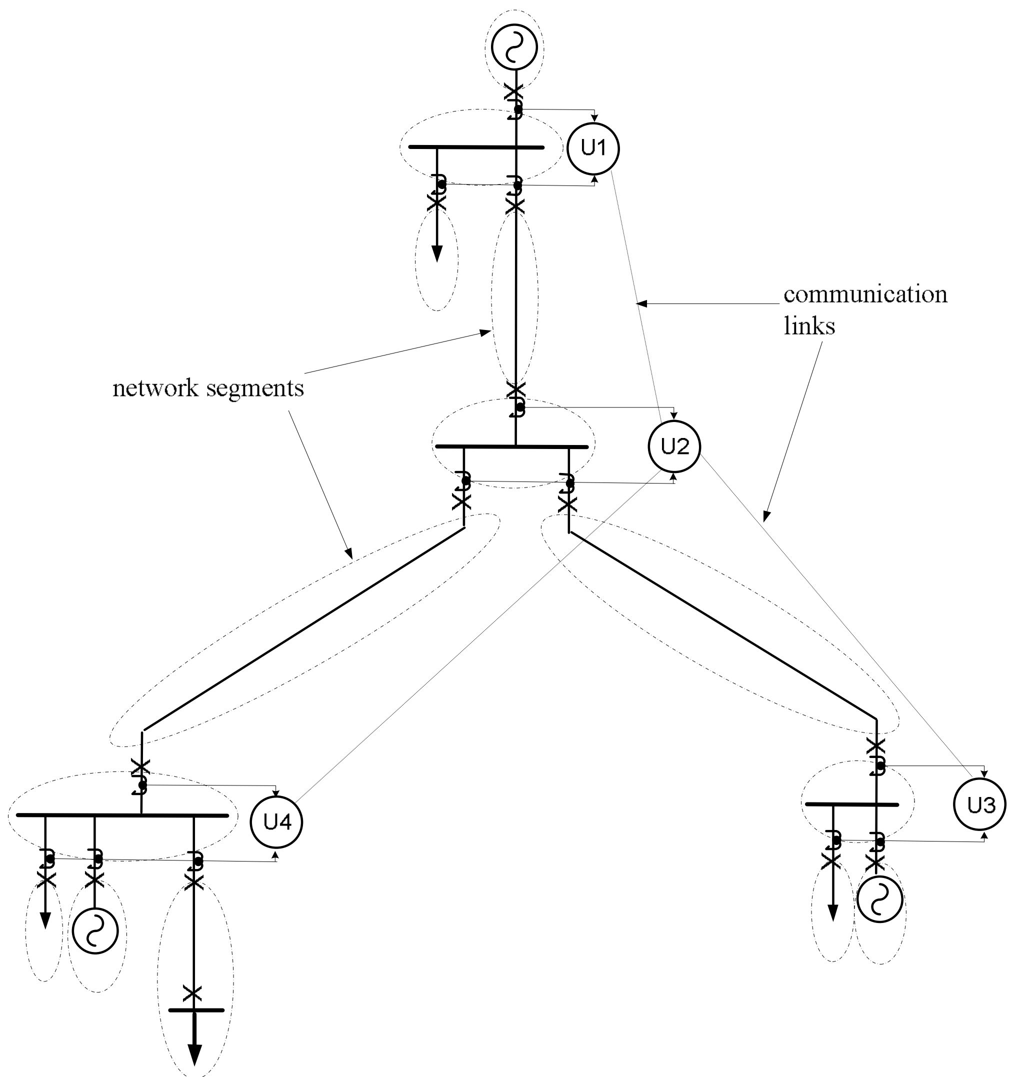

Figure 3-7 : Structure of the proposed protection scheme

Faulty segment identification requires the exchange of fault direction information among the decision making units installed at different stations on the transmission network via telecommunication links as illustrated in Figure 3-7. Note that the communication links between different decision making units closely follow the topology of the network. A decision making unit communicates only with the other decision making units that are directly connected with it. The steps involved in the faulty segment identification process are summarized in the flowchart shown in Figure 3-8.

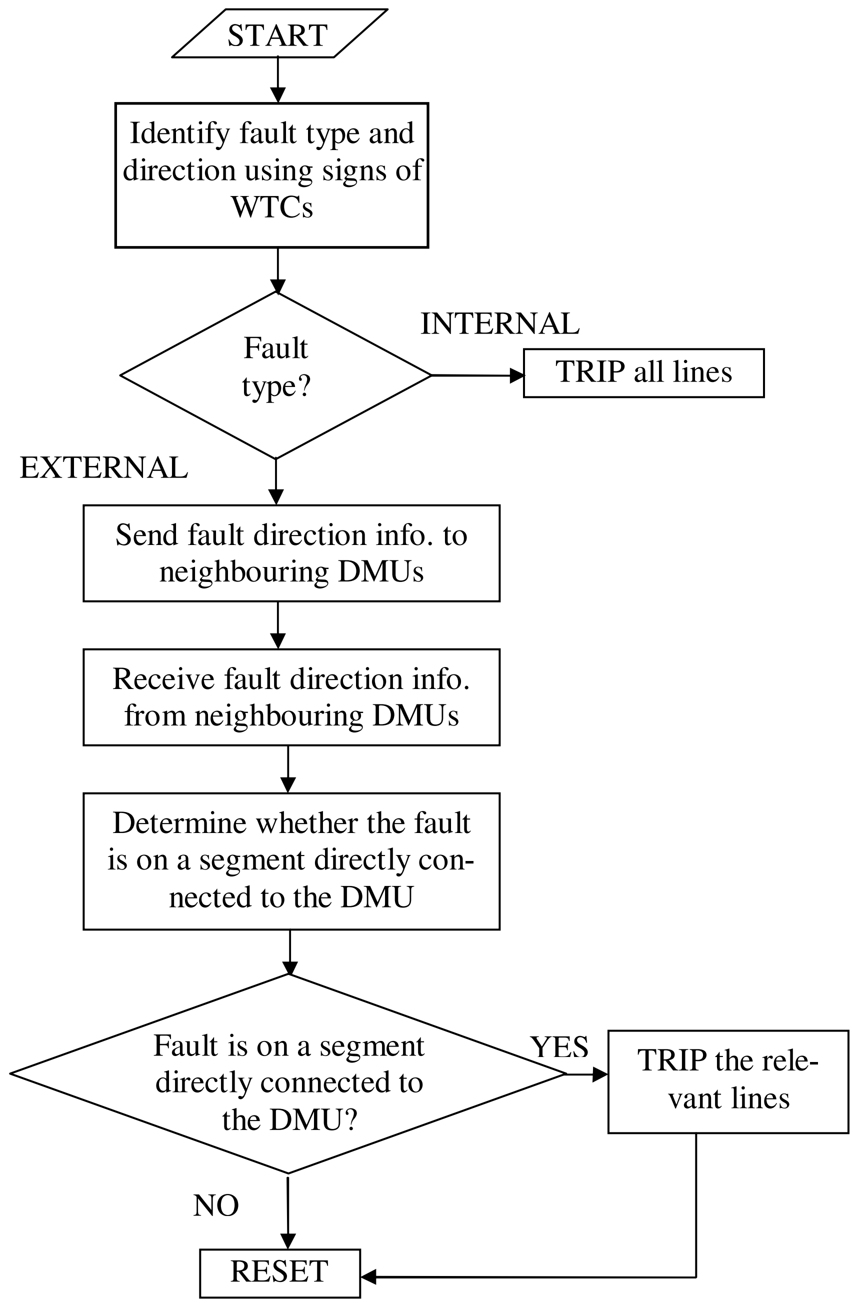

Figure 3-8 : Algorithm for faulty segment identification

The following rules are applied in communicating the fault direction information to the neighbouring DMUs to determine the faulty network segment.

I. If the fault category is internal, then a signal representing a logical value of "0" is transmitted to all neighbouring relay agents.

II. If the fault category is external, then a logical value of "1" is transmitted to the relay agent in the direction of the fault and a logical value of "0" is transmitted to all the other relay agents.

III. If there is no relay agent in the direction of the fault (remote end), or if the incoming communication from the neighbouring relay agent in the direction of the fault is not forthcoming (broken communication link), the incoming signal is assumed to be a logic value of "1".

IV. If there are parallel lines connected between two decision making units, a separate logic value corresponding to each line is transmitted.

Note that based on the above rules, only a logic value, '0' or '1' needs to be transmitted between two adjacent DMUs. Thus communication bandwidth requirements and the possible errors due to noise and interference are minimal. The communication requirements are similar to those used in inter-tripping schemes used with the traditional distance protection, and much less demanding compared to line differential protection.

A DMU requires (i) sign information from all SPUs connected to it, and (ii) the fault direction information from all other DMUs directly connected with it (via telecommunication channels), to make a trip decision. The logic functions of a DMU located at a node connected with n-branches is shown in Figure 3-9. The WTC sign information received from the signal processing units on each branch (S_i values) are used to determine the fault direction information value sent to the DMU at the other end of the i^{th} branch, D_{Si}. The values of D_{Si} and D_{Ri} (fault direction information received from the other end) are used to derive the trip signal T_i for the breaker on the i^{th} branch. In case of an internal fault (D_{Si} = 0 for all i), breakers on the all the branches are tripped.

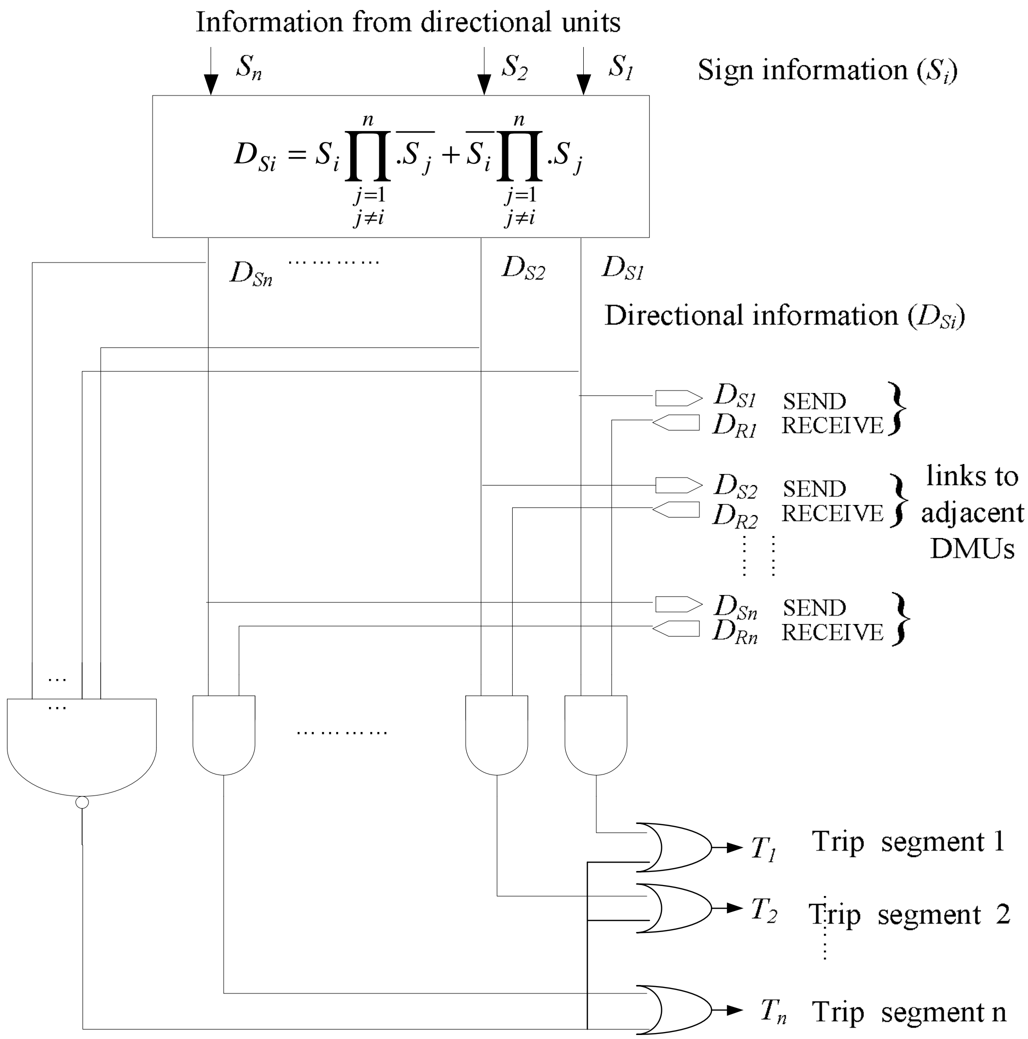

Figure 3-9 : Logic processing involved in faulty segment identification

The following example cases illustrate the faulty segment identification procedure for different scenarios.

3.4.1 Busbar Fault

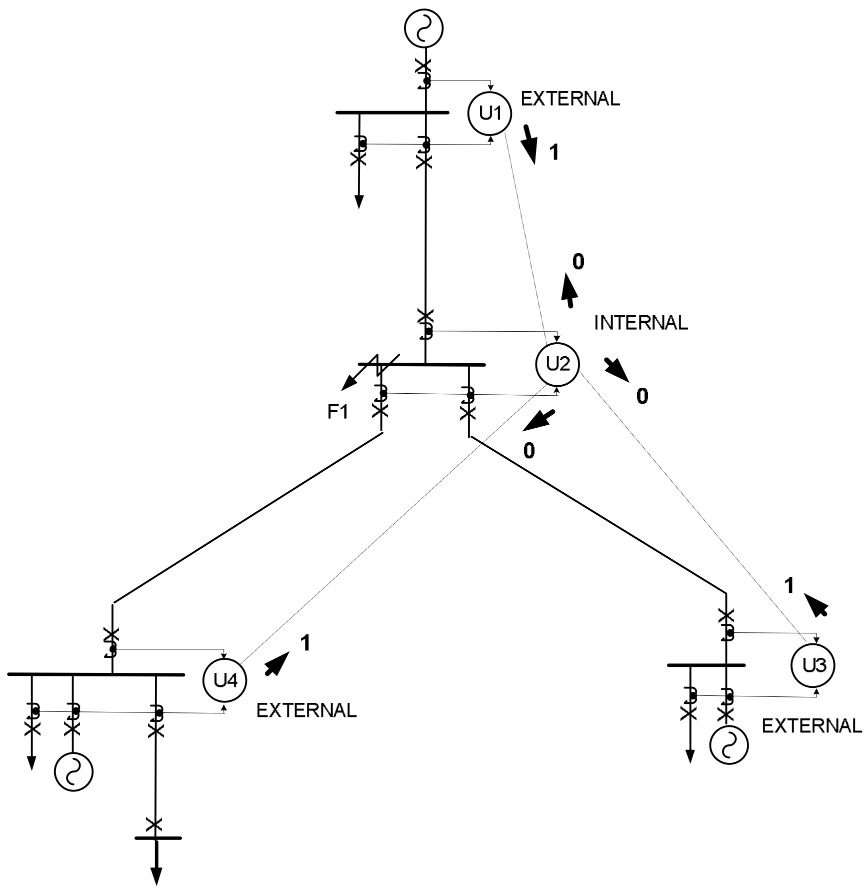

Figure 3-10 : Illustration of faulty segment identification for a busbar fault

Consider the 4-bus power system shown in Figure 3-10. The fault F1 is on the busbar corresponding to DMU U2. For this fault, observations at U2 would indicate it as an internal fault. The observations at U1, U3 and U4 would indicate it as an external fault, and find the direction of fault with respect to the DMU's location. The information (1 or 0) exchanged between the DMUs based on the fault directions determined is also shown in Figure 3-10. The arrows indicate the direction of transmission. Based on the logic described earlier, DMU U2 can immediately isolate the internal fault by operating all the circuit breakers connected to it. At the same time, information exchanged among the

DMUs will prevent other DMUs from taking actions against this fault. This provides very fast busbar protection.

3.4.2 Network Segment Fault

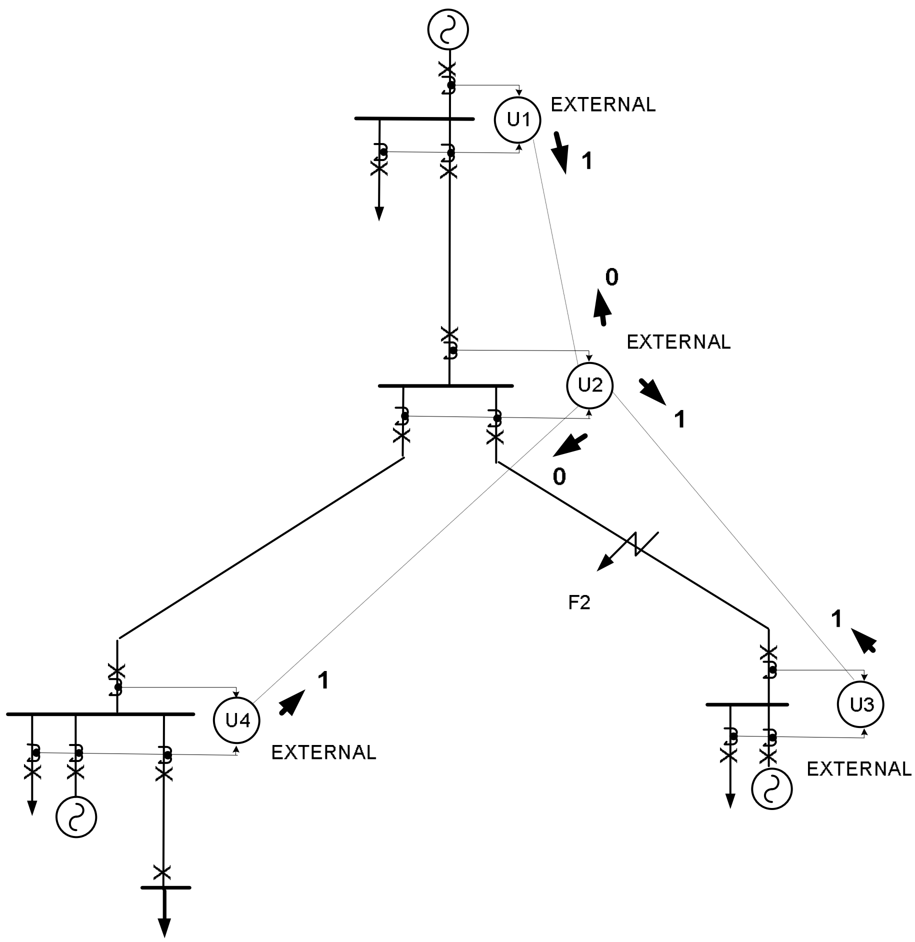

Figure 3-11: Illustration of faulty segment identification for a network fault

For this discussion, consider the fault F2 on the transmission line connecting the busbars corresponding to DMUs U2 and U3 as shown in Figure 3-11. In this case, the observations at all DMU locations would have indicated it as an external fault. The information exchanged among the DMUs based on the fault directions determined by each DMU would be as indicated in Figure 3-11. For this fault, DMU U2 sends ‘1’ to U3 and receives ‘1’ from U3; and DMU U3 sends ‘1’ to U2 and receives ‘1’ from U2. This confirms the existence of a fault between them. DMUs U2 and U3 can issue trip signals to isolate the line segment between them. DMUs U1 and U4 send ‘1’ to DMU U2, but receive ‘0’ from U2. That confirms there is no fault in the lines between U1 and U2, and U4 and U2.

3.4.3 Remote End Fault

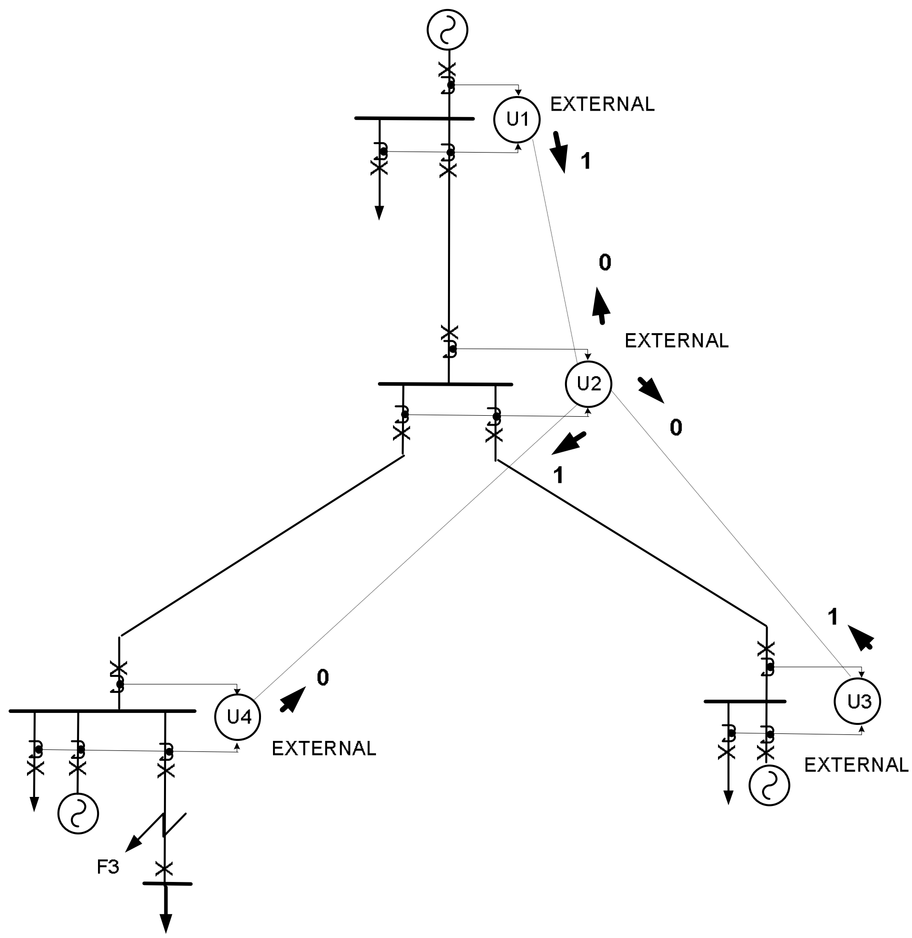

Figure 3-12: Illustration of faulty segment identification for a remote end fault

Fault F3 is located on one of the remote feeders of the network as shown in Figure 3-12. For this fault, DMU U4 finds the fault direction towards the remote terminal. When there is no DMU in the direction of the fault, U4 assumes incoming signal to be logical “1”. This results in correct identification of the faulted network segment. The fault direction information exchanged between U4 and U2, U2 and U1, and U2 and U3 confirms that that the line segments between respective DMUs are healthy.

3.4.4 Busbar with Two Line Segments

When there are only two lines connected to a busbar a DMU can only provide the protection against the internal (busbar) faults, because in this situation, the DMU cannot determine the fault direction based on the wavelet coefficients’ signs. Such situations can result from the opening of circuit breakers in the system and need to be handled differently. If there are only two segments connected to the busbar, the DMU determines the fault category, but avoids responding for the external faults. In case of an external fault, the decision making unit waits for the fault direction information from the neighbouring DMUs and passes that information to the opposite sides. The fault in this case is allowed to handle by the two neighbouring DMUs.

The example case shown in Figure 3-13a illustrate such a scenario. The transmission line between the DMUs U2 and U4 is tripped, leaving only two branches connected to DMU U2. Monitoring of circuit breaker status allows DMU U2 to be aware of the situation. For the fault shown in Figure 3-13a, DMU U2 waits for the direction information from U1 and passes that value to U3, in place of the direction determined by itself. Similarly, the direction information received from U3 is passed to U1, as illustrated in Figure 3-13a. This will result in the DMU U1 opening the breaker in the branch between U1 and U2, and the DMU U3 opening the breaker in the branch between U3 and U2, thus isolating the fault. In this case, the two line segments and bus-2 are disconnected to isolate the fault. Although two line segments and a bus is removed to clear the fault in this case, no additional loads (or generators) are interrupted. If a load (or a generator) was connected to the node at U2, the fault direction can be determined using the load (generator) as the third branch.

On the other hand, an internal fault such as F5 on the busbar of U1shown in Figure 3-13b does not result in tripping of the breakers at U3, if the same rule is followed with regard to the direction information sent by U2. The fault F5 will be cleared by the breakers operated by U1 as intended. In order to handle this type of situation, it is required to enhance the basic logic function shown in Figure 3-9, using the circuit breaker status signals.

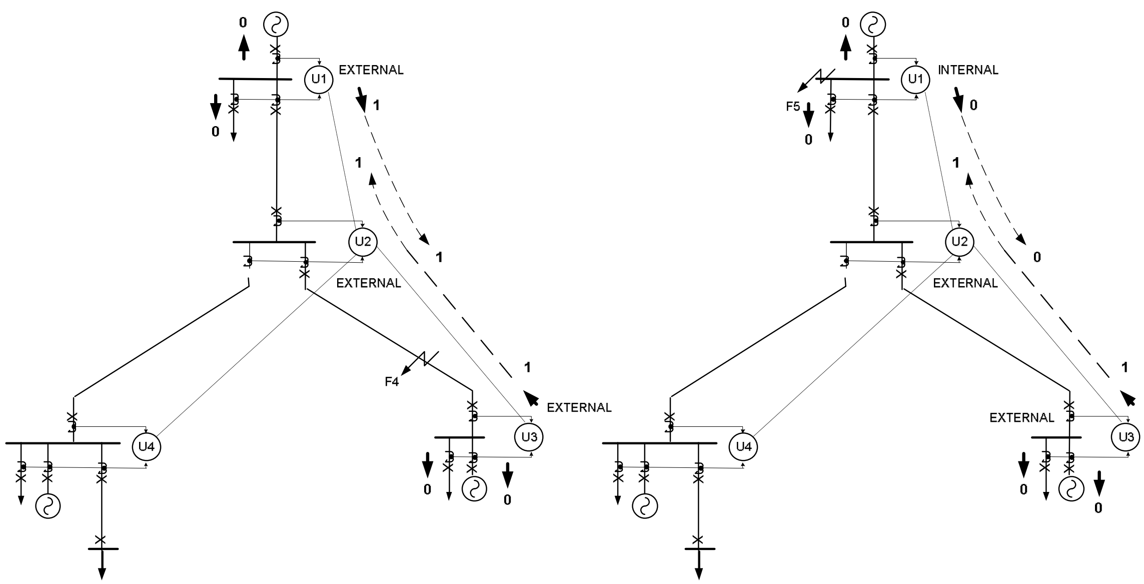

(a) (b)

Figure 3-13: Faulty segment identification when there are only two active segments connected

3.4.5 Faults on Parallel Line Segments

In order to demonstrate the fault segment identification procedure for faults on parallel lines, consider the modified transmission network with two parallel lines connecting the busbars corresponding to DMUs U2 and U3 as shown in Figure 3-14. As there are two parallel lines, the DMUs U2 and U3 require two directional values exchanged between each other. In this case, the fault F5 is located on one of the parallel lines. For this fault, DMU U2 sends ‘1, 0’ to U3 and receives ‘1, 0’ from U3; and DMU U3 sends ‘1, 0’ to U2 and receives ‘1, 0’ from U2. This allows the DMUs U2 and U3 to correctly identify the faulted line segment out of the two parallel lines.

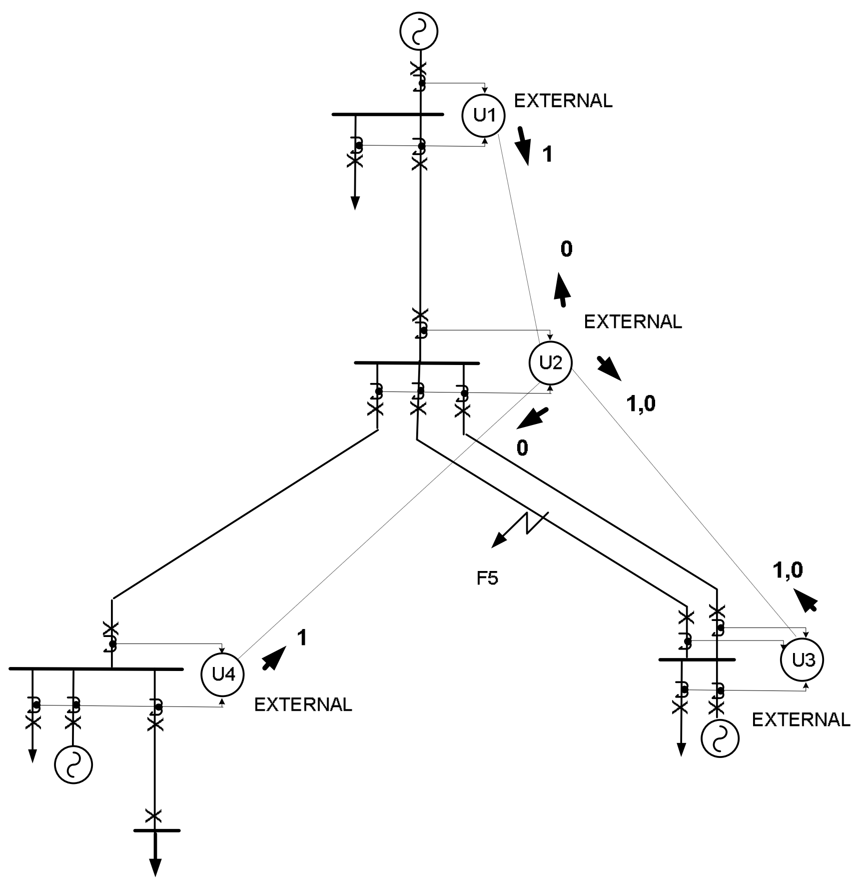

Figure 3-14: Illustration of faulty segment identification for parallel line fault

3.4.6 Communication between Relays

The operation of the proposed protection scheme relies on the information exchanged between the DMUs located at different substations. Thus the protection scheme must be feasible to implement using currently available communication facilities. The IEC 61850 is the latest international standard for communication that enables integration of all protection, control, measurement and monitoring functions. The protocol provides the means for high-speed substation protection applications, interlocking and inter-tripping [29]. The main features of IEC 61850 architecture is given in Appendix-I.

The proposed protection scheme can be easily designed to be compatible with the GSSE (Generic Substation State Events) or GOOSE (Generic Object Oriented Substation Event) messaging facility provided in the IEC 61850 framework. The GOOSE is a control model in which any format of data (status, value) is grouped into a data set and transmitted within a time period of 4 milliseconds. GSSE on the other hand allows transmission of only status data, which is sufficient for this application. More details about the GOOSE and GSSE messaging facilities are given in the Appendix-I. In the proposed protection scheme, the logical information corresponding to fault directions can be exchanged between the neighboring relays using GOOSE/GSSE messaging facility.

3.5 Simulation Studies

A comprehensive simulation study was carried out to investigate the performance of the proposed protection scheme. Figure 3-15 shows the high voltage power transmission system [45] used for the simulation studies. The parameters of the system are given in Appendix-II. The power system was simulated using PSCAD/EMTDC software. The transmission lines were simulated using frequency dependent phase domain transmission line models that take into account details such as skin effect. The Bus-9 was modeled as an infinite bus and the generators G2, G3 and G4 were modeled as salient pole synchronous generators. The complete generator models included exciters, turbines and governors. The three-phase transformers were modeled with the effects of saturation. The current transformers were also simulated using a detailed model [46]. Simulations were carried out with a 5μs time step, since it is required to capture high frequency transient signals.

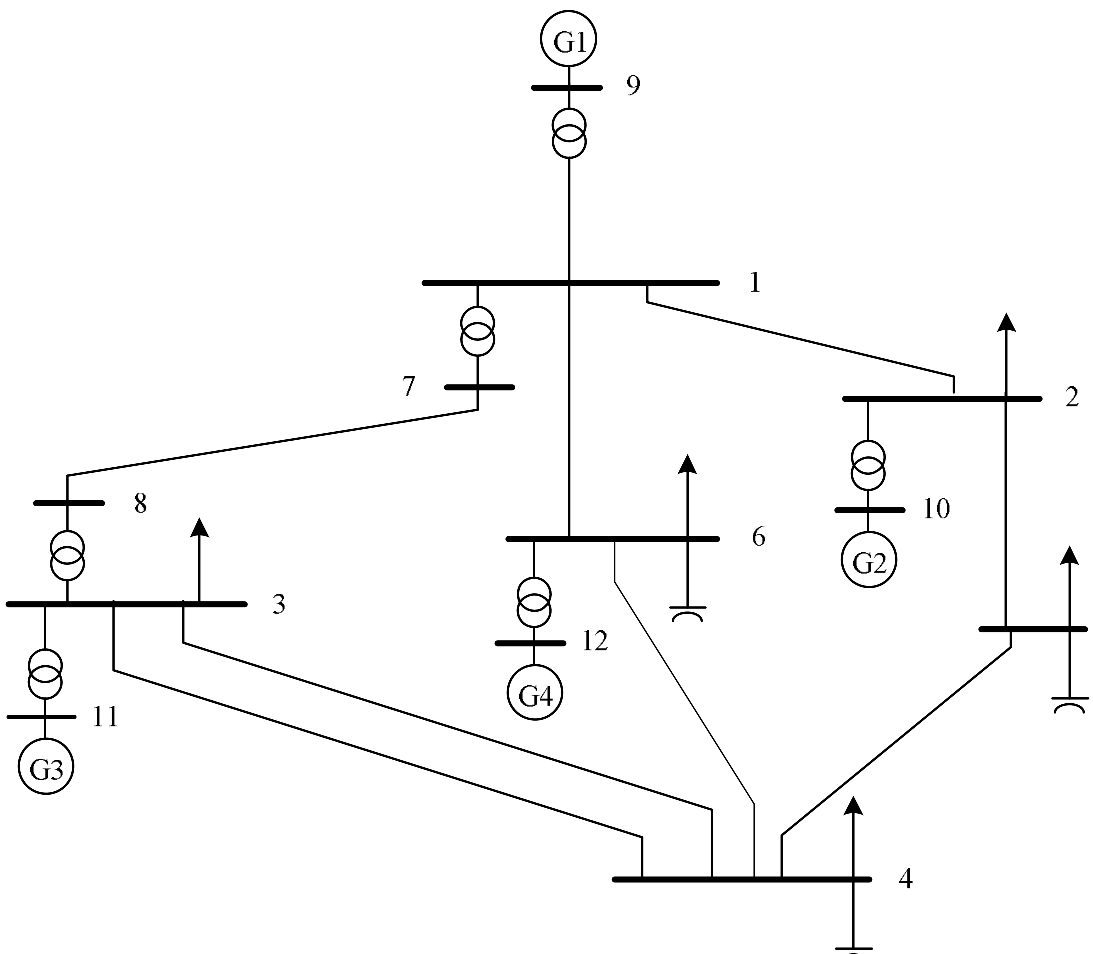

Figure 3-15 : HV test system

3.5.1 Development of the Relay Algorithm

This section describes the implementation of the fault location algorithm used in the PSCAD/EMTDC simulation program. Figure 3-16 shows the arrangement of the DMUs U1-U6 in the high voltage test power system.

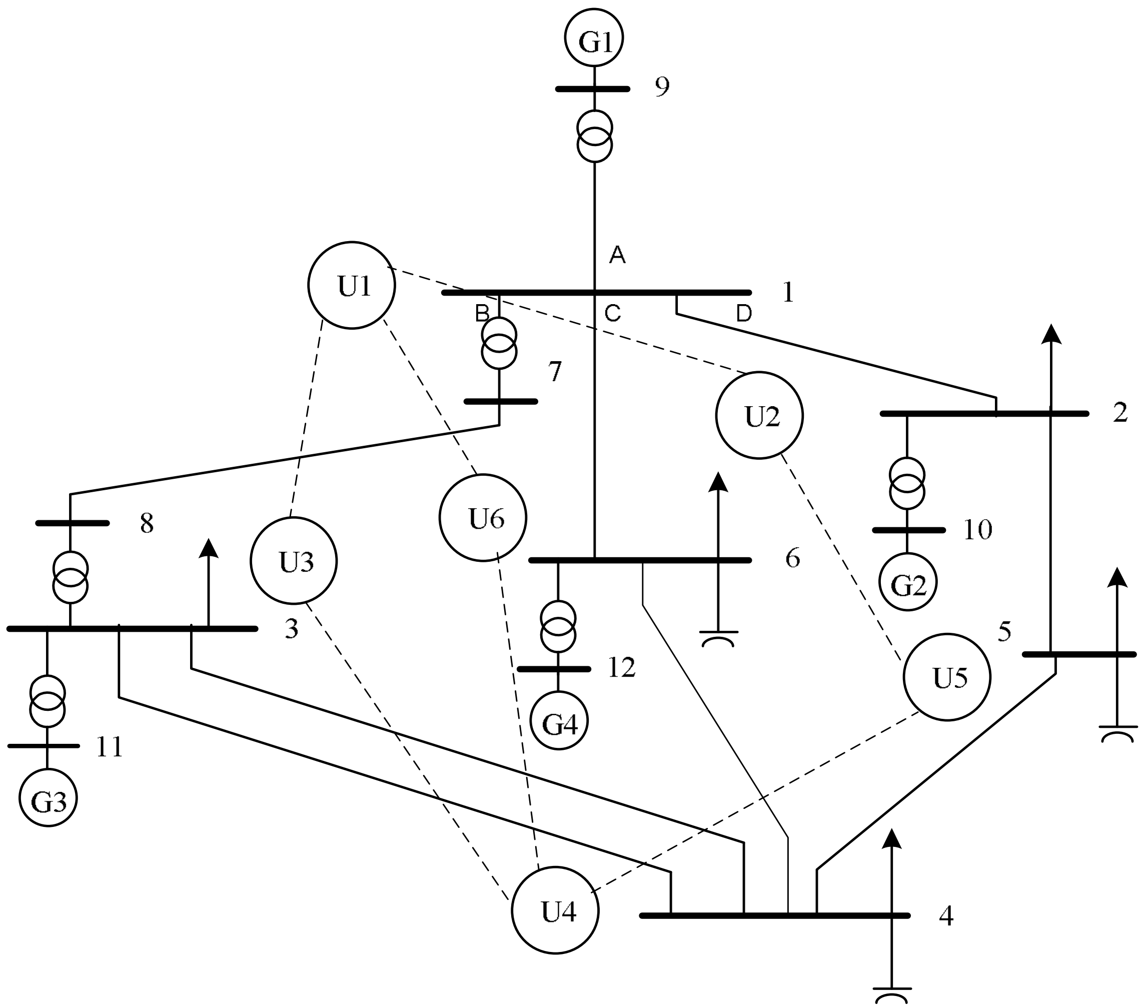

Figure 3-16 : Relay arrangement

Signal Processing Unit

The current signals were sampled at 20 kHz. The Clarke's transformation was applied to the three-phase currents and the three modal components were extracted. Then the wavelet coefficients of the modal currents were obtained using a custom module developed to perform the discrete wavelet transformation (DWT) [47]. In order to determine the fault direction, the wavelet coefficients of the modal current signals were compared with a reference wavelet. The cross correlation between the wavelet coefficient and the reference wavelet was used to determine whether two signals are had the same sign or not.

As a standard component to perform the cross-correlation is not available in the PSCAD/EMTDC master library, a custom model was developed to perform the identification of the sign of a wavelet coefficient with respect to a specified reference wavelet. This custom model is shown in Figure 3-17.

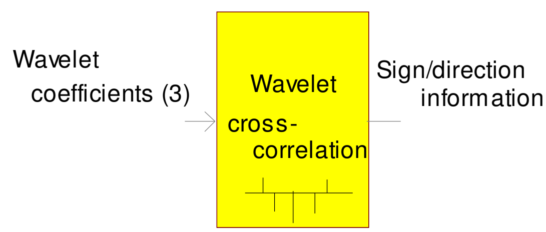

Figure 3-17 : Simulation model of the cross-correlation based wavelet sign detection unit

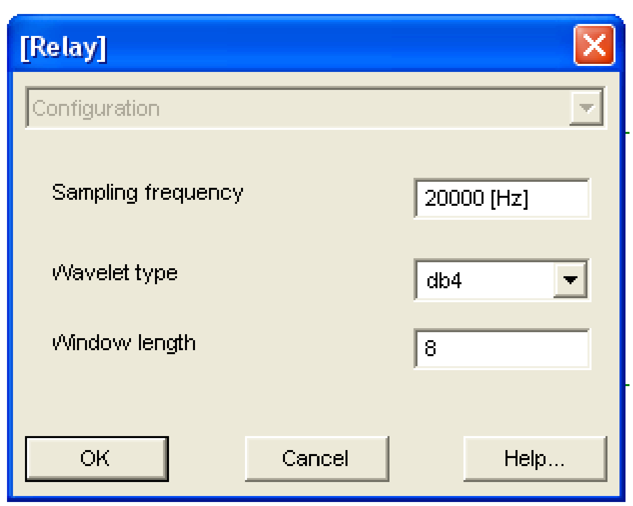

Figure 3-18: Input parameter window for the cross-correlation based wavelet sign detection

The input to the model is the wavelet coefficients of the three modal components of the current measured on a line segment connected to the relay. The output of the model is the sign of the wavelet coefficient ("1" for the positive and "0" for negative). The sign information is transmitted to the decision making unit to identify the direction of the fault.

Figure 3-18 shows the screen shot of the input parameter window for the cross-correlation based wavelet sign detection unit. The user can specify the sampling frequency, type of the mother wavelet and the length of the sampling window.

Decision Making Unit

The model of the DMU implemented in PSCAD/EMTDC is shown in Figure 3-19. The signs of the wavelet coefficients found by the directional units are the inputs to the model. The trip signals are the outputs of the model. The category and the direction of a fault are determined using the information received from the signal processing units. The information "0" or "1" is exchanged via the communication port as shown in Figure 3-19. This model allows the user to specify the number of line segments connected to the relay. Finally the trip signals are generated based on the information received by the model.

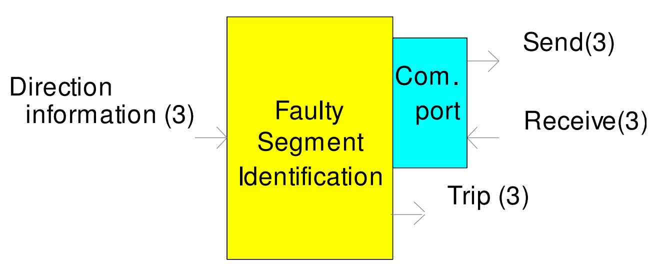

Figure 3-19: Simulation model developed to identify the faulty segment

.

3.5.2 Faulty Segment Identification

In order to investigate the performance of the proposed faulty segment identification models, faults were simulated at different locations in the network with different fault impedances. The signals we sampled at a frequency of 20 kHz. In these simulations, a communication delay of 4 ms was assumed between the relays.

Bus Fault Identification

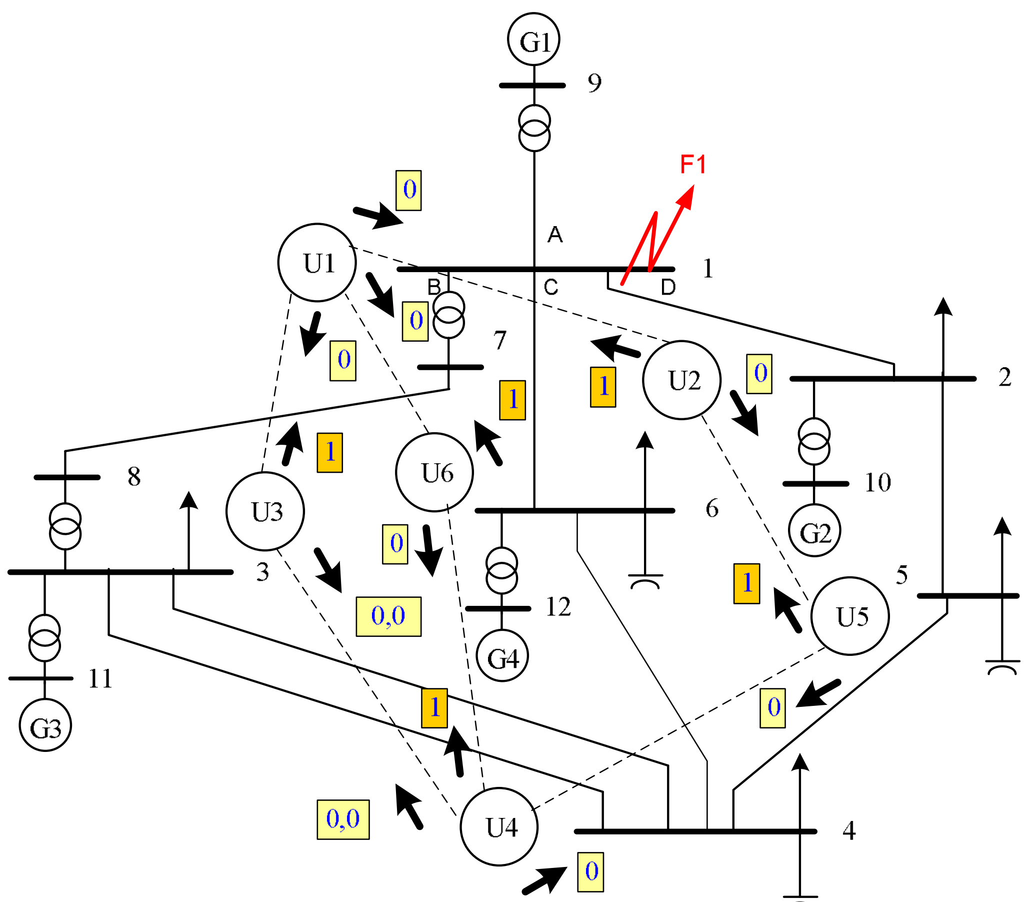

Figure 3-20: Fault directions identified for fault F1

In order to demonstrate the operation of the protection scheme during an internal fault, a three phase to ground fault (F1) was simulated on bus 1 as shown in Figure 3-20. The variation of three phase currents and the most significant Clarke components observed by all the signal processing units on bus-1 are shown in Figure 3-21.

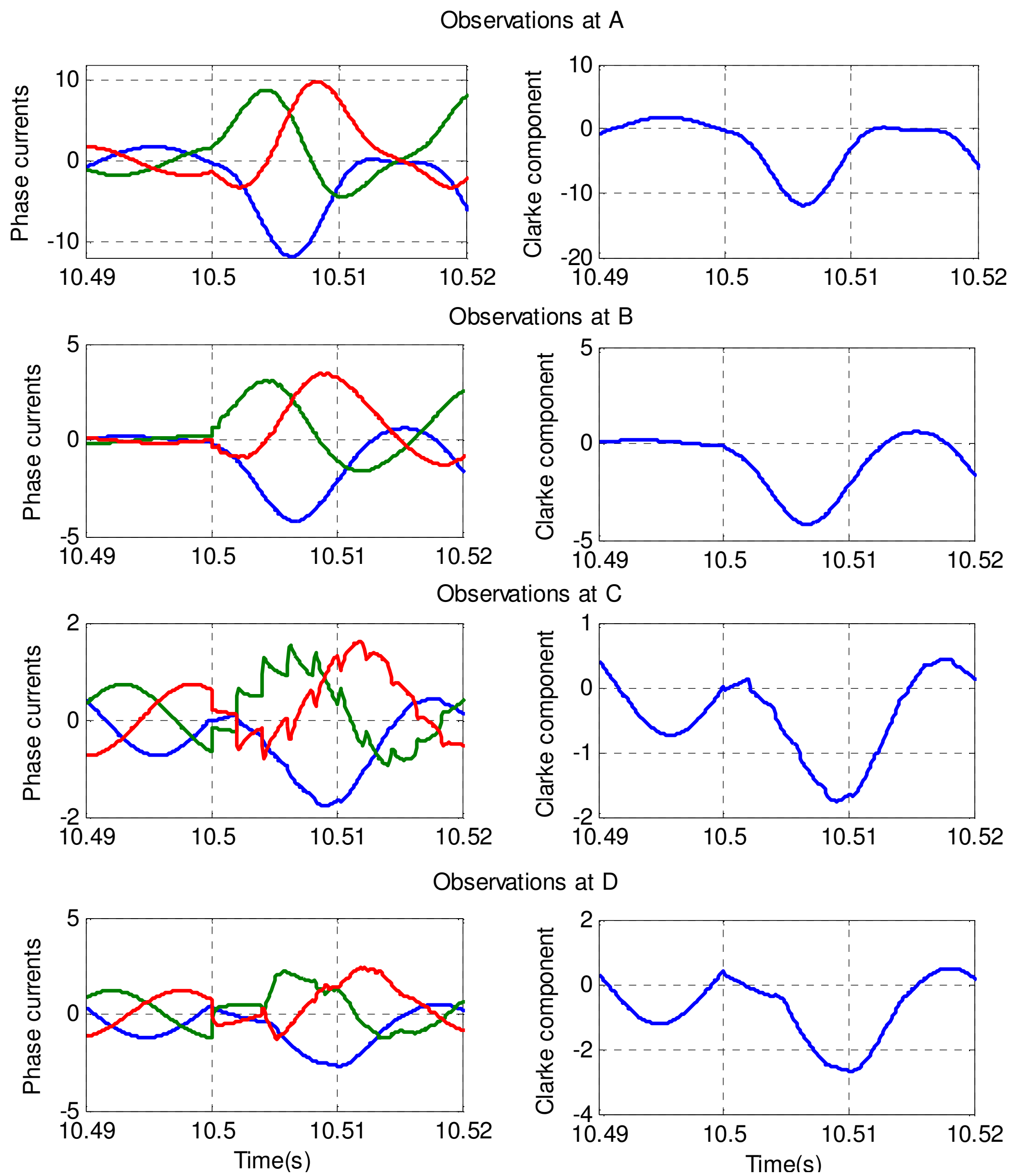

Figure 3-21: Three-phase current signals and most significant Clarke component during fault F1

The WTCs and the coefficients of cross-correlation corresponding to each measurement point are shown in Figure 3-22. As it can be clearly seen from Figure 3-22, the maximum values of all four coefficients of cross-correlation are of the same sign (i.e.

negative). Based on this information, the DMU U1 would correctly identify this situation as an internal fault. Similarly other units have identified this event as an external fault. The fault direction information determined by all six DMUs during this fault are shown in Figure 3-20. As this is an internal fault, the DMU U1 can locally make necessary actions to isolate the fault irrespective of the fault direction information received from the other neighboring DMUs.

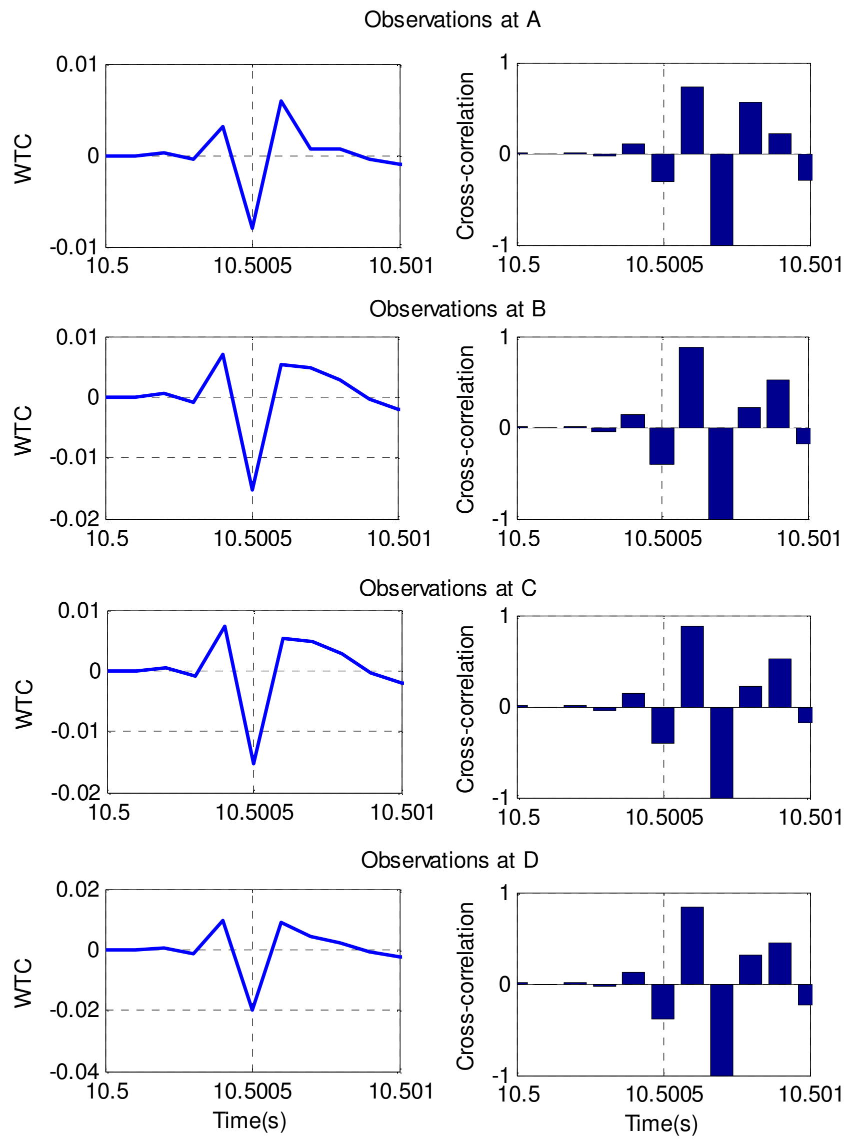

Figure 3-22: WTCs and coefficients of correlation for fault F1

The response of the DMU U1 is shown in Figure 3-23. As it can be seen from Figure 3-23 the DMU U1 was able to detect the fault within 3 ms. In this case, the decision is made independent of the fault direction information from other units and therefore the operation is not delayed due to the communication effects.

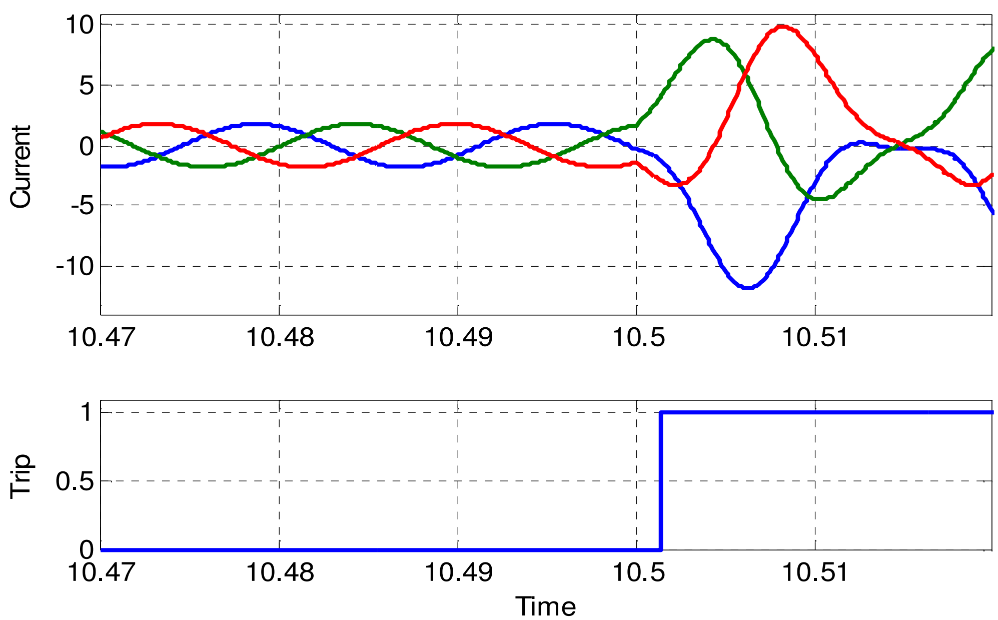

Figure 3-23: Time response of the protection scheme for fault F1

External Fault Identification

In order to demonstrate the operation of the proposed protection scheme during external faults, consider the line-to-line fault F2 simulated at the middle of the transmission line connecting buses 1 and 6 as shown in Figure 3-24. The WTCs and coefficients of cross-correlation observed by the devices simulated on bus 2 during this external fault are shown in Figure 3-25.

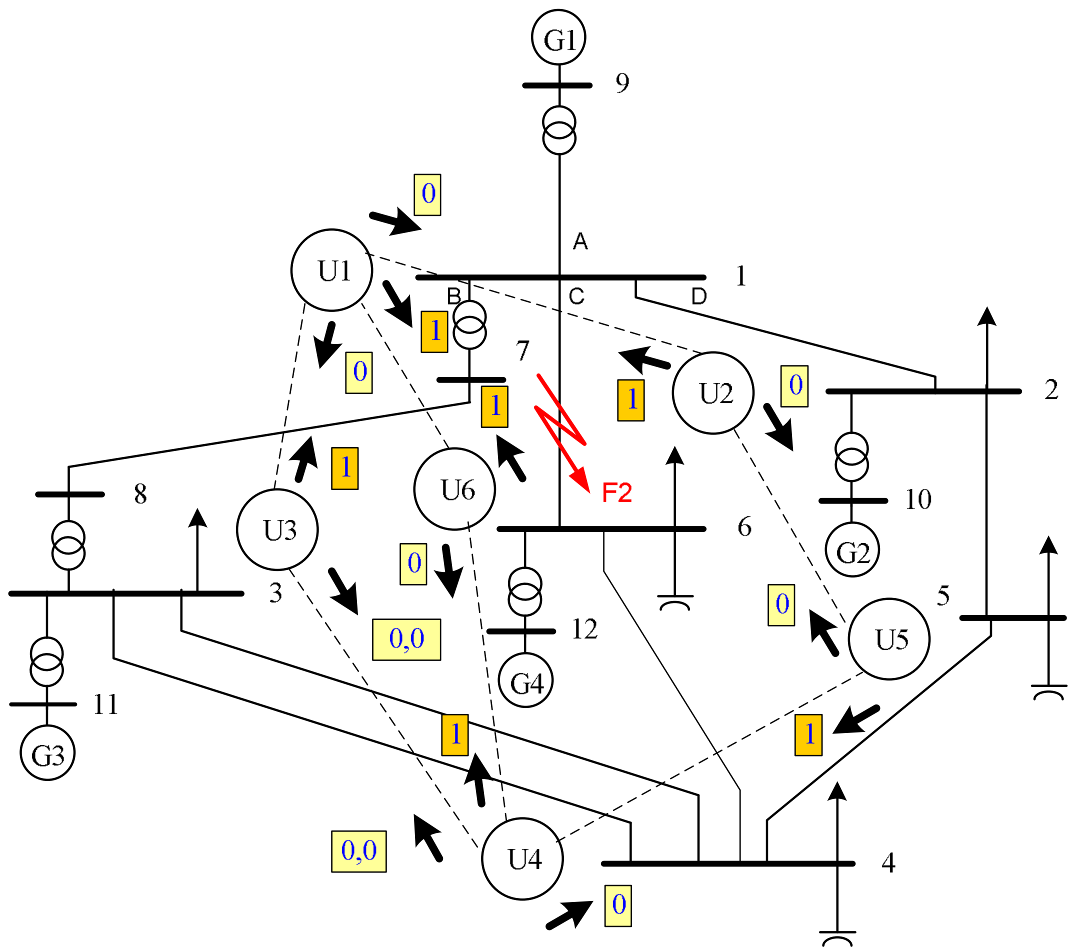

Figure 3-24: Fault directions identified for the fault F2

As it can be clearly seen from Figure 3-25 the maximum coefficient of cross-correlation observed at C has a sign opposite to the signs of the maximum cross-correlation coefficients observed at the other three measurement locations. Based on this information, U1 was able to categorize this fault as 'external' and the fault direction as U6. Similarly the other units have identified this fault as 'external'. The fault directions identified by each unit and fault direction information exchanged between each decision making units during this fault are shown in Figure 3-24. As it can be seen from Figure 3-24, the decision making unit U6 located on bus-6 has identified the fault direction as U1. Based on the fault direction information exchanged between each unit, the decision making units U1 and U6 can correctly identify the faulted line segment.

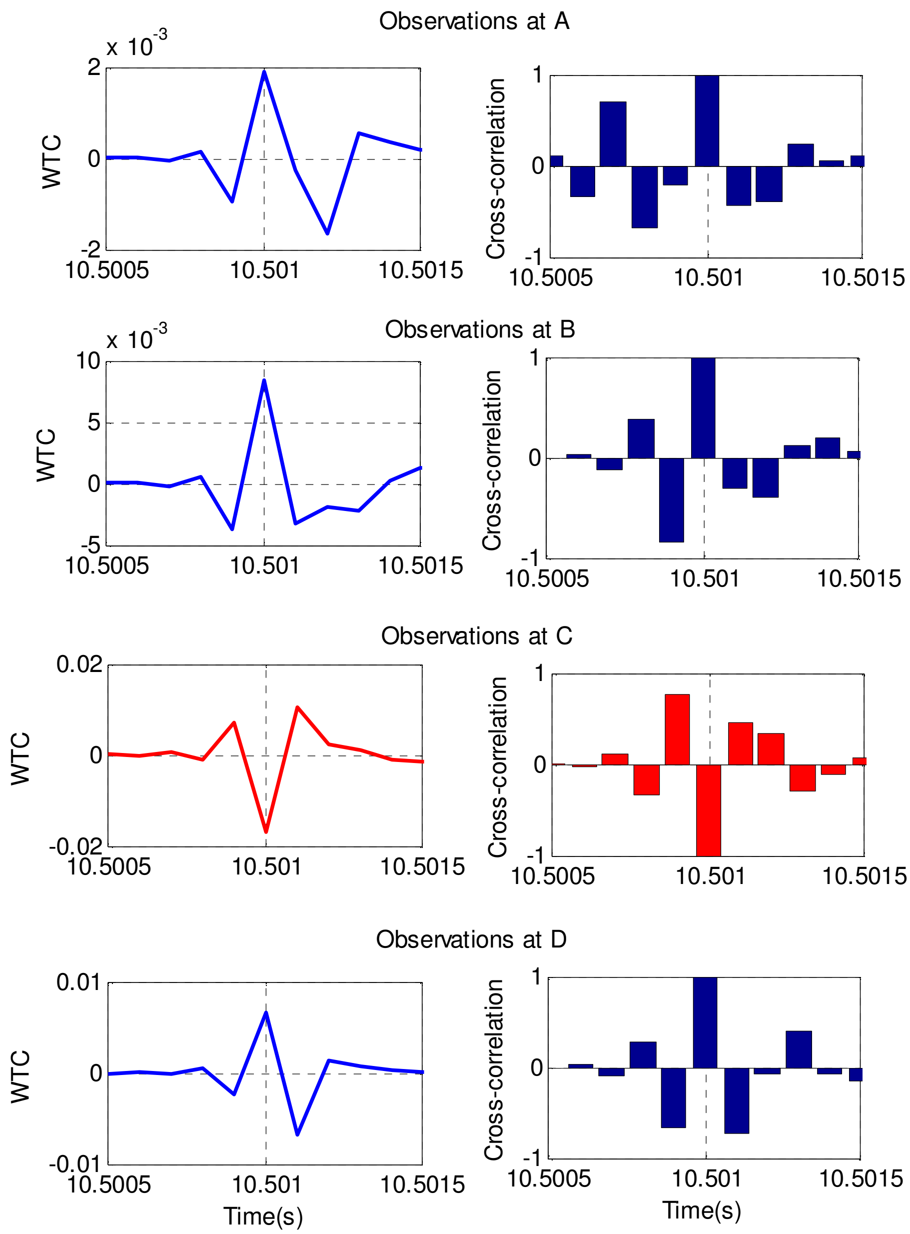

Figure 3-25: WTCs and coefficients of correlation for fault F2

External Fault on Double Circuit Line

Double circuit lines are commonly used in many practical transmission systems. Investigation of the applicability of the proposed protection scheme in such systems is essential.

In order to demonstrate the operation of the proposed protection scheme for faults on double circuit lines, consider the fault F3 shown in Figure 3-26. The WTCs and coefficients of correlations observed by the DMU U3 are shown in Figure 3-27. As it can be seen from Figure 3-27, the WTC observed on the faulted line is having an opposite sign to that of the others. Thus, the maximum coefficient of correlation observed on the faulted line is having opposite sign compared to the others. Based on this information, U3 was able to identify the fault direction correctly.

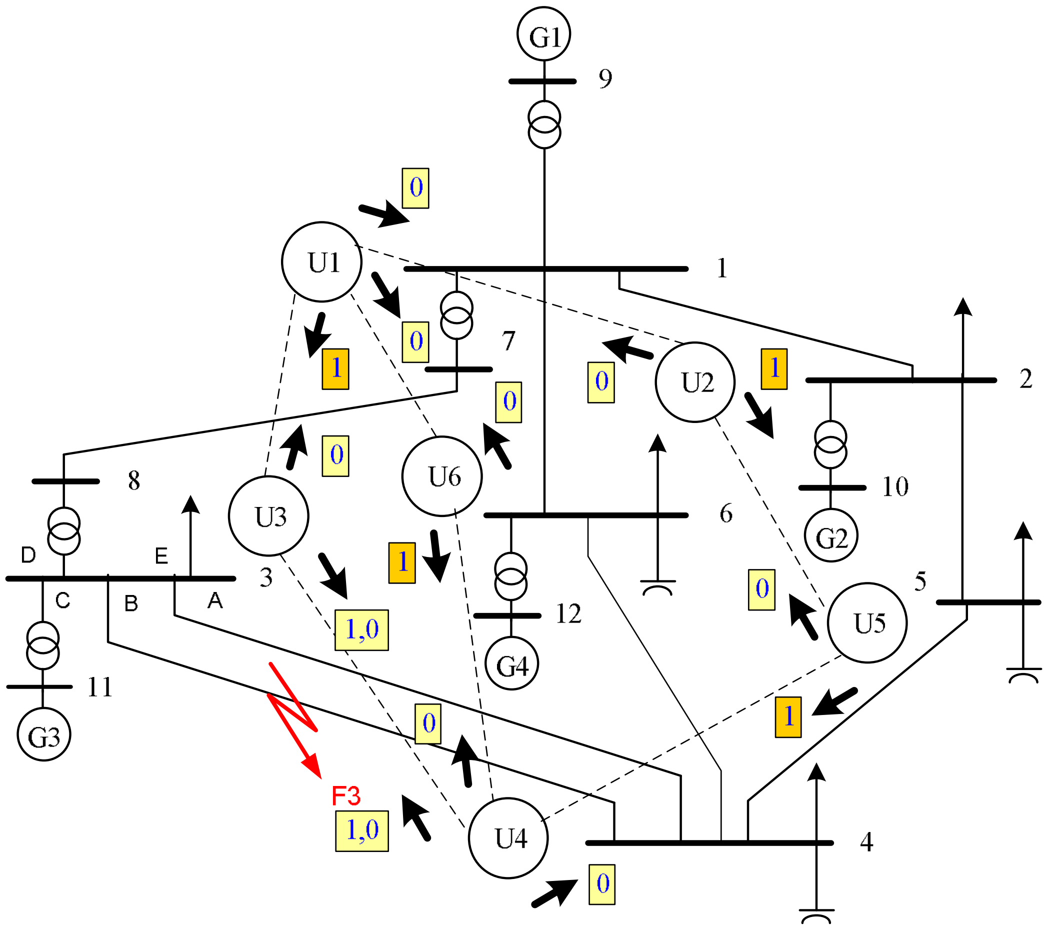

Figure 3-26: Fault directions identified for the fault F3

Similarly the DMU U4 was able to correctly identify the fault direction from the other side. This allows the protection scheme to correctly identify the faulted line. The fault direction information exchanged by all DMUs during this event is shown in Figure 3-26.

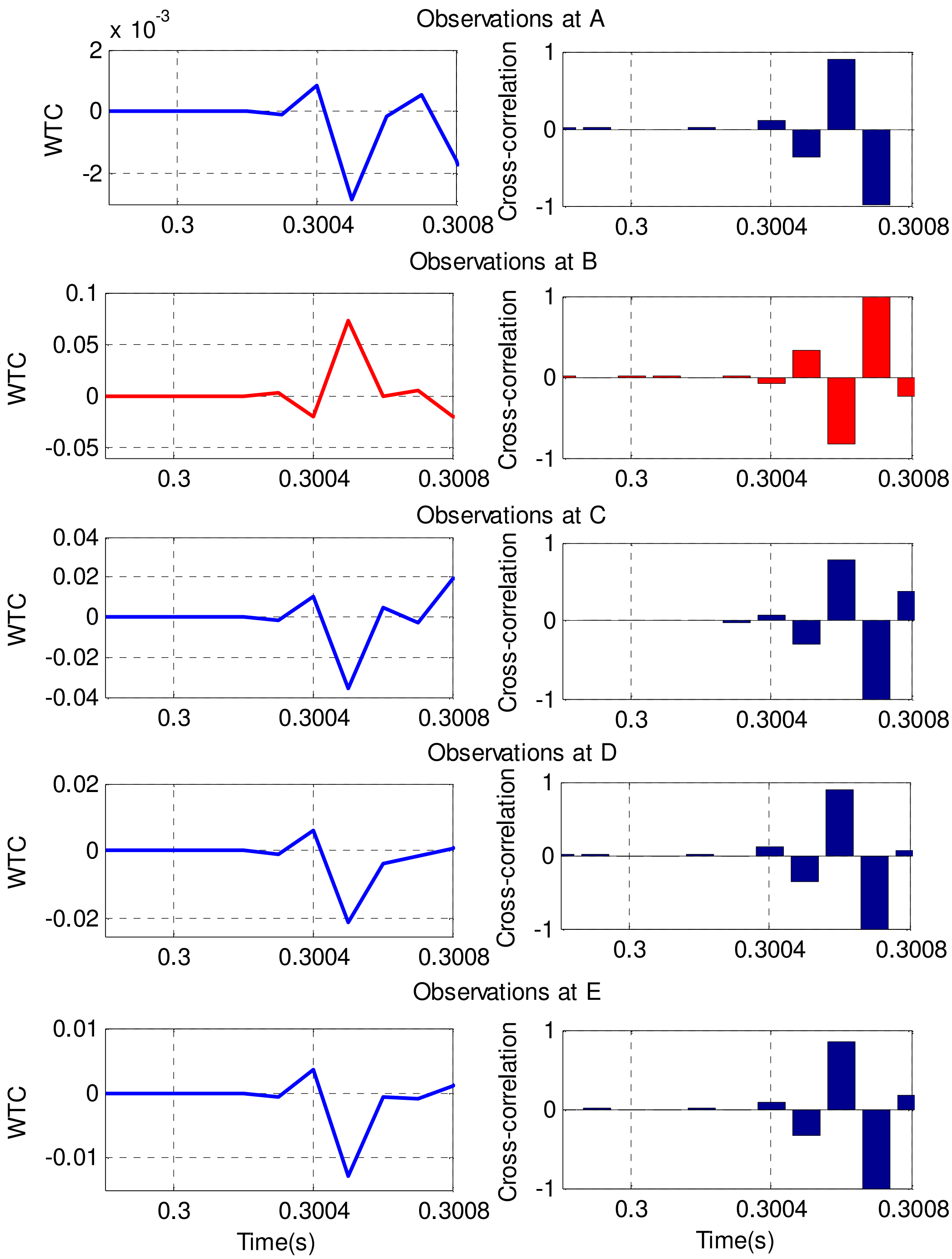

Figure 3-27: WTCs and coefficients of correlation observed by U3 during the fault F3

In order to further investigate the performance of the proposed protection scheme, simulations were repeated for different types of faults simulated at different locations of the network with different fault impedances, source impedances and fault inception angles. Table 3-I summarizes the fault categories and directions identified by the relays for some of the faults simulated in the network. In Table 3-I, R_f is the fault impendence. Entries in the table are the identified fault categories ("I" for internal and "E" for external), and the fault directions identified by each of the relays. For example, for fault F4, the entry corresponding to decision making unit U2 is "E(U1)". This means that U2 categorized the fault as an "external fault" in the direction of U1. The same fault is identified by U1 as an internal fault.

Table 3-I : Faulty Segment Identification Results

Fault	Loc. (bus)	Type	R_f (Ω)	U1	U2	U3	U4	U5	U6
F4	1	AC-G	0	I	E(U1)	E(U1)	E(U6)	E(U2)	E(U1)
F5	1-2	ABC-G	100	E(U2)	E(U1)	E(-)	E(U6)	E(U2)	E(-)
F6	2	A-G	10	E(U2)	I	E(U1)	E(-)	E(U1)	E(-)
F7	1-3	AB	0	E(U3)	E(U1)	E(U1)	E(-)	E(-)	E(-)
F8	6	BC	0	E(U6)	E(U1)	E(-)	E(-)	E(-)	I
F9	6(L)	BC	100	E(U6)	E(U1)	E(-)	EX(-)	E(-)	E(L)
F10	4	ABC-G	100	E(U3)	E(-)	E(-)	I	E(U4)	E(-)
F11	4-6	AB	10	E(-)	E(-)	E(-)	E(U6)	E(U4)	E(U4)

'I': internal, 'E': external, ' - ': no direction found

The results presented in Table 3-II show accurate faulty segment identification for all simulated cases. These studies revealed that the proposed approach can identify the faulty line segments correctly even for the high impedance faults irrespective of fault inception angle. The results obtained using the investigations carried out based on the previous method [17] were successfully achieved using the proposed new modular implementation.

3.5.3 Effect of Communication Delays

Since the proposed protection scheme requires the exchange of information between each decision making unit to make trip decisions in the case of external faults, communication delays affect the operating time. The simulations show that fault directions can be determined within 2 to 3 ms after the arrival of fault transient at the measurement point. Depending on the location of the fault and the length of the line, the fault generated travelling waves may take few milliseconds to reach the measuring points. Therefore, the units located at different busbars do not see the transient at the same time. Final trip decisions can be made only after receiving the information from the neighbouring DMUs. Thus the total detection time includes the propagation delay, signal processing time (approximately 2 to 3 ms) and the communication delay. In order to confirm this, investigations were carried out by measuring the trip time under different communication delays. Operation of U1 and U6 during the fault F2 shown in Figure 3-24 was considered for the study on the effects of communication delays. A fixed delay is added for communication between the two units in each simulation. The response times of U1 and U6 are summarized in Table 3-II.

The total response time given in Table 3-II is the time from the inception of a fault to the issuing of trip signals. Thus, apart from the communication delay, the total response time also includes transient propagation delays and the time involved with signal processing. The length of the transmission line used in this study was 300 km long and the fault is located 150 km from bus-1. It takes approximately 0.5 ms for the current transient to propagate to bus-1, and 0.5 ms for the transients to reach bus-6. The signal processing time involved with fault direction identification is approximately 3 ms. As it can be seen from the results, the total response time of the protection scheme varies proportionately with the communication delay.

Table 3-II : Effect of Communication Delays

Communication Delay(ms)	**Total response time (ms)** **propagation time + processing time + communication delay**	
	DMU - U1	DMU - U6
4	8	8
6	10	11
8	12	12
10	13	14
20	24	23

3.5.4 Speed Comparison with Conventional Distance Protection

In this section, the speed of the proposed protection scheme is compared with that of a distance protection scheme. The conventional standard distance protection scheme does not require communication, but trip decisions can be accelerated with the assistance of telecommunication using a transfer tripping arrangement. Since the proposed protection scheme is also using communication facilities similar to those used in transfer tripping schemes for reaching trip decisions, speed comparison will be more fair if compared with communication aided high speed distance protection schemes. In this thesis, a distance protection scheme with covenantal permissive over-reach transfer trip (POTT) arrangement was used [41]. The arrangement of the distance relay in the conventional POTT scheme used in this study is shown in Figure 3-28. The distance relays were simulated with mho characteristics. The directional elements of the relays were also simulated. The trip logic of the POTT scheme is given in Figure 3-29. Communication delays between the relays were assumed as 4ms.

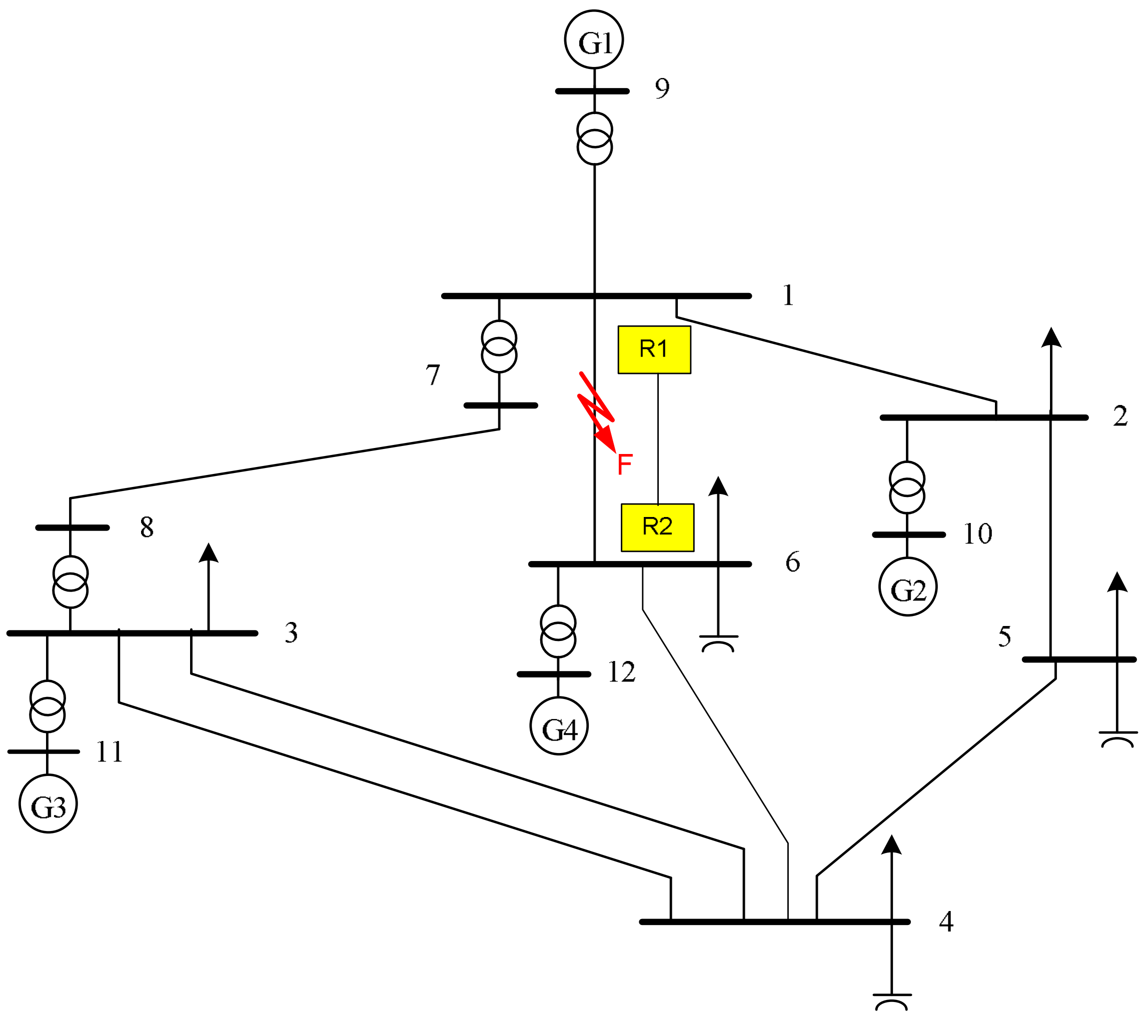

Figure 3-28: Communication aided distance protection scheme

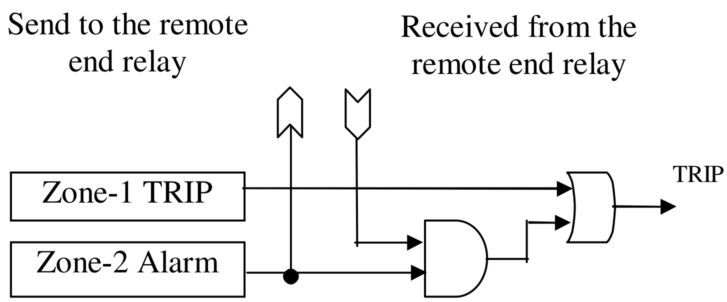

Figure 3-29: Trip logic for POTT Scheme

Table 3-III : Comparison with Conventional Distance Protection

Fault type	Distance % from R1	Inception angle (deg)	Operation			
			Proposed Method (4ms com. Delay)		Conventional Distance with POTT (4ms com. Delay)	
			TRIP	Response Time (ms)	TRIP	Response Time (ms)
AG	10	0	Yes	7	Yes	12
BC	10	90	Yes	8	Yes	10
ABC	10	180	Yes	7	Yes	9
BCG	10	270	Yes	7	Yes	10
ABCG	10	0	Yes	7	Yes	9
AG	50	180	Yes	7	Yes	14
BC	50	270	Yes	8	Yes	12
ABC	50	0	Yes	8	Yes	12
BCG	50	90	Yes	7	Yes	13
ABCG	50	180	Yes	7	Yes	12
AG	75	270	Yes	7	Yes	17
BC	75	0	Yes	7	Yes	15
ABC	75	90	Yes	7	Yes	14
BCG	75	180	Yes	8	Yes	14
ABCG	75	270	Yes	8	Yes	14
AG	90	0	Yes	7	Yes	17
BC	90	90	Yes	7	Yes	15.0
ABC	90	180	Yes	6	Yes	12
BCG	90	270	Yes	6	Yes	15
ABCG	90	0	Yes	6	Yes	12

In order to evaluate the speed of the operation, different types of faults (LG, LL, LLG, LLL, etc.) were simulated at different distances on the line. Response times corresponding to both protection schemes (for the relays associated with bus-1) were determined and presented in Table 3-III. As it can be seen from these results, the proposed transient based protection scheme is capable of identifying the faults faster than the distance protection scheme. The response time of the conventional protection scheme depends on the location of the fault where as the response time of the proposed transient based protection scheme is more or less unaffected by the location of the fault.

3.5.5 Effect of Series Capacitors

In transmission systems, series capacitors are used to increase the power transfer capability of the system by reducing the effective series impedance of the line. Although they are being widely used, providing an adequate protection using conventional distance relays is problematic due to the interaction of the series capacitors. Inclusion of series capacitors may sometimes lead to invert the voltage or current phasors, which will eventually result in malfunction of the distance relays protecting the line. On the other hand, behaviour of the devices used to protect the capacitors such as Metal Oxide Varistors (MOVs), bypassing switches, etc. is highly unpredictable and this may also lead to under-reach and over-reach problems in the distance element. In order to overcome these problems, several methods have been proposed for distance relays [41]. These methods include the use of various compensation methods for directional and impedance functions. The main shortcoming of these methods is the requirement of complicated settings depending on the network configuration, location of PTs/CVTs, amount of series compensation, etc.. Thus it would be very beneficial if the proposed transient based protection scheme would provide a reliable protection to series compensated lines without additional complexities. This possibility is investigated in this section through detailed simulations.

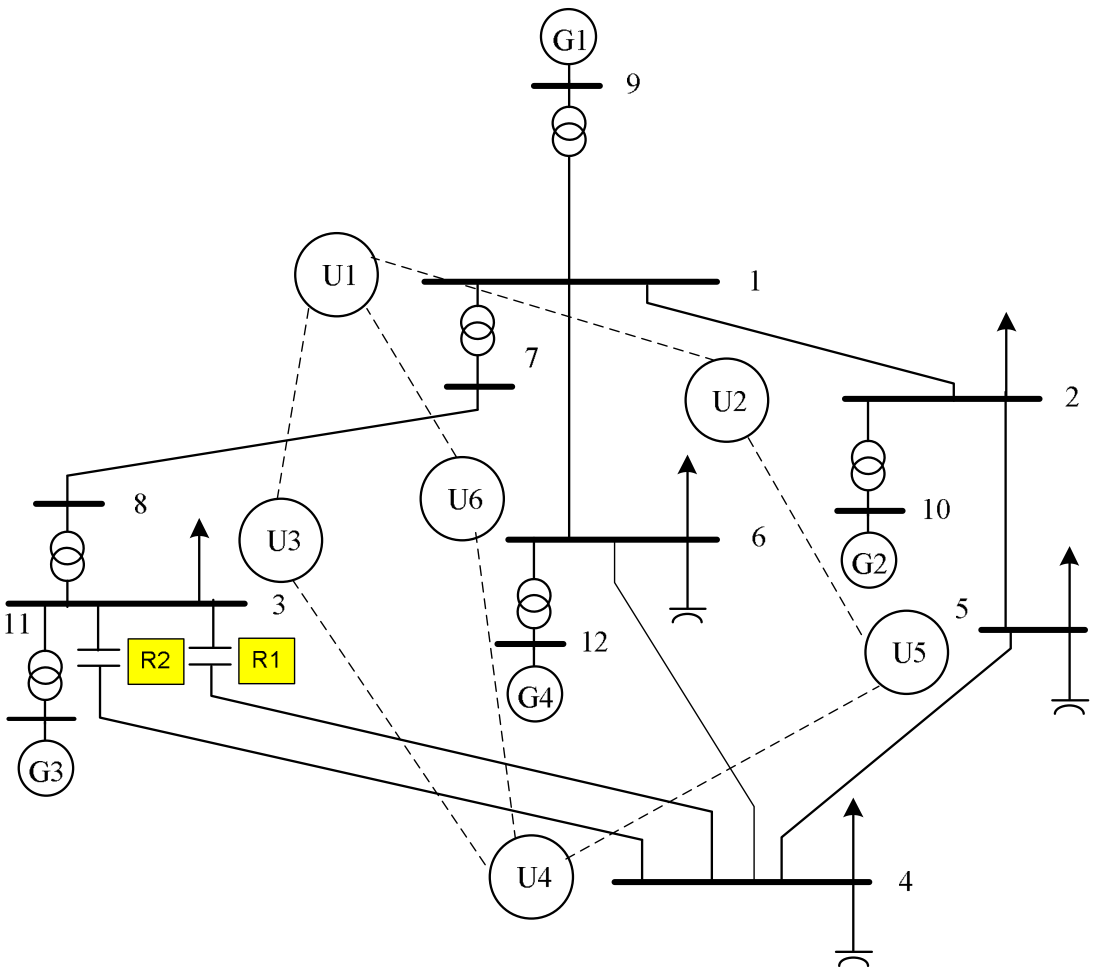

Figure 3-30: Series capacitor simulated on double circuit transmission line

In order to evaluate the performance of the proposed transient directional protection scheme for series compensated transmission lines, the test power system was modified to include series capacitors on the double circuit transmission line connecting buses 3 and 4 as shown in Figure 3-30. Performance of the proposed protection schemes was evaluated under different fault scenarios in which the conventional protection scheme fails. Results obtained in this simulation are summarized below.

Performance during Voltage Inversion

A significant change in the voltage phase angles during a fault, caused by the series capacitor, is referred to as voltage inversion. This may sometimes affect the performances of conventional distance relays. A distance relay protecting one line of the double circuit transmission system would malfunction during a reverse fault on the other line.

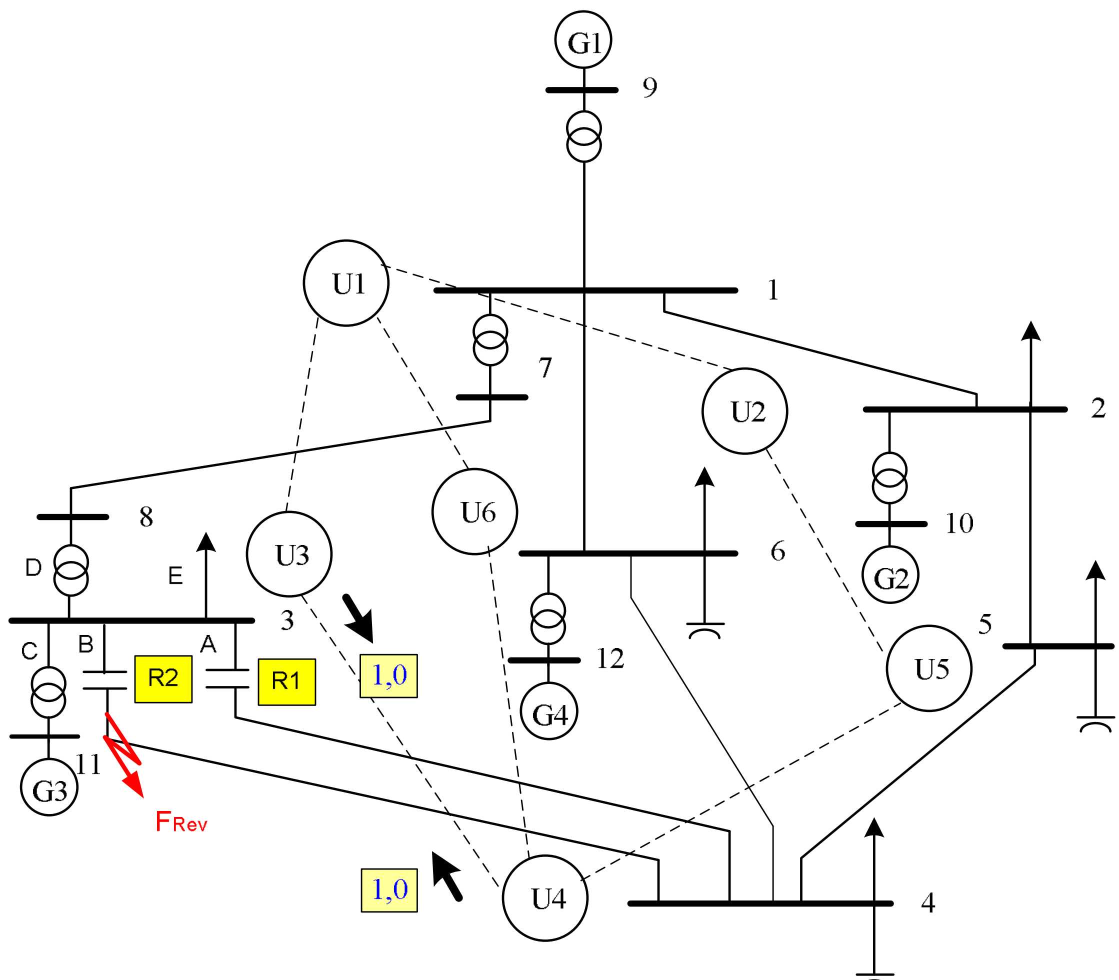

Figure 3-31: Fault directions identified for the reverse fault

In order to demonstrate the operation of proposed protection scheme during voltage inversions, consider a solid three phase fault (F $_{Rev}$) simulated on circuit-2 of the double circuit line shown in Figure 3-31. The variations of impedances observed by the phase units of the conventional distance relay on the non-faulted circuit are shown in Figure 3-32. Although the fault is not on the protected line, the measured impedances are traverse through the Zone-1 of the relay. The wavelet coefficients observed by the DMU U3 during this fault are shown in Figure 3-33. As it can be seen from Figure 3-33, the wavelet coefficient on the faulted line is having an opposite polarity compared to those of the others. Similarly DMU U4 was able to identify the fault direction correctly. Exchange of correct of direction information allows the protection scheme to identify the faulted line. Simulations were repeated for other types of reverse faults and results confirmed that the proposed the transient based protection scheme correctly determines the faulted segment regardless of the presence of the series capacitor.

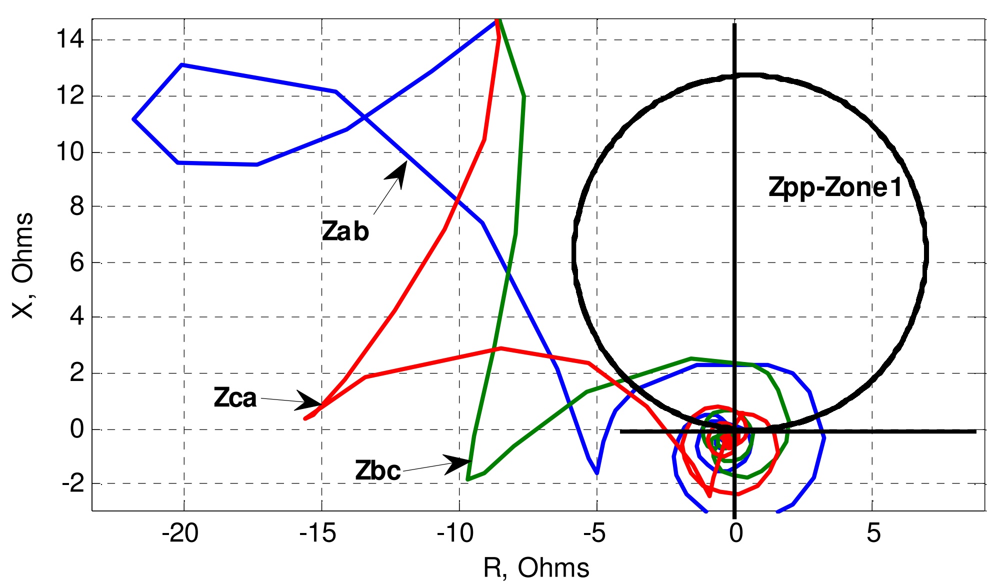

Figure 3-32: Operation of the impedance element (phase) of R2 during the reverse fault

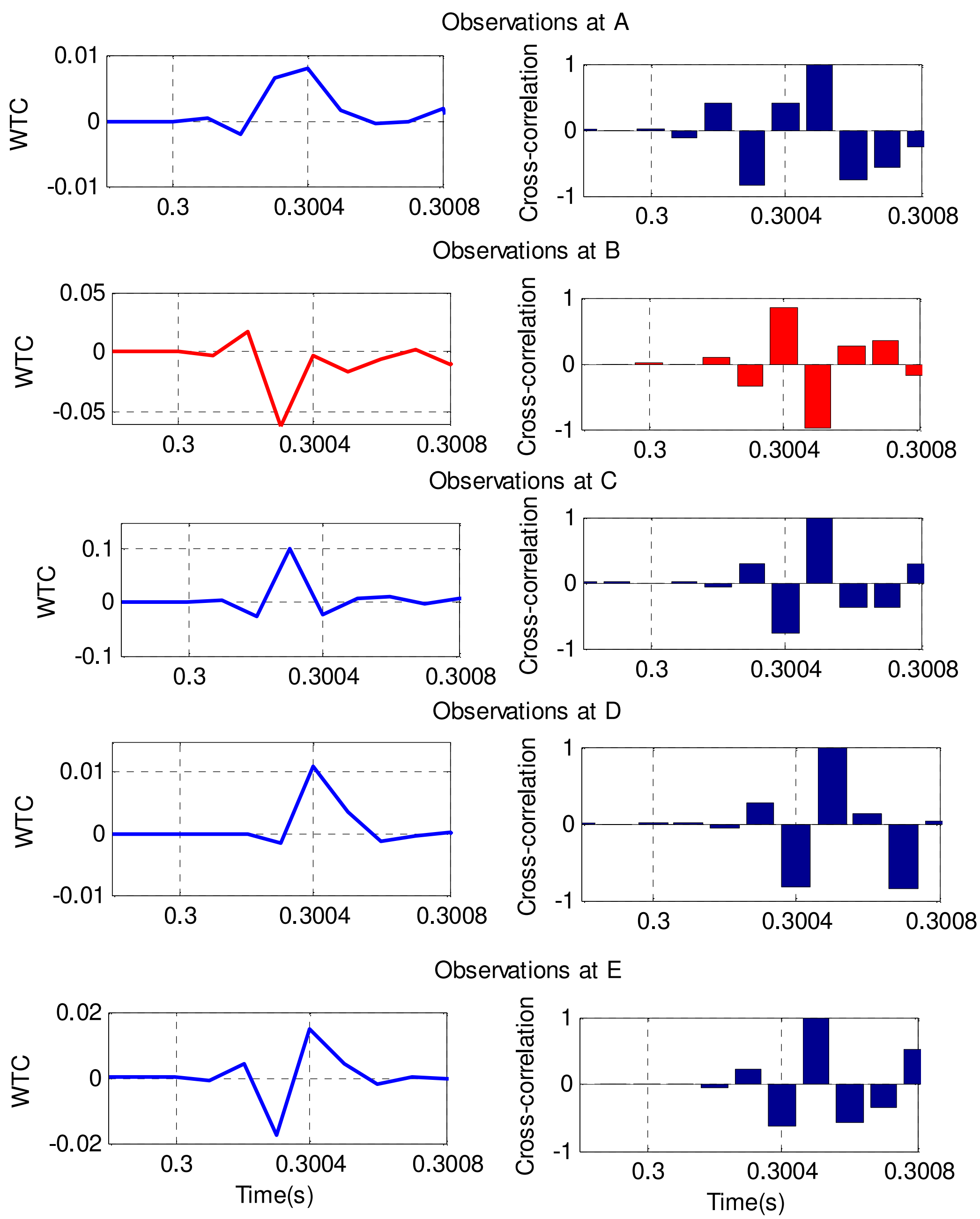

Figure 3-33: WTCs and coefficients of correlation observed by U3 during the reverse fault

Performance during Current Inversion

Current inversion is another common phenomenon that occurs during the faults on series compensated lines, if one side of the line system is capacitive while the other side is inductive. This condition may affect the performance of distance and directional functions.

Current inversion can occur during a close-in high impedance (R_f=25 Ω) fault on the protected line, such as F_{Fwd} shown in Figure 3-34.

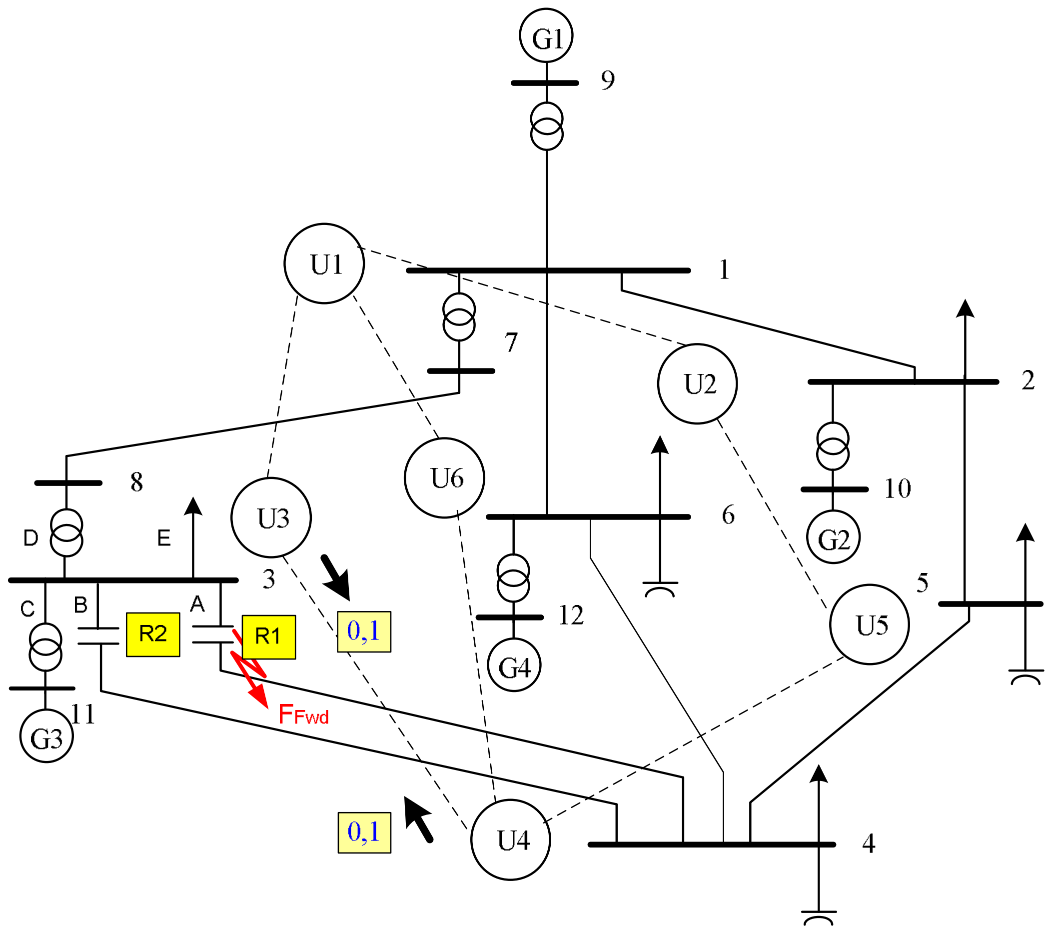

Figure 3-34: Fault directions identified for the fault F_{Fwd}

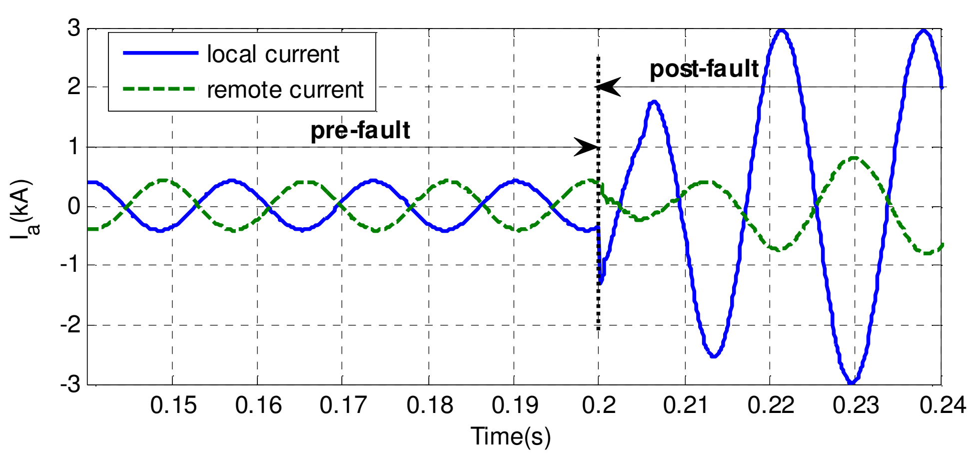

Figure 3-35: Variation of phase-A current observed at both ends during phase A-G high impedance forward fault

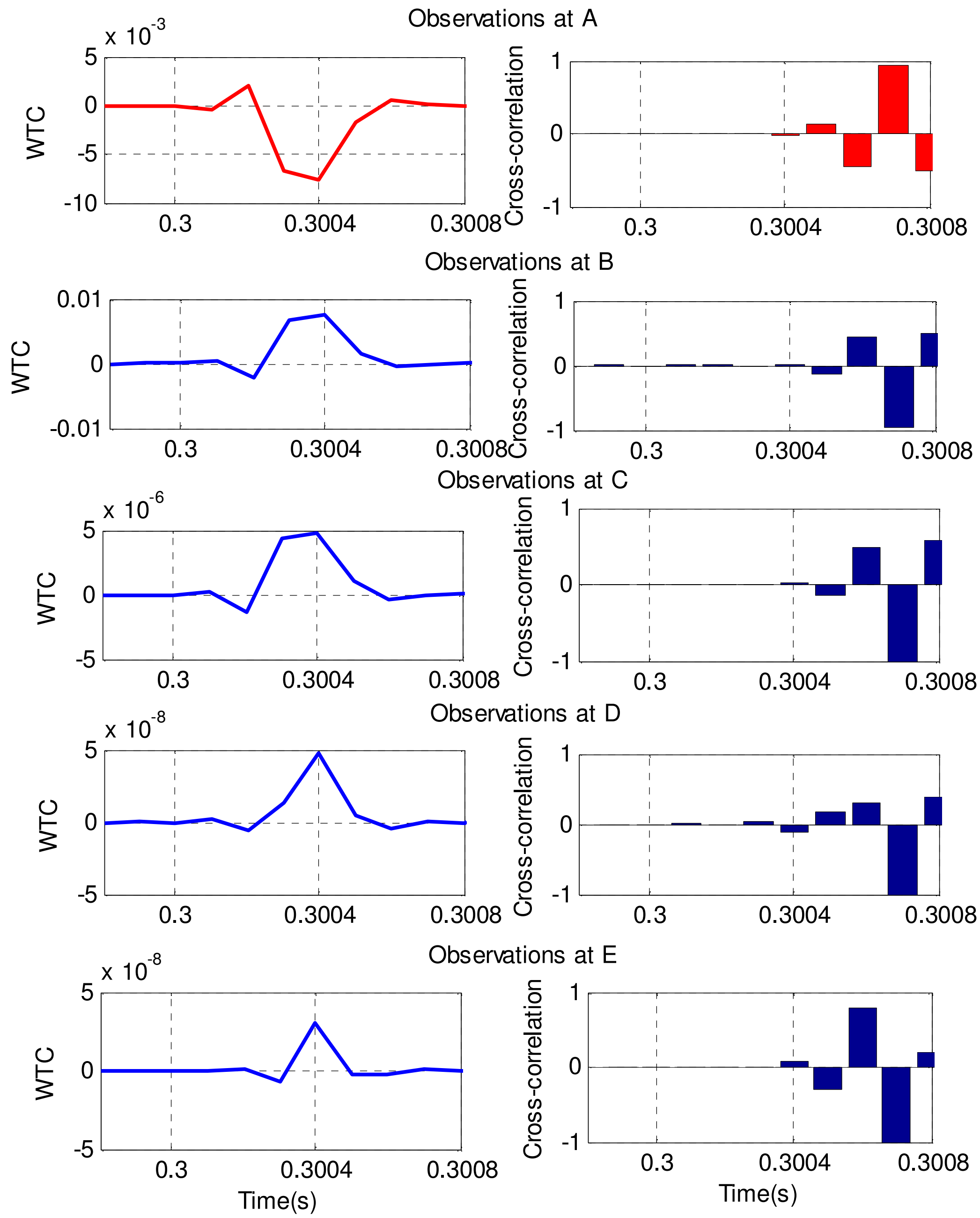

Figure 3-36: WTCs and coefficients of correlation observed by U3 during the forward high impedance fault

The variation of phase-A current observed at both ends during a phase A-G fault is shown in Figure 3-35. As it can be seen from Figure 3-35, the phase difference between the currents observed at two ends reverses after the fault F_{Fwd}. Due to this current inversion, the voltage measurement would also be reversed resulting in malfunction of the directional elements.

However, the operation of the proposed protection method is independent of current inversion. Figure 3-36 shows the wavelet coefficients observed by the DMUs U3 and U4 during this fault. As it can be seen from Figure 3-36, the wavelet coefficient on the faulted line has an opposite polarity when compared to those of the others, enabling correct fault direction identification at both U3 and U4.

3.5.6 Effect of Sampling Frequency

Based on the simulation results presented above, the use of a 20 kHz sampling rate enables correct identification of fault directions within 2 to 3 ms after the arrival of the transients. In order to investigate the effect of sampling rates on the performance of fault detection speed, some of the above simulations were repeated for 10 kHz sampling rate. The results obtained in this study showed correct faulty segment identification, but the fault directions identification time was extended to 5 to 6 ms range.

3.6 Backup Protection

Operation of the proposed scheme relies on the fault direction information exchanged between decision making units. Any failure in communication would make it impossible to determine the faulted segment. Although modern dedicated communication schemes are highly reliable, some form of defence against possible communication failure is required. The proposed protection scheme can be integrated with the conventional distance protection scheme to develop a hybrid protection scheme. Such a hybrid scheme can provide fast and secure protection against closed-in fault with the conventional distance protection while using the proposed method for remote end faults. In case of a communication breakdown, backup protection will also be provided with distance protection.

3.7 Chapter Summary

A faulty segment identification method using wavelet coefficients of the current transients was proposed for transmission systems. This requires one directional unit per branch and one decision making unit per busbar. This implementation structure is capable of exploiting the communication capabilities of new IEC 61850 protocol. The communication resources required are minimal as only a few logical signals are transmitted in the event of a fault, and the communication is required only between the adjacent relay agents. The decision making process is distributed and there is no central computer receiving all the fault direction information. Investigations were carried out using a high voltage transmission system simulated in PSCAD/EMTDC simulation program. The on-line models required to simulate the protection system was developed. Operation of the protection scheme was investigated for different types of faults simulated at different locations of the transmission system. A performance of the proposed protection scheme for series compensated transmission lines was also investigated. Results obtained in this study showed the capability of implementing a fast faulty segment identification methodology using the proposed transient based protection approach. Implementation and testing of a hardware prototype of the proposed protection scheme will be presented in the next chapter.

Chapter 4

Prototype Implementation

4.1 Introduction

This chapter investigates the development of a prototype of the proposed protection scheme. Prototyping and testing is an important step in the verification process of the protection concept. Successful testing of a hardware prototype will provide confidence for the next level of verification, which is the field testing of the protection scheme. Although the protection concept was proven through simulations, there were numerous challenges to overcome in the real-time implementation such as algorithm optimization for real-time calculations, reducing the computational time and maintaining high calculation accuracy.

The proposed protection scheme requires one decision making unit per each bus and several signal processing units per line (branch). Therefore, the implementation of the complete scheme requires several signal processing units. Although this arrangement is feasible for an actual system, implementation of a system in laboratory environment requires significant resources. In order to overcome this problem, three phase current signals recorded on all the branches during a disturbance were fed into the same signal processing unit and the responses of the unit were then combined to determine a fault direction corresponding to each bus.

The proposed relay algorithms require high frequency sampling and high calculation accuracy, especially in the wavelet analysis of high frequency transients. A high speed floating point digital signal processor (DSP) development board was selected for this implementation. The implementation details and the results obtained using the prototype are presented in the following sub-sections.

4.2 Design Considerations

4.2.1 Requirement of Higher Sampling Frequency

The proposed relay algorithm requires simultaneous sampling of three phase current signals at 20 kHz. The requirement of a multi-channel, high frequency sampling rate is one of the main requirements in this implementation.

4.2.2 Calculation Accuracy

The techniques proposed in this algorithm use wavelet transform and correlation calculations to identify the fault directions. These mathematical methods involve floating point calculations which require high computational power. The development of a hardware platform that is capable of handling floating point calculations at a high sampling rate is one of the key requirements.

4.2.3 Minimize the Noise

Noise can significantly affect the performance of hardware devices that process high frequency signals at a high rate. The noise can sometimes be generated internally in the hardware components or from external interferences. In a prototype it is essential to reduce the occurrence of noise from both these sources.

4.3 Development of Hardware Platform

The Texas Instruments (TI) TMS320C6713 floating-point DSP development system was selected for the hardware platform. This is one of the powerful floating point platforms commonly used in implementing complex algorithms in real time. The floating point DSPs are specifically designed to do floating point processing. Recent literature has reported several successful protection algorithms implemented using floating point DSPs [3], [48].

The key features of the TMS320C6713 DSP platform are [49]:

- 225 MHz processor
- 16 Mbytes of synchronous DRAM
- 512 Kbytes of Flash memory
- Standard expansion connectors for daughter card use
- JTAG emulation through on-board JTAG emulator with USB host interface or external interface
- Supported by the Code Composer Studio development environment

The functional block diagram of the TMSC6713 DSP is given in the Appendix-III

4.3.1 Hardware Assembly

Figure 4-1 shows the block diagram of the hardware prototype that includes amplifiers, low pass filters, Analog to Digital Converter (ADC), digital signal processor, etc.. A photograph of the laboratory prototype implementation is shown in Figure 4-2.

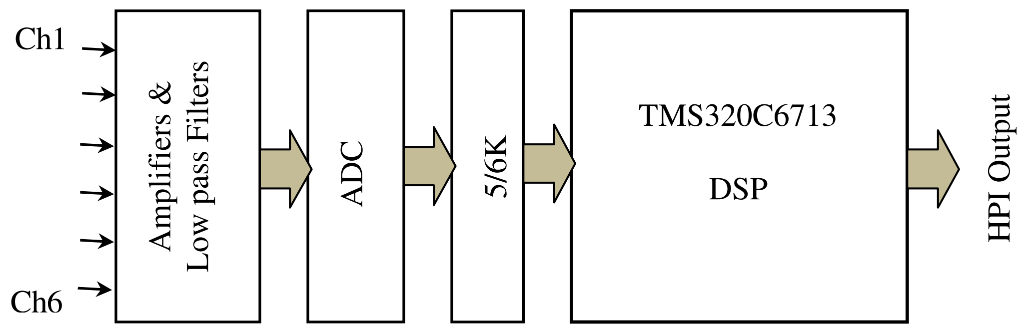

Figure 4-1: Block diagram of hardware platform

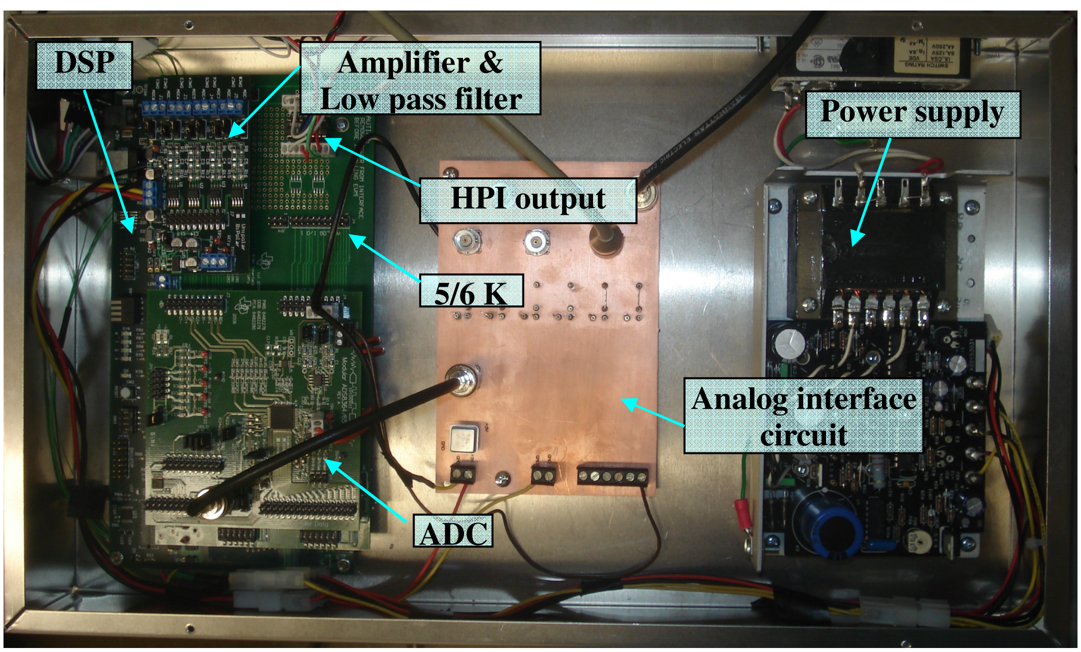

Figure 4-2: Laboratory prototype

4.3.2 ADS8364 EVM ADC

The TI six-channel ADC module, ADS8364 EVM was used to digitize the analog input signals. The main features of the ADS8364 ADC are [50]:

- 16 bit, six channels, simultaneous sampling
- Analog inputs can be configured as single-ended or differential
- Modular design allows direct connection to the selected DSP platforms through the 5/6K Interface Boards
- Built-in reference
- High-speed parallel interface

4.3.3 5/6K Interfacing Board

The TI 5/6K interfacing board maintains a compatible interface with the selected DSP family [51]. It includes two signal conditioning sites, two serial interfacing sites, and a parallel interfacing site. In this implementation, a direct interface was provided between the DSP and the ADC through the parallel interfacing site of the 5/6K interfacing board. The dc power required for the ADC was also obtained through the standard power connector of the interface board. A schematic diagram of the 5/6K interfacing board is given in the Appendix III.

4.3.4 Analog Amplification Circuit

The TI signal conditioning unit [52] is a standard amplification device compatible with TI data converters. The signal conditioning unit scales the measurements from ±10 V to the required range of 0-4.5 V for the ADC. The channel configuration of the signal conditioning unit is given in the Appendix III. The unit includes four such channels.

4.3.5 Analog Filtering

The input to any data sampling system requires an anti-aliasing filter to band-limit the sampled signal to prevent aliasing of measurements. Simple low-pass R-C analog filters were used for this purpose. The low-pass filters were integrated into the analog amplification circuits.

4.3.6 Power Supply

A linear power supply was selected instead of a non-linear power supply to reduce the noise generated from the power supply. The specifications of the power supply are given in the Appendix III.

4.3.7 Digital Outputs

The DSP contains a Host Post Interface (HPI) port that can be configured as either digital inputs or digital outputs. In this implementation, digital outputs were used. More detailed information about the HPI port and its operation can be found in [53].

4.4 Development of System Software

The TI Code Composer Studio (CCS) [54] provides an integrated development environment for real-time signal processing. The CCS was used to develop the prototype system's software. The CCS software allows for development with the C programming language and includes a C compiler, an assembler, and a linker. The CCS software provides the infrastructure and hardware abstraction for the application software development. Figure 4-3 shows the structure of the system software implemented using the CCS that links with the application software and hardware resources. The system software is capable of managing hardware resources and processing resources. The hardware resources that must be managed by the system software include the peripherals such as DRAM, on-chip memory, Host Port Interface (HPI), ADC, etc.. The main processing resource that must be managed is the DSP. The DSP includes the user defined computational functions that are implemented using standard mathematical libraries specific to the processor. The real time operating system (RTOS) and memory manager are the main components of the system software layer responsible for performing various tasks required for the software application. The RTOS is responsible for managing and arbitrating the real-time aspects of the application whereas the memory manager is responsible for allocating, freeing, and protecting code and memory.

The system scheduler is one of the key elements in the RTOS, which is responsible for coordinating and controlling various real time tasks according to their priorities. In this implementation, the system scheduler was developed in a way that the users can assign their own priorities to ADC, HPI and user defined computational modules according to the application requirements as shown in Figure 4-4. In addition to that, users can select different sampling rates for the ADC.

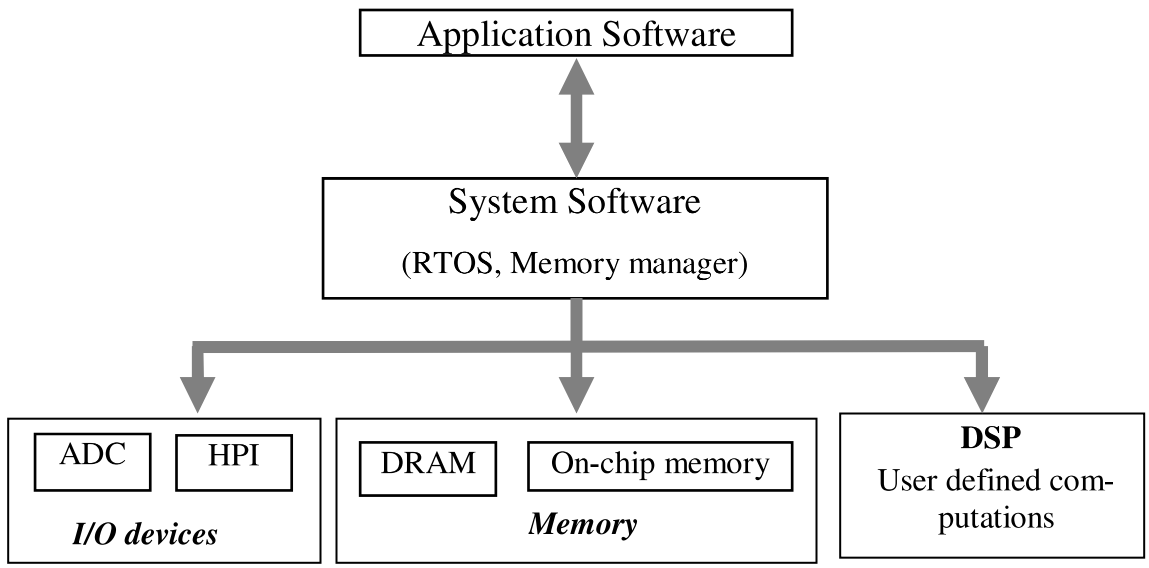

Figure 4-3: System Software Layer

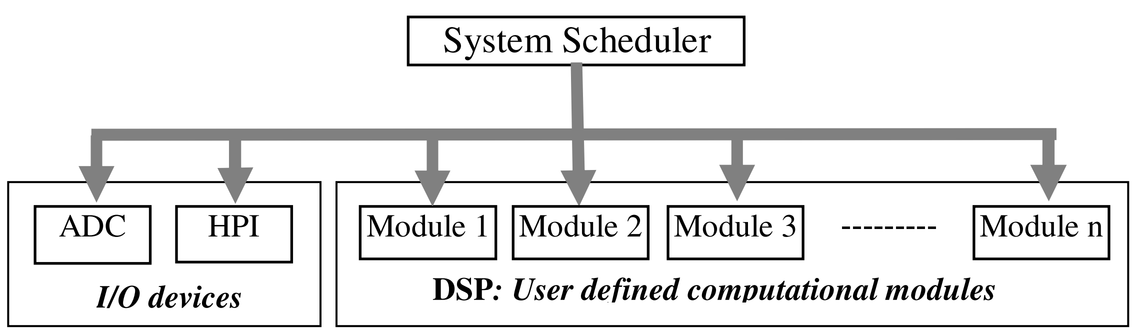

Figure 4-4: System Scheduler

In order to validate the operation of the system software, some preliminary investigations were carried out and the results are presented in the Appendix-IV.

4.5 Implementation of Algorithm for Signal Processing Unit

This section explains the main steps involved in the implementation of the algorithm for the signal processing unit presented in chapter 3. The algorithm for the signal processing unit is shown in Figure 4-5. First, the modal components of the three-phase signals were obtained using the constant Clarke transformation. The implementation of the Clarke transform is shown in Figure 4-6.

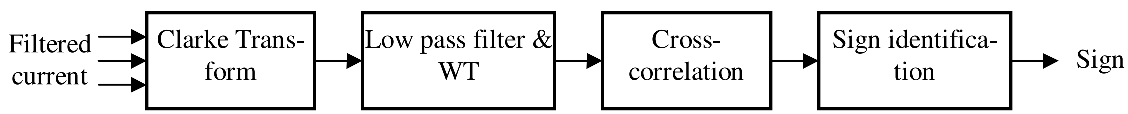

Figure 4-5 : Algorithm for Signal Processing Unit

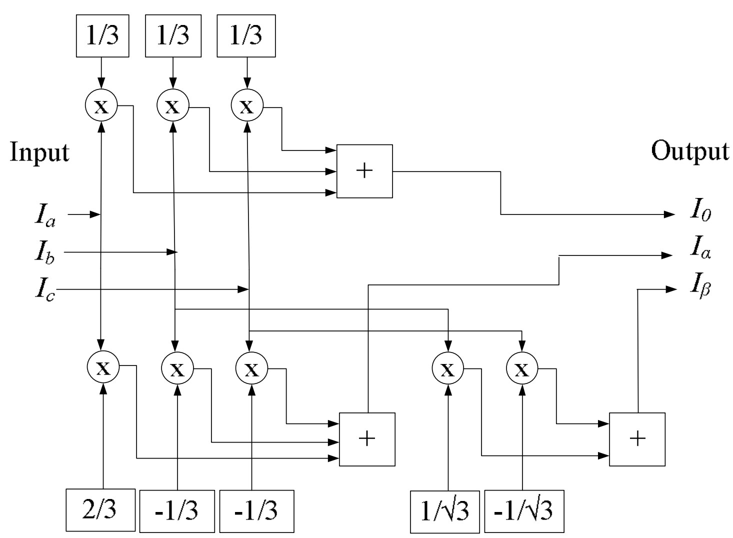

Figure 4-6 : Implementation of Clarke transformation

Before computing the wavelet coefficients of the modal currents, the high frequency components inside the sampling bandwidth were removed by passing them through a digital low-pass filter with down sampling. Then the wavelet coefficients of the modal currents were obtained via the continuous wavelet transformation of 'DB4' mother wavelet [55]. The implementation of the digital low-pass filter and the continues wavelet transform is shown in Figure 4-7.

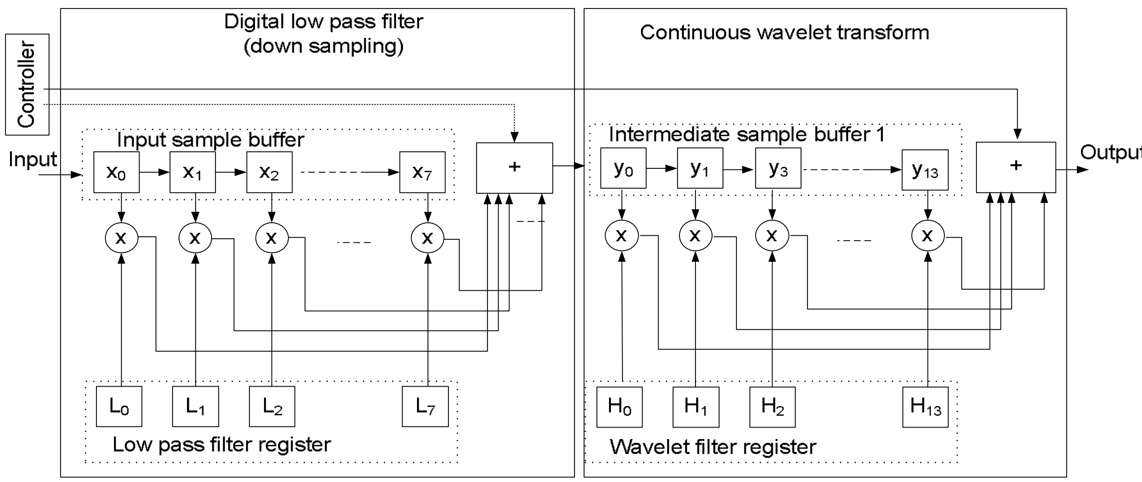

Figure 4-7 : Implementation of Digital low pass filter and CWT

The cross-correlation coefficients between the CWT coefficient of each modal current component and the reference wavelet were then computed. The mean removed coefficients of cross-correlation (r) for a data sequence of x with reference to the reference wavelet w is given by [56],

$$r = \frac{1}{n}\sum_{i=0}^{n-1}\left(w_i - \overline{w}\right)\left(x_i - \overline{x}\right) \tag{4.1}$$

where $\overline{w}$ and $\overline{x}$ are the mean values of two data sequences and n is the size of the data set. However, the mean value of the wavelet function can be approximated to zero; therefore the Eq. (4.1) can be approximated as,

$$r = \frac{1}{n}\sum_{i=0}^{n-1} w_i x_i \tag{4.2}$$

The calculation of the cross-correlation coefficients of the reference wavelet and the computed wavelet coefficient was implemented as shown in Figure 4-8.

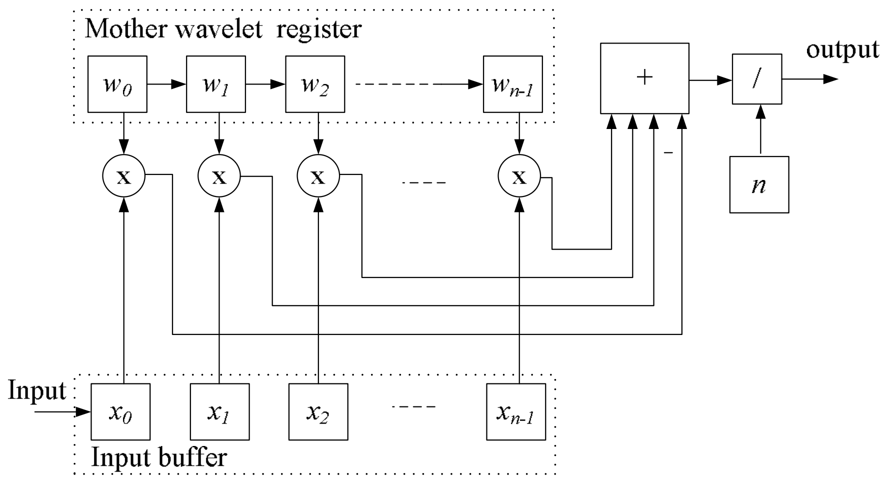

Figure 4-8 : Implementation of coefficients of cross-correlation

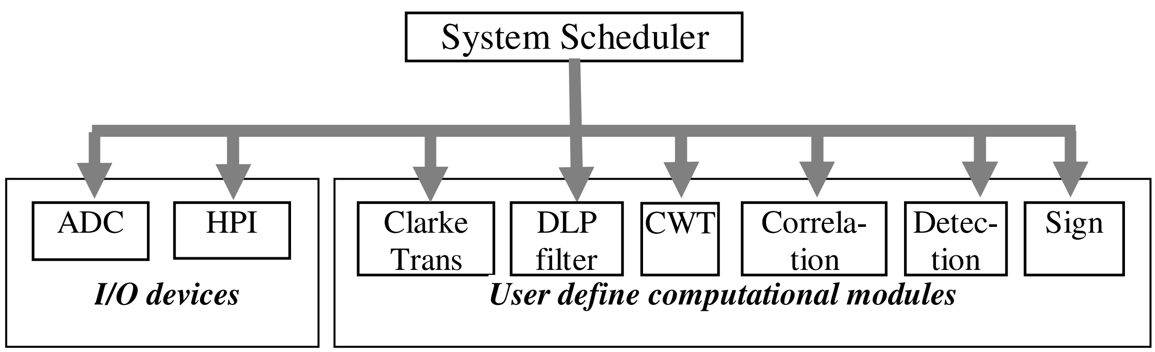

Figure 4-9 : System Scheduler

Finally, the sign of the wavelet was determined by the cross-correlation coefficient relevant to the largest Clarke component observed during the transient (which depends on the type (L-G, L-L, etc.) and the phases involved in the fault). A detection signal that indicates the occurrence of a transient was generated by comparing the magnitude of wavelet coefficients with a threshold value. The threshold was set at 50% above the pre-fault steady state values of the respective wavelet coefficients.

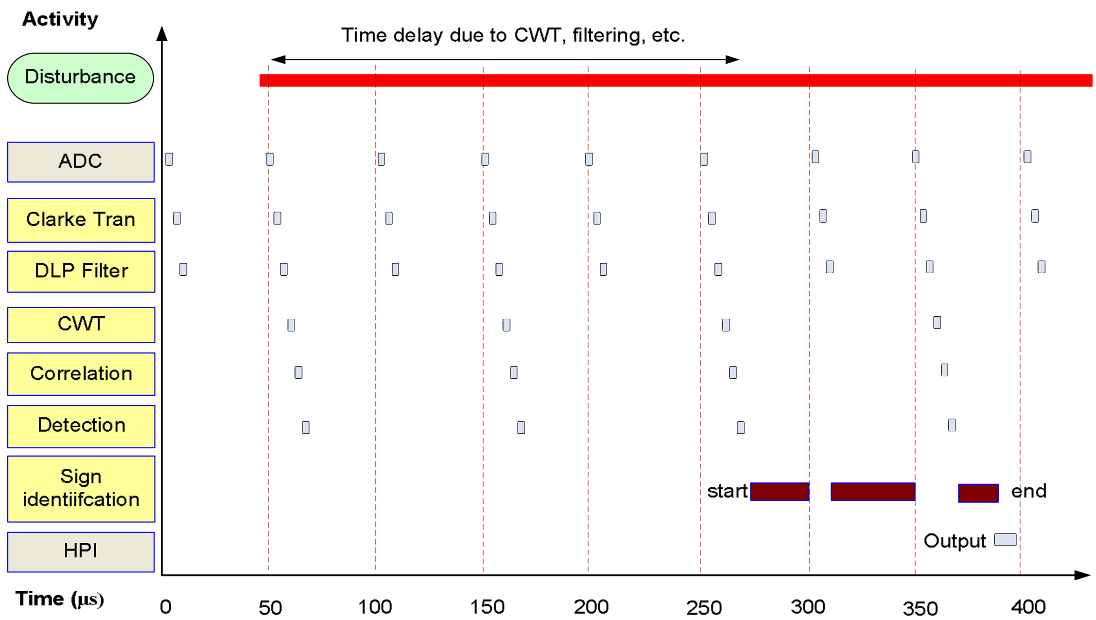

Figure 4-10 : Real-time operation of prototype

The system scheduler corresponds to the signal processing unit algorithm implemented on the DSP is shown in Figure 4-9. The computational models required to perform the Clarke transform, digital filtering, CWT, etc. were implemented on the DSP. The algorithm for sign identification is enabled only when a transient is detected by the system. The HPI output signals are enabled upon the completion of the sign identification algorithm.

Real time operation of the prototype during a fault disturbance is shown in Figure 4-10. Time delays shown here are for demonstration purpose only.

4.6 Test Setup

Testing is an integral part of prototype implementation. The power system waveform generator Real Time Playback (RTP) [57] was used to test the performance of the prototype unit. The RTP is capable of generating the waveforms recorded by actual fault recorders and electromagnetic transient (EMT) type simulations. Figure 4-11 shows a photograph of the test setup. The user interfaces for the RTP and DSP were provided using a personal computer.

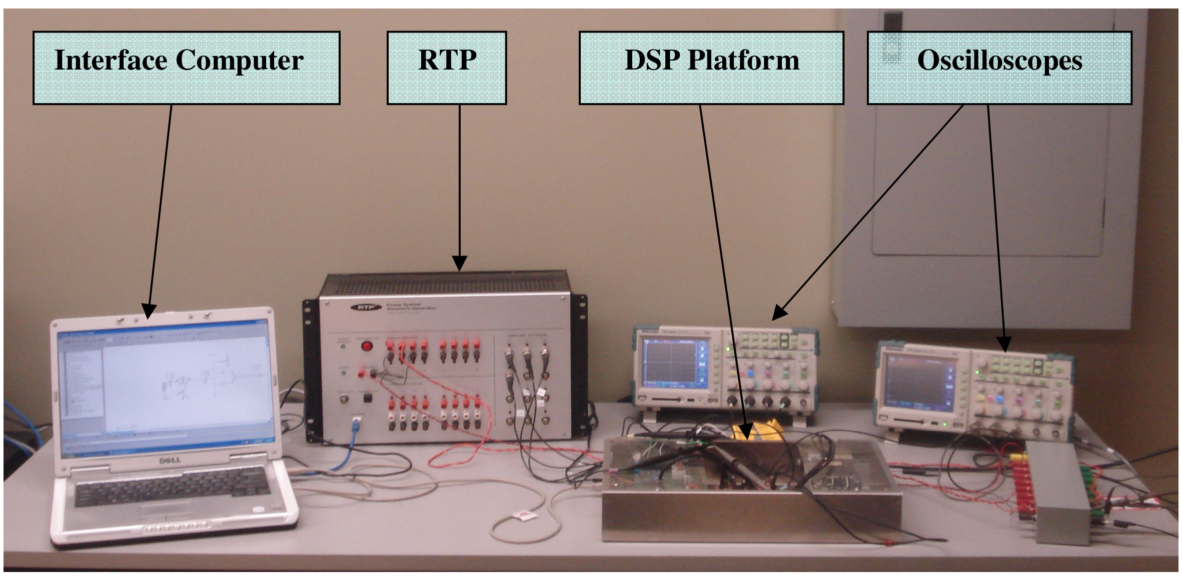

Figure 4-11 : Test setup

In order to investigate the performance of the hardware prototype, recorded waveforms obtained using a test transmission system simulated in PSCAD/EMTDC^{TM} were played back using a RTP. Results obtained in this study are described in the following section.

4.7 Test Results

4.7.1 Test System

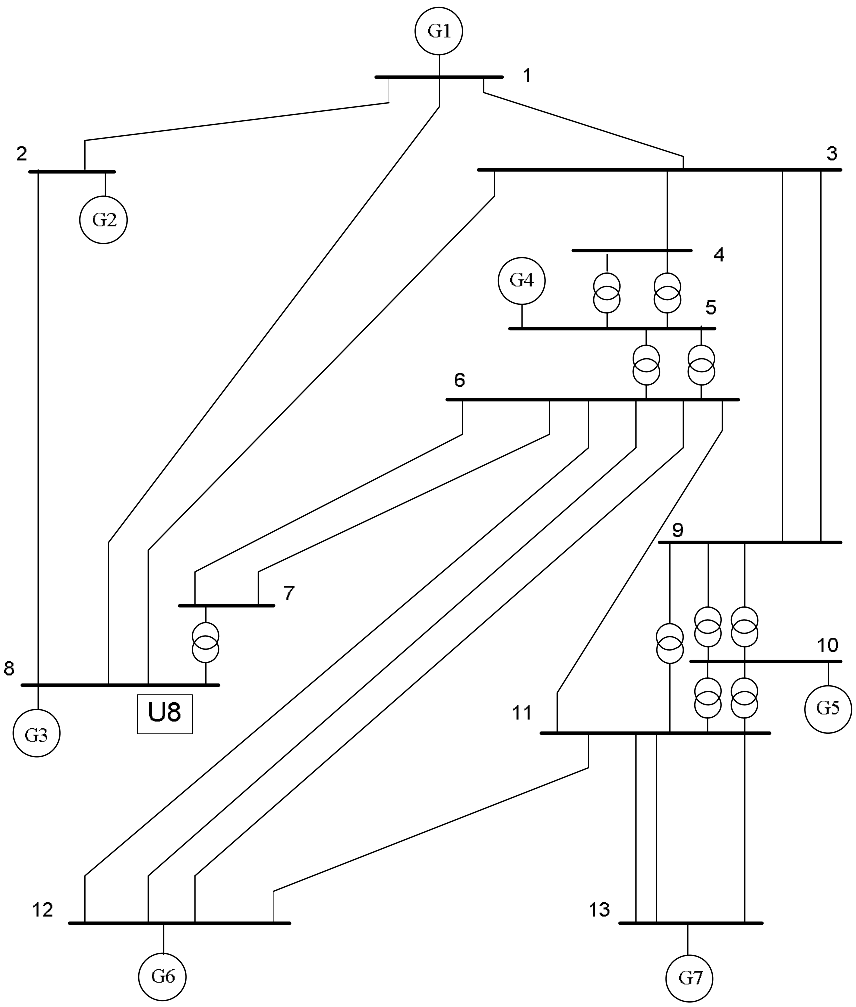

Figure 4-12 : 765/400/230kV transmission system

The transmission network shown in Figure 4-12, closely represents a real 756 kV power system, was simulated in PSCAD/EMTDC^{TM} electromagnetic transient simulation software. The frequency dependent phase domain transmission line models were used to simulate transmission lines. The current signals were measured using the current transformers modeled considering the saturation characteristics. The generators were modeled as voltage sources. The transformers were modeled with the saturation effects. The three-phase waveforms generated using simulations were recorded and played back using the RTP. A simulation time step of 5 μs was used. Investigations were carried out using different types of faults simulated at different locations in the system with different fault impedances.

4.7.2 Busbar Fault

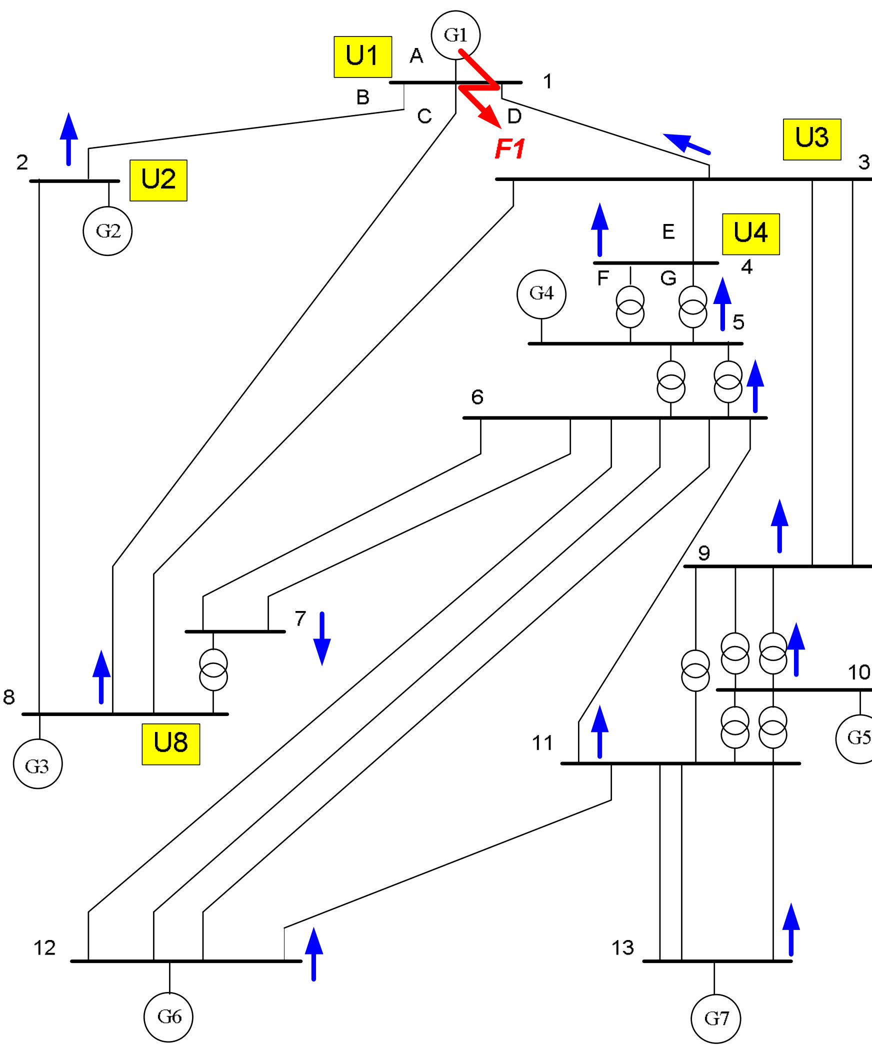

Figure 4-13 : Fault directions identified for F1

The first test was a solid three phase to ground solid fault on bus-1 as shown in Figure 4-13. The three-phase current waveforms recorded on bus-1 during this fault were played back using the RTP. Figure 4-14 shows the three-phase current waveforms and the output signals observed at each of the branches connected to bus-1. The coefficients of correlation observed at each of the branches are also shown in Figure 4-14. The yellow (light grey) curve on the output signals graph in Figure 4-14 represents the detection of transient which triggers the calculation of coefficient of correlation. The blue curve (dark grey) on the output graph represents the sign of the wavelet coefficient. This signal takes value "1" if the computed wavelet coefficient has the same sign as the reference mother wavelet, that is when the sign of the correlation coefficient with the largest magnitude is positive. The signal takes value "0" when the wavelet coefficient has a sign opposite to the reference wavelet. For the case shown in Figure 4-13, the wavelet coefficients of all four branches have the same sign (negative), thus the decision making unit on bus-1 recognizes this fault as a busbar fault and isolates the faulted busbar.

The observations at each of the branches connected to bus-4 during the same event are also shown in Figure 4-15. The output signals that represent the sign of the wavelet coefficients indicate that branch-E coefficient has a sign different to the other two branches. Therefore, the decision making unit on bus-4 recognizes this event as an external fault in the direction of bus-3. Signals collected at all other branches were processed in the same manner using the prototype.

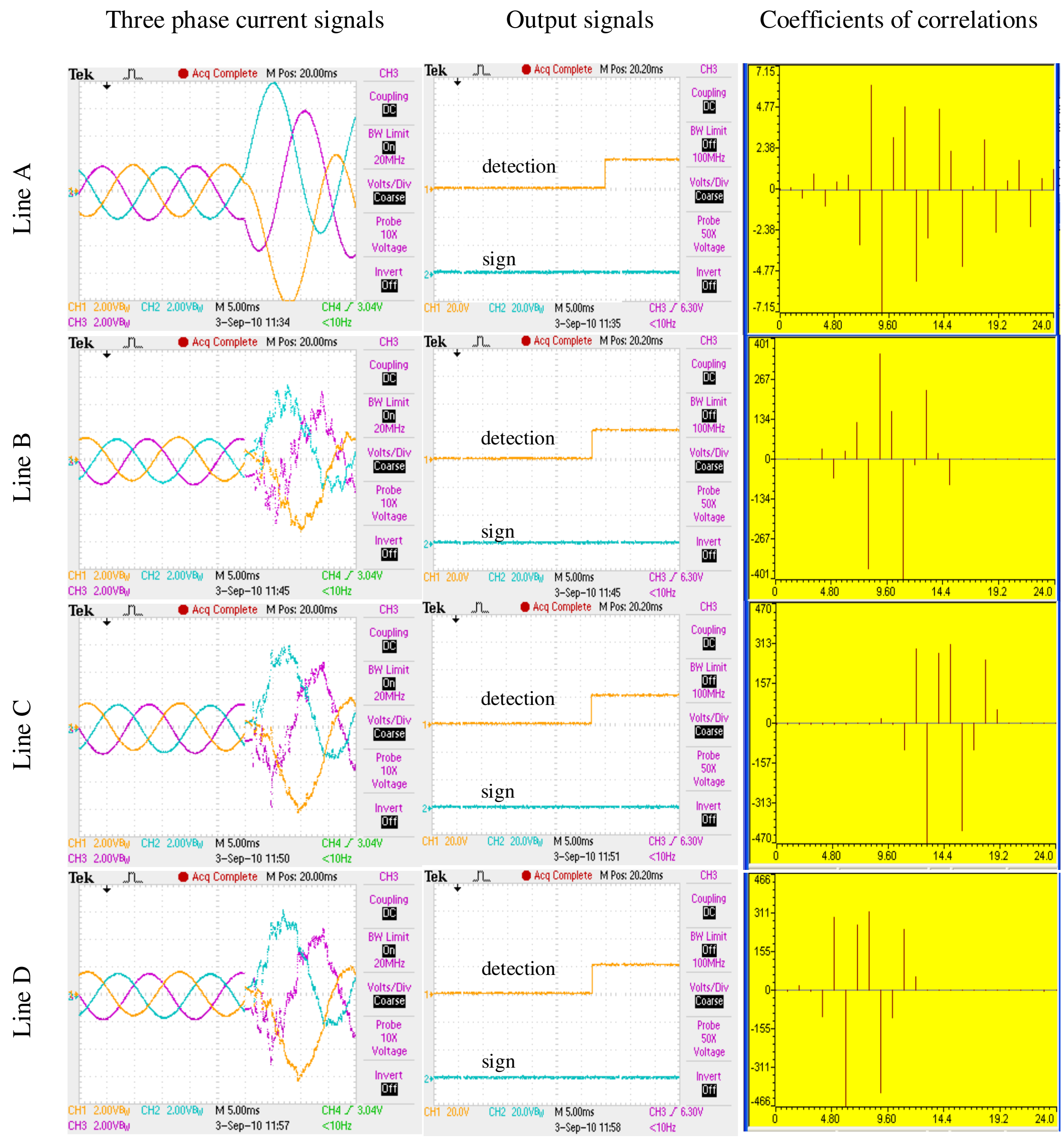

Figure 4-14 : Observation at U1 for F1

The fault directions identified by all the decision making units during the fault are also indicated on Figure 4-13 by arrows. Information exchanged between the decision making units (numbered based on the busbar number) located closest to the fault are shown in Table 4-I. The table also indicates the fault category determined by each decision making unit. Since this fault is an internal one, all units received a signal that is opposite to the transmitted signal.

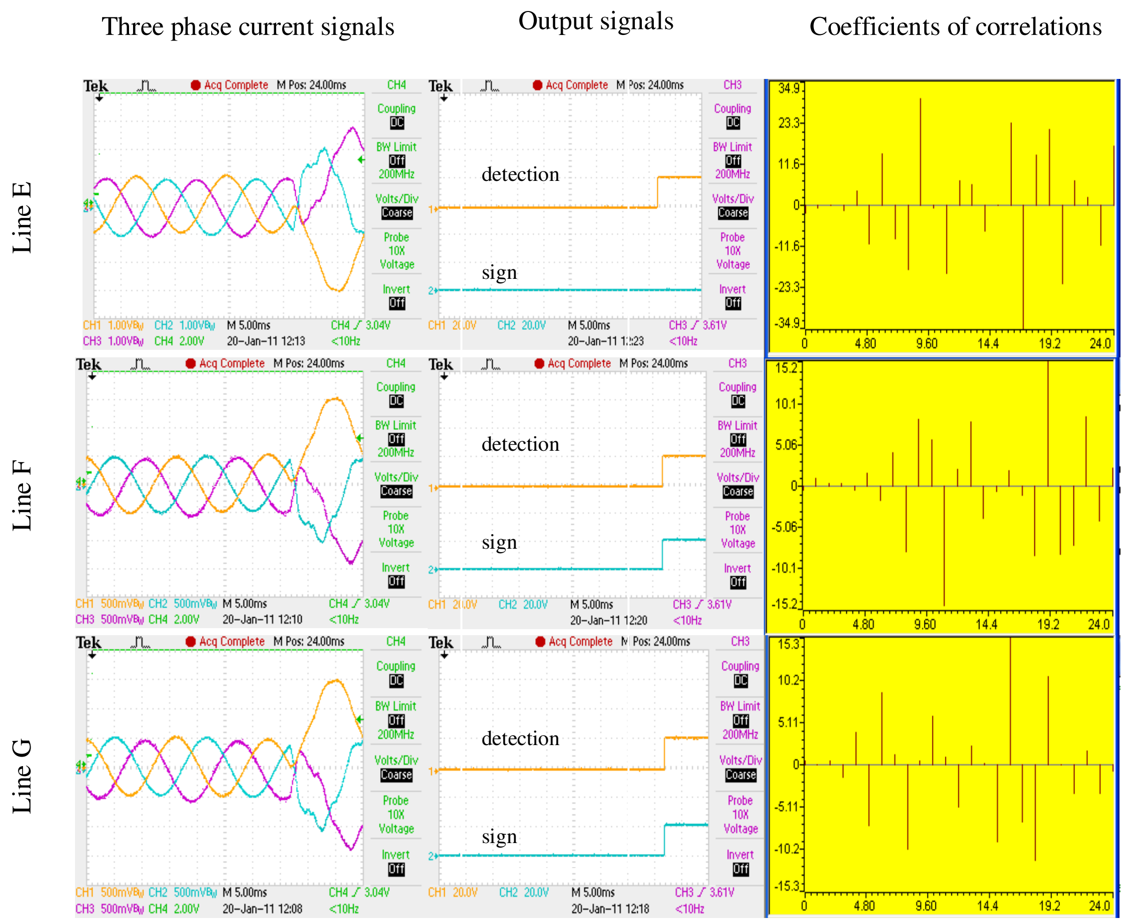

Figure 4-15 : Observation at U4 for F1

Table 4-I : Information Exchanged During Fault F1

Unit	Type	Information sent to\ received from unit				
		U1	U2	U3	U4	U8
U1	Internal	-	1 / 0	1 / 0	-	1 / 0
U2	External	0 / 1	-	-	-	0 / 0
U3	External	0 / 1	-	-	1 / 0	0 / 0
U4	External	-	-	0 / 1	-	-
U8	External	0 / 1	0 / 0	0 / 0	-	-

The prototype was tested with waveforms from several other busbar faults of different types and locations, including a fault on bus-6, which connects eight segments. All tests verified the correct operation in terms of recognizing the faulted element.

4.7.3 Line Fault

The results shown in this section is for a solid line to ground fault on the line segment connecting bus-1 and bus-8. The fault location is shown in Figure 4-16. The recorded waveforms on the buses-1 and-8 were played back using the RTP.

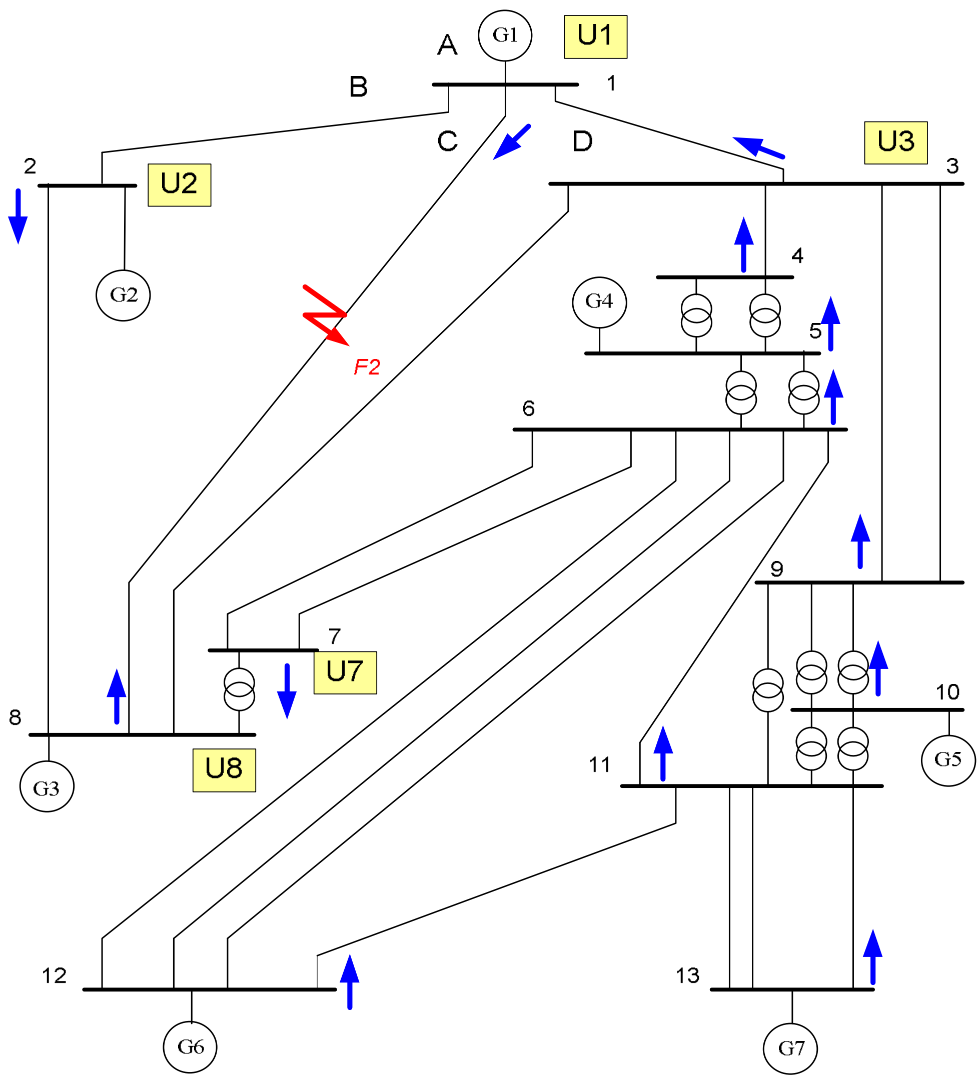

Figure 4-16 : Fault directions identified for F2

Figure 4-17 shows the three phase current waveforms, output signals and coefficients of correlations observed at bus-1. By combining the output signals, the decision making unit on bus-1 can recognize this event as an external fault in the direction of bus-8. Similarly, the decision making unit on bus-8 can recognize this event as an external fault in the direction of bus-1. The fault directions identified by all other units during this fault are also shown in Figure 4-16 by arrows.

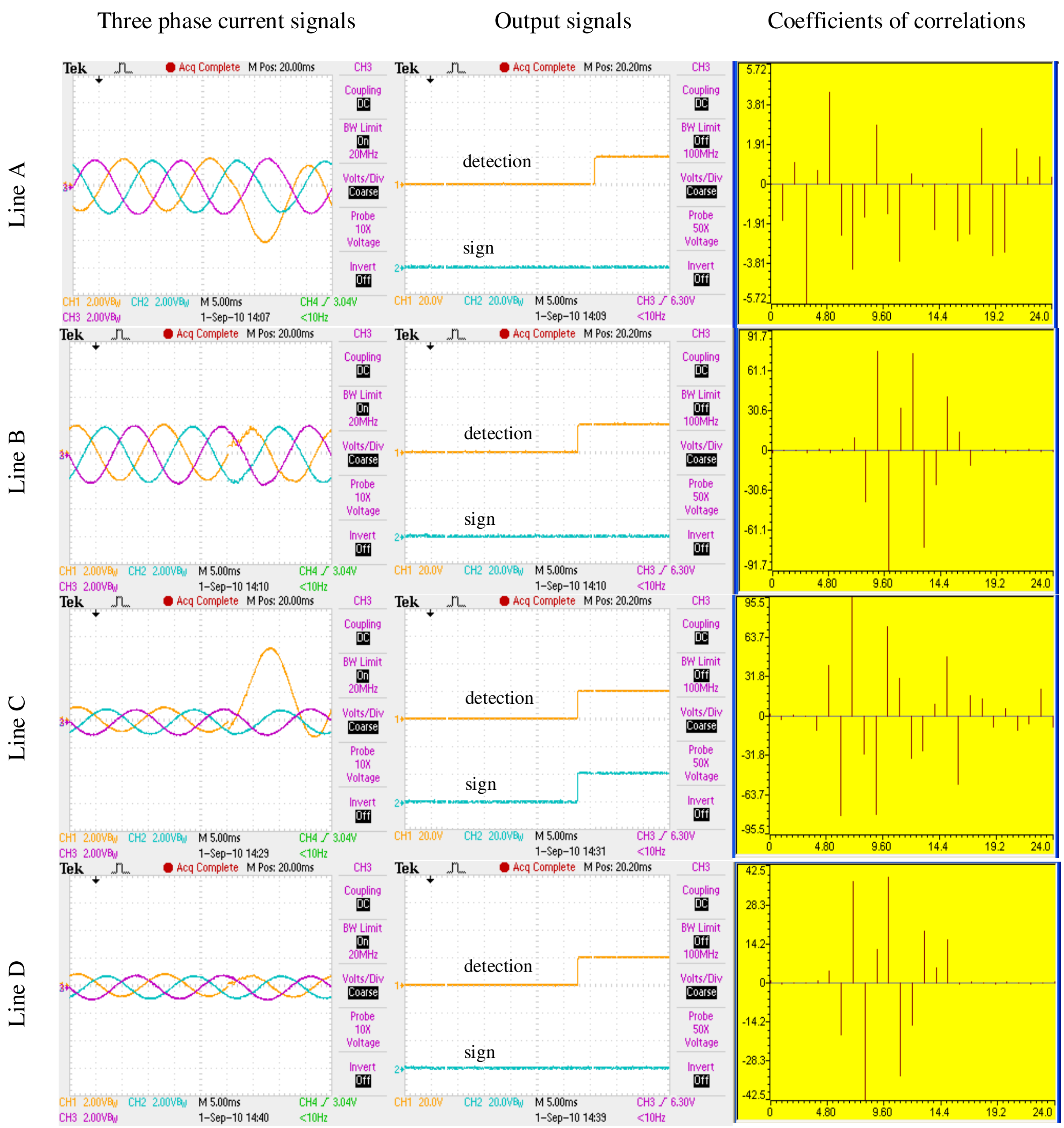

Figure 4-17 : Observations at U4 for F2

The type of the fault and the information exchanged between the decision making units located on the buses closest to the fault are shown in Table 4-II. As it can be seen from the Table 4-II, the decision making units on buses-1 and -8 have sent a “1” and received a ‘1’. Thus, both these units can conclude that the fault is on the line connecting buses-1 and -8. The prototype was tested for several other line faults including terminal faults. The results show accurate faulty segment identification.

Table 4-II : Information Exchanged During Fault F2

Unit	Type	Information send to\ received from unit				
		U1	U2	U3	U7	U8
U1	External	-	0 0	1 0	-	**1** **1**
U2	External	0 0	-	-	-	0 1
U3	External	0 1	-	-	-	0 0
U7	External	-	-	-	-	0 1
U8	External	**1** **1**	1 0	0 0	1 0	-

4.7.4 Parallel Line Fault

The test results shown in this section are for a fault on one of the two parallel transmission lines. The simulated fault was a line to line fault on one of the two lines connected between buses 6 and 7 as shown in Figure 4-18. Figure 4-19 shows the three phase current waveforms, output signals and coefficients of correlations observed at bus-7. Table 4- III shows the information exchanged between the decision making units U6, U7 and U8 (located close to the fault) during the fault.

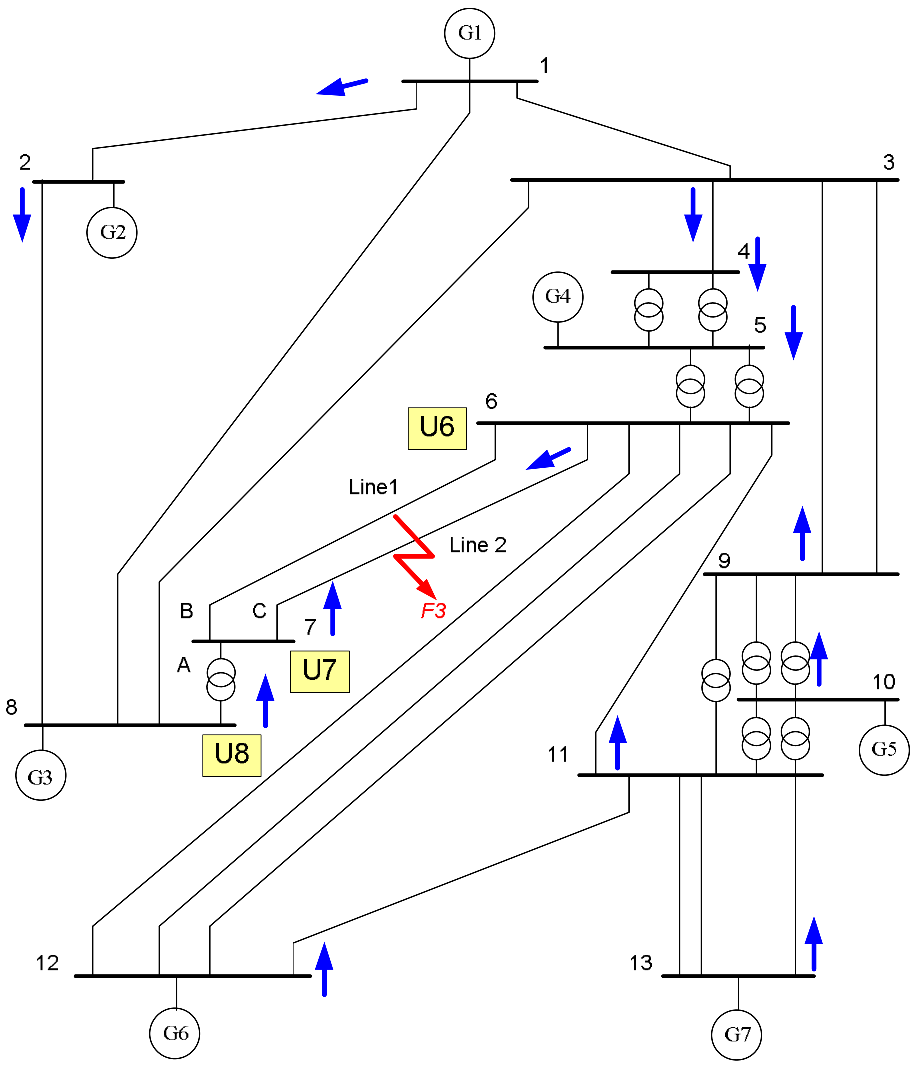

Figure 4-18 : Fault directions identified for F3

Table 4-III : Information Exchanged During Fault F3

Unit	Type	Information send to\received from unit		
		U6	U7	U8
U6	External	-	Line-1: 0 / 0 Line-2: **1** / **1**	-
U7	External	Line-1: 0 / 0 Line-2: **1** / **1**	-	1 / 0
U8	External	-	0 / 1	-

As it can be seen from the table above, the signals exchanged by U6 and U7 correspond to line-2 are '1'. Based on this information the protection scheme can correctly identify line-2 as the faulted segment. The prototype was tested for several other line faults including terminal faults. The results have shown accurate faulty segment identification.

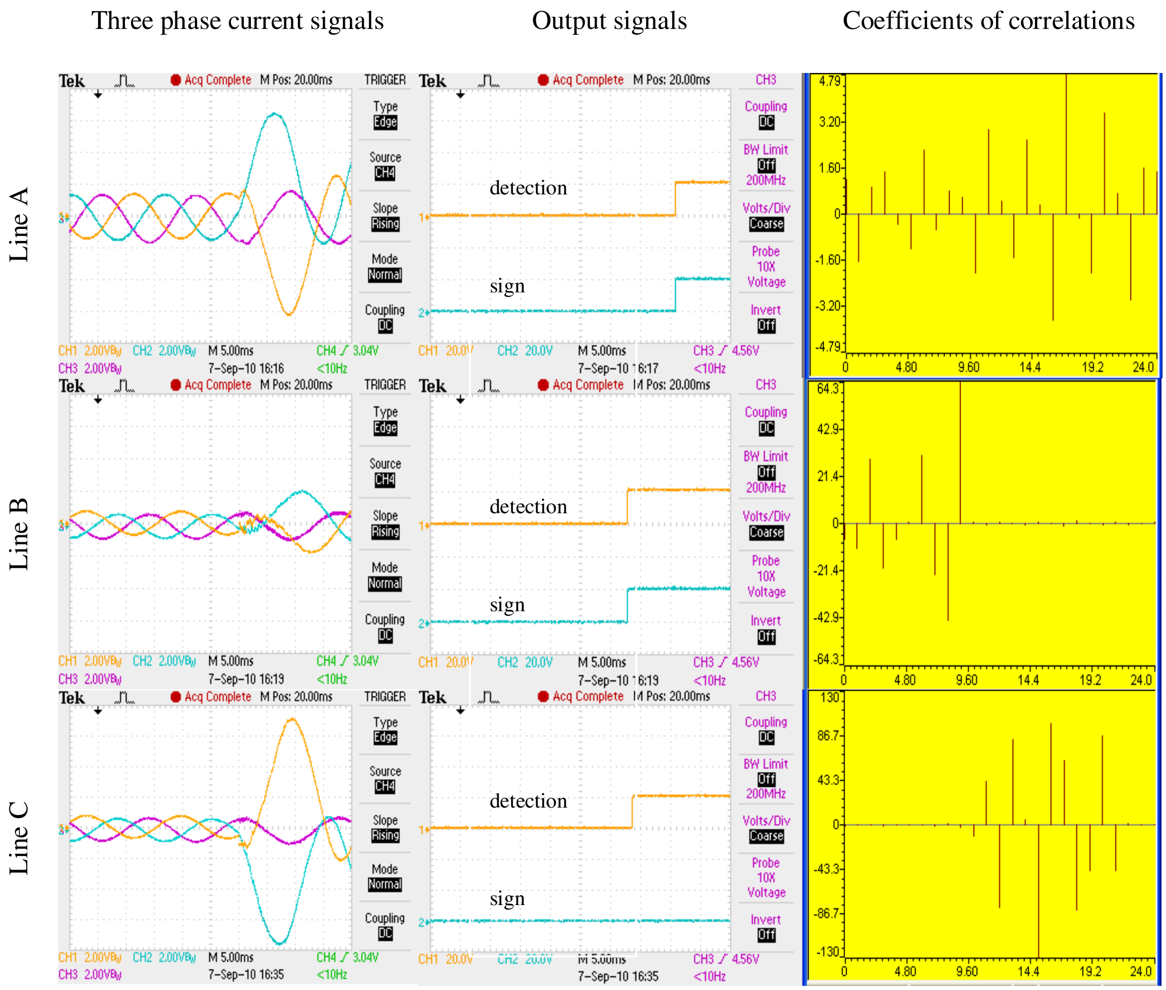

Figure 4-19 : Observations at U7 for F3

4.7.5 Effect of CT Saturation

Current transformer saturation is one of the common scenarios observed during the faults in real power systems. As mentioned in chapter 1, transient based protection is not expected to be affected by CT saturation. In order to verify this claim, some tests were carried out. Figure 4-20 shows the operation of the signal processing unit for the same line to ground fault simulated with and without CT saturation. As shown in Figure 4-20, the method proposed in this thesis uses the initial transient originating from the fault which is observed well before the occurrence of CT saturation. Thus, the operation of the signal processing unit is independent of the effect of the CT saturation.

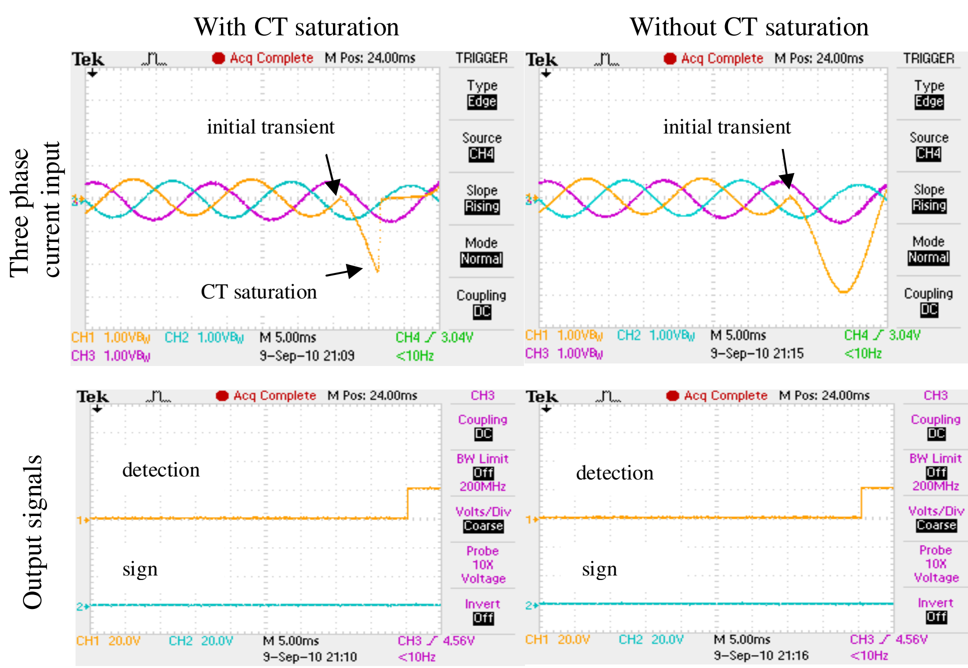

Figure 4-20 : Effect of CT saturation

4.7.6 Effect of Noise

Investigations were carried out to evaluate the performance of the proposed method under the influence of noise. Noisy waveforms were generated using the simulation program with different noise levels ranging from 45 dB to 100 dB. The investigations carried out using the played back waveforms revealed that the threshold level of the triggering algorithm needs to be adjusted according to the level of the noise present in the input signals. Increased threshold in the detection algorithm results in a lower sensitivity to high impedance faults. According to the investigation, the prototype implemented in research was capable of identifying solid faults for signal to noise ratios above 60 dB.

4.7.7 Response Time

The line protection in the proposed scheme requires the exchange of information between relays, and is therefore, affected by communication delays. The average response time of the protection scheme was estimated to be 10 ms with a 4 ms communication delay. Although the operating time observed here approaches that of a conventional distance relay with a fast phasor extraction algorithm, the proposed protection scheme is capable of providing fast protection against the faults on 100% of the line in contrast to the conventional Zone-1 setting of 80-85%. The response time is not affected by the communications delays, in the case of busbar faults.

4.7.8 Effect of Switching Events

Malfunction due to the transients originating from non-faulty events is one of the commonly reported problems of the transient type protection methods. Investigations showed that the proposed protection scheme is also susceptible to false triggering due to switching disturbances and lightning strokes. In order to overcome this problem, a fault recognition scheme that can distinguish faulty transients from non-faulty transients can be used to supervise the proposed protection scheme.

4.8 Chapter Summary

A hardware prototype of the proposed fault direction identification scheme was implemented on a DSP platform and tested using simulated waveforms played back on a real-time waveform generator. The test waveforms were obtained from an high voltage transmission system simulated on an electromagnetic transient simulation program. Numerous tests on the prototype under different practical scenarios such as measurement noise and CT saturation, verified the correct operation of the proposed protection concept. The test results demonstrate the potential for successful development of a transient directional protection scheme for fast clearing of the faults in transmission systems, irrespective of the fault location on the transmission lines.

Although the proposed method has shown correct fault direction and segment identification, malfunction due to the transients originating from non-faulty transients such as line switching, load switching, etc. was observed. Investigations carried out to develop a transient recognition scheme to distinguish the transients originating from faults from those originating from switching events are described in the next chapter.

Chapter 5

Transient Recognition System

5.1 Introduction

Possible malfunction of the transient based protection scheme proposed in chapter-3 due to switching transients is a major concern that has to be overcome. As a solution to the problem, a transient classification system that can supervise the decision making unit to prevent issuing false trip signals is proposed in this chapter. This transient classifier is expected to distinguish the fault transients from non-fault transients, and block the relay, if the transients observed are not due to a fault. This chapter is devoted to describe the development of this transient classification system, including the identification of features and classification methods suitable for the application. The initial investigations were carried out to select a suitable classification method based on an off-line analysis of a system, using the waveforms generated through electromagnetic transient (EMT) simulations. In the end, a prototype of the selected classification method was implemented and tested with the simulated waveforms as well as with few recorded waveforms obtained from a practical extra high voltage system.

5.2 Transient Classification System

The structure of the proposed transient classification system is shown in Figure 5-1. The system takes three phase current measurements (CT outputs) as the inputs. Only the current measurements are considered as inputs to be consistent with the transient based protection scheme proposed in chapter 3. This again avoids bandwidth issues related to measurements of voltages using CVTs. These currents are pre-processed using the wavelet transform to extract features used for the classification. As shown in Figure 5-1, the proposed classification system consists of three individual classifiers; one for each phase. Each classifier is trained using the disturbances recorded from the phase to which it is connected. The final trip decision is made by a post processing decision making module that considers the outputs of all three classifiers. This arrangement also enables determination of the phases involved in a fault.

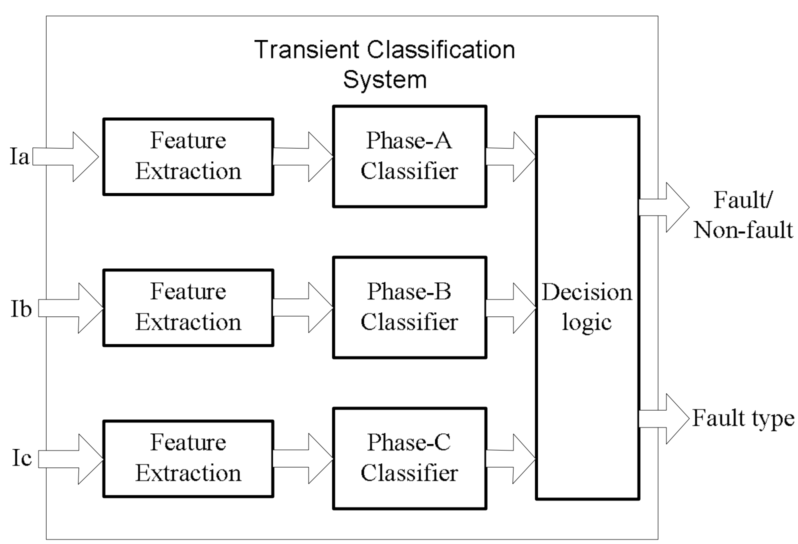

Figure 5-1 : Structure of the transient classifier

5.2.1 Feature Selection and Extraction

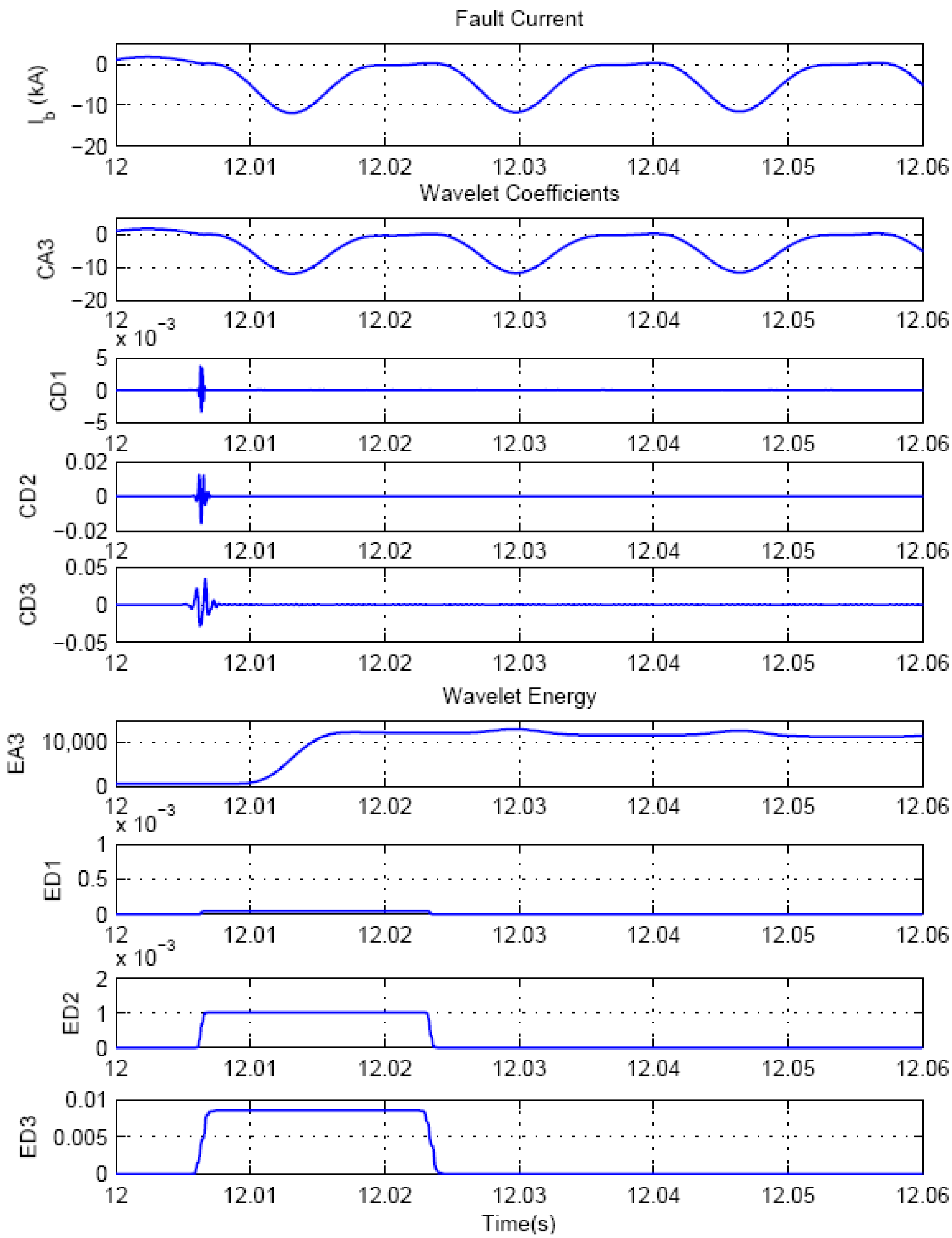

Figure 5-2 : Current during a fault, its wavelet coefficients, and the corresponding wavelet energies

The success of any classification system is highly dependent on the input features used. The composition of different frequency components in a signal discloses its characteristics. The wavelet transform is a technique well suited for decomposing an aperiodic signal into different frequency bands. Wavelet transformation also allows time-frequency analysis. Therefore, the wavelet transform has been successfully used in several applications that required the analysis of high frequency transients [37],[39].

In this research, feature vectors were generated using DB4 mother wavelet. Results of previous studies related to the power quality disturbance classification [37],[39] indicates that the 'DB4 mother wavelet' is a good choice for analyzing the power system signals. Using the selected mother wavelet, a signal is decomposed into several components in different frequency bands. The decomposed signal components are known as "reconstruction wavelet coefficients" of different levels (scales). Superposition of these reconstruction wavelet coefficients, which are sampled signals, yields the original signal. As the frequency increases (scale decreases), the width of the frequency band also increases. The lowest frequency component is called the approximation wavelet coefficient while the other components are called detail wavelet coefficients of various levels. The input features to the classifiers used in this study were the energies associated with the reconstruction wavelet coefficients, in a moving time window. The wavelet transform was carried out up to three levels. The energy of the approximation wavelet coefficients (*EA3*) and the detail wavelet coefficients (*ED1- ED3*) were calculated using (5.1) and (5.2).

$$EA3 = \sum_{j=1}^{N} \left| CA3_j \right|^2 \tag{5.1}$$

$$EDi = \sum_{j=1}^{N} \left| CDi_j \right|^2, i = 1,2,3 \tag{5.2}$$

Here, N denotes the length of the moving window in terms of the number of sample points, $CA3_j$ denotes the j^{th} sample of level 3 approximation wavelet coefficient and CDi_j denotes the j^{th} sample of level i detail wavelet coefficient.

Figure 5-2 shows the current observed in phase-B during a B-G fault, the corresponding approximation and detail wavelet coefficients (*CA3*, *CD1-CD3*), and their wavelet energies (*EA3*, *ED1-ED3*). The window length considered for energy calculation is 15 *ms*. Figure 5-3 and 5-4 show the currents and the wavelet energies observed during a capacitive load switching disturbance and a line switching disturbance respectively. Some notable differences exist in the distribution of energy levels among the wavelet coefficients of different scales. These differences are exploited for the classification.

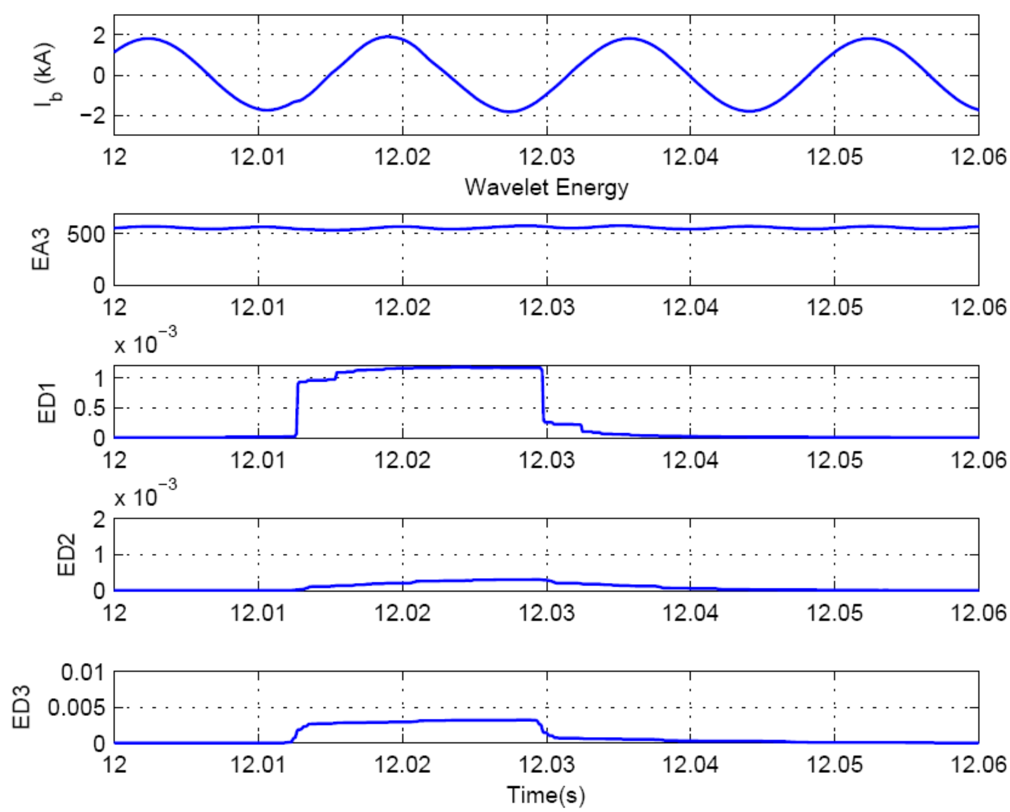

Figure 5-3 : Current and wavelet energies for a capacitive load switching event

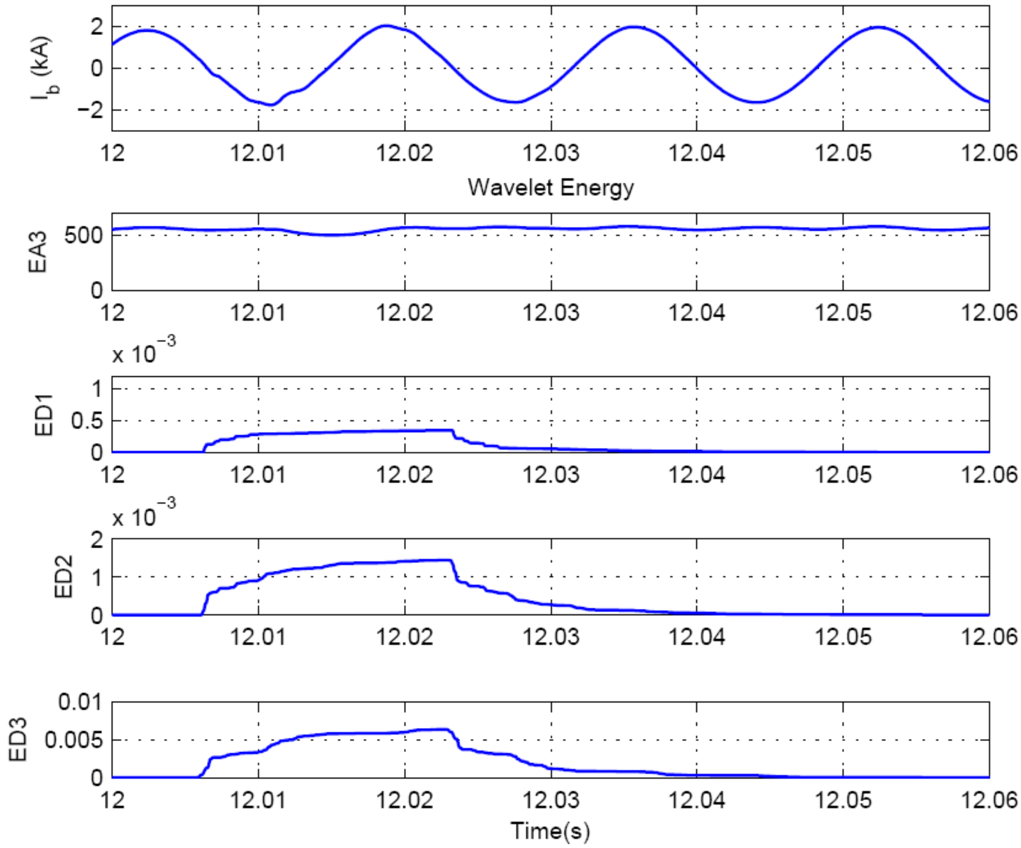

Figure 5-4 : Current and wavelet energies for a line switching event

5.2.2 Classification Methods

The performance of different classification methods may vary from application to application. Therefore it is important to select the most suitable classification method for the application considered, in this case for differentiating the fault transients from the non-fault transients. In this research, three techniques, Decision Trees (DTs), Hidden Markov Models (HMMs) and Probabilistic Neural Networks (PNNs) were examined as candidate classification methods. These techniques have shown promising results in some of the previous studies reported in literature [19],[58]-[63]. A brief description of these three classification methods are given below.

Decision Trees

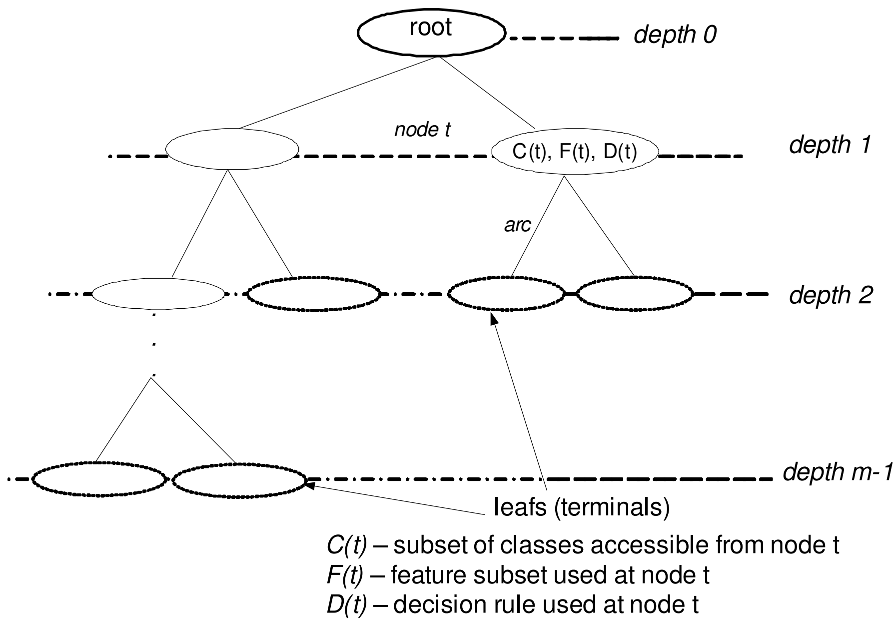

Figure 5-5 : DT Structure

The structure of a general DT is shown in Figure 5-5. An interior node corresponds to a feature whereas an arc to a child represents a possible value of that feature. A leaf represents the predicted class of the target feature, given that the values of the features are represented by the path from the root.

A decision tree can be learned by splitting the source feature set into subsets based on an attribute value test. This process is repeated on each derived subset in a recursive manner. The recursion is completed when splitting is either non-feasible, or a singular classification can be applied to each element of the derived subset. The depth of a node is the length of the path from the root to the node.

The main objectives of training a DT based classifier is to correctly classify as much of the training samples as possible and generalize the samples beyond the training samples. This is done so that unseen samples could be classified as accurately as possible and making it easier to update as more training samples become available and have as simple a structure as possible. More details about training and testing of a DT classifier can be found in [59].

Hidden Markov Models

A Hidden Markov Model (HMM) , λ, with N states and M observation symbols can be mathematically expressed in a simplified form as,

$$\lambda(\mathbf{A}, \mathbf{B}, \boldsymbol{\pi}) \tag{5.3}$$

where, **A** denotes the state transition probability distribution, **B** denotes observation symbol probability distribution and $\boldsymbol{\pi}$ denotes initial state distribution [64]. The HMM used in this research is assumed to have two states and four observations symbols as shown in Figure 5-6. In Figure 5-6, S_i denotes the state i ($i = 1 \ldots N$, $N = 2$), $E(k)$ denotes the observation symbol k, ($k = 1 \ldots M$, $M = 4$).

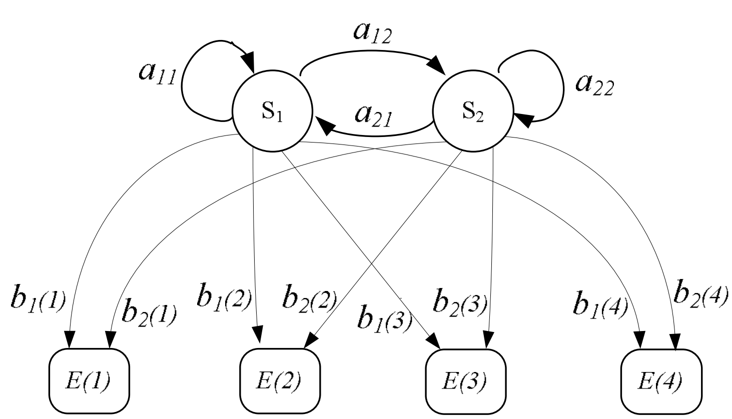

Figure 5-6 : Hidden Markov Model with two states and four observation symbols

The parameters that describe an HMM are the state transition probability distribution

$$\mathbf{A} = \lfloor a_{i,j} \rfloor_{N \times N} \tag{5.4}$$

where, $a_{i,j}$ is the state transition probability from i^{th} state to j^{th} state, the observation symbol probability distribution

$$\mathbf{B} = [b_i(k)] \qquad i = 1 \cdots N, k = 1 \cdots M \tag{5.5}$$

where $b_i(k)$ is probability of occurring the k^{th} observation symbol when in the i^{th} state, and the initial state probability distribution

$$\boldsymbol{\pi} = [\alpha_i] \qquad i = 1 \cdots N \tag{5.6}$$

where α_i is the initial probability of i^{th} state. With appropriate values of N, M, $\mathbf{A}$, $\mathbf{B}$ and $\boldsymbol{\pi}$, an HMM can be used to generate sequence of observations or as a model for given observation sequence. The latter use is applied in classification.

In a Gaussian mixture HMM, the observation symbol probabilities are expressed as mixer of M-variate Gaussians [63].

$$\mathbf{B} = \left[\sum_{l=1}^{G} c_i^l \aleph(\boldsymbol{\mu}_\mathbf{i}^\mathbf{l}, \boldsymbol{\Sigma}_\mathbf{i}^\mathbf{l})\right] \quad l = 1 \cdots G \tag{5.7}$$

Here $\boldsymbol{\mu}_i^l$, is a ($1 \times M$) vector of the mean values and Σ_i^l is a ($M \times M$) matrix of covariance values of the observation symbol probability distribution of i^{th} state in l^{th} Gaussian. c_i^l are the mixing weights and G is the number of Gaussians. In this thesis a mixer of two Gaussians were used and therefore $G = 2$.

The likelihood of given input feature set, $\mathbf{E}$, belonging to HMM, λ, is estimated using a log like-likelihood function.

$$f(\mathbf{E} \mid \lambda) = \log\left(\sum_{i=1}^{N}\left(\alpha_i \sum_{l=1}^{G} L_i^l\right)\right) \tag{5.8}$$

where,

$$L_i^l = \frac{c_i^l}{(2\pi)^{M/2}\left|\boldsymbol{\Sigma}_i^l\right|^{1/2}} \exp\left\{-\frac{1}{2}\left(\mathbf{E} - \boldsymbol{\mu}_i^l\right)^T \boldsymbol{\Sigma}_i^{l\,-1}\left(\mathbf{E} - \boldsymbol{\mu}_i^l\right)\right\} \tag{5.9}$$

The classification criterion ξ given in (5.10) was used to classify the disturbances into two different classes (fault and non fault).

$$\xi = \frac{f(\mathbf{E} \mid \lambda_F)}{f(\mathbf{E} \mid \lambda_{NF})} \tag{5.10}$$

where, E is the input feature set (i.e. wavelet energies) and λ_F and λ_{NF} are the HMMs of faulty and non-faulty classes. If ξ is greater than 1, the likelihood of the event is being a fault is greater than that of a non fault event. Then event is classified as a fault and vice versa [64].

Training of an HMM involves estimation of the parameters **A**, **B** and $\boldsymbol{\pi}$. In order to estimate the HMM parameters, expectation maximization method, which is also known as Baum-Welch method [64] can be used. In this approach, the initial model parameters are randomly selected and the first estimate of the HMM is made. Next the log-like likelihood is estimated and compared against the log-like likelihood calculated in the previous iteration to obtain the optimum parameter values of $\lambda(\mathbf{A},\mathbf{B},\boldsymbol{\pi})$ for each classification class (fault and non-fault) using the training data set [64].

Probabilistic Neural Networks

The PNN was introduced by Specht in 1990 [60]. It is fundamentally based on the well-known Bayesian classifier technique commonly used in many classical pattern-recognition systems. The nonparametric estimation technique known as Parzen windows is used to construct the class-dependent probability density functions for each classification category. This is then used to determine the probability of a given vector pattern belonging to a particular category. The Parzen estimate of the probability for input x belonging to category A is given by the probability density function

$$F_A(x) = \frac{1}{(2\pi)^{m/2}\sigma^m n} \sum_{j=1}^{n} \exp\left[\frac{(x - x_j)^T (x - x_j)}{2\sigma^2}\right] \tag{5.11}$$

where x is the m dimensional input pattern vector, j is the pattern number, x_j is the j^{th} training pattern for category A, n is the number of training patterns, m is the input space dimension, and σ is an adjustable "smoothing parameter." The parameter σ must be determined experimentally [65]. An input is assigned to the category for which it has the highest probability value. With PNN, no time consuming training is involved and online adaptation to new patterns can be easily implemented by way of modifying its training database with new patterns and their correct categories.

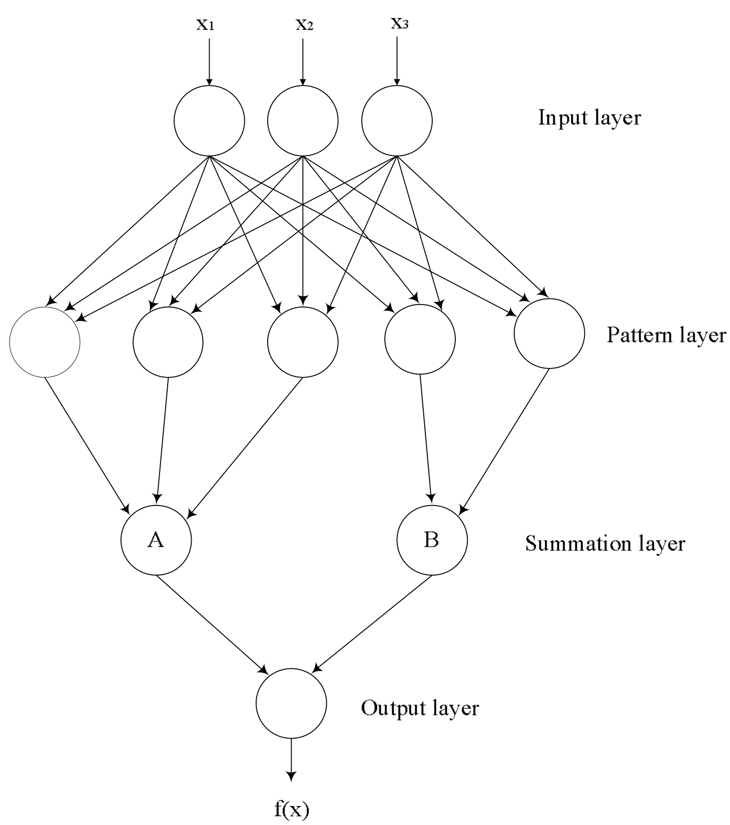

Figure 5-7 : Structure of the Probabilistic Neural Network

Figure 5-7 shows the probabilistic neural network structure used to implement the decision rule for classifying the input disturbances into two classes. This network consists of four layers: input layer, pattern layer, summation layer and output layer. The input layer represents the input variables (x_1, x_2, x_3). The pattern layer is fully connected to the input layer, with one neuron for each pattern in the training set. The summation layer sums the outputs from the pattern-layer neurons. Each neuron in the summation layer corresponds to a particular category classification problem. A summation layer neuron sums up the outputs of pattern layer neurons which belong to the category it represents. The output-layer neuron produces a binary output value corresponding to the highest probability value [54].

5.3 Simulations and Results

In order to investigate the performance of different classification methods in classifying the faulty and non-faulty transients, investigations were carried out using the 12-bus high voltage test system and the actual transmission system described in chapter 4.

5.3.1 12-Bus Transmission System

Figure 5-8 shows the location of the transient classifier on the simulated HV test system. In order to generate the high frequency components of the signals, simulations were carried out at a simulation time step of 5 μs. The transient classifier uses three phase current signals obtained through current transformers as inputs. The current transformers were also modeled in the simulation. Current signals obtained during different types of fault scenarios, capacitor switching, and load switching occurrences were sampled at 20 kHz sampling frequency and recorded. They were used to generate required feature vectors to train the classifier. The detail and approximation wavelet energies calculated up to three levels were used for the analysis.

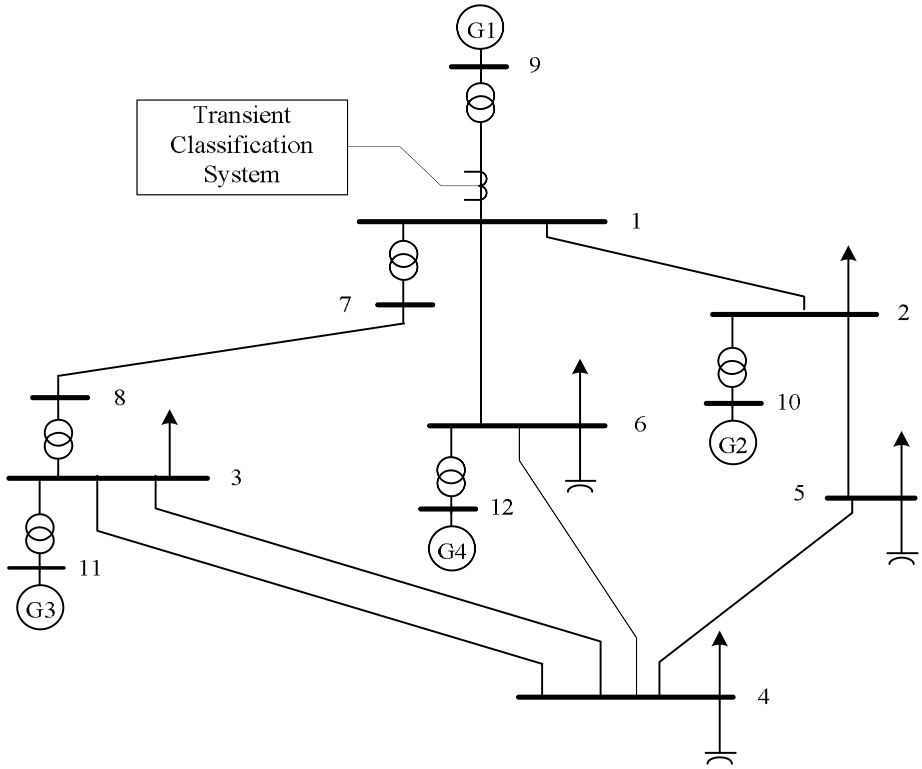

Figure 5-8 : 12-bus power system used for testing the transient classification system

Training and Testing Database

A 140 fault events and 250 non-fault switching events were generated using the simulations. The fault data set including different types of faults (ABC-G, ABC, AB, AG, BG, etc.), and were created with different fault impendence values and different fault inception angles. The non-fault events include transients occurred during load, line and capacitor bank switching, as well as steady state non-transient signals. A total of 325 cases consisting of 105 fault disturbances and 220 switching disturbances were used as the training data set. The rest of the disturbances were used as the test data set.

Training of the Classifier

All three classifiers were trained off-line using the feature vectors generated using the training database. The wavelet toolbox in MATLAB was used to perform the wavelet transformation to extract the feature vectors. The CART software [66] was used to train and simulate the DT classifier. The HMM Classifier was trained and tested in MATLAB using the HMM toolbox developed in [67]. The PNN was fully simulated in MATLAB. Finally all three classifiers were tested for the same test data and results are presented in the next section.

Classification Results

The trained classifiers were tested with the unseen examples in the testing data set. The classification results obtained with the DT classifier are summarized in Table 5-I. According to the classification results obtained, all the non-fault transients were classified correctly, however, 11 percent of the fault transients were misclassified as non-fault.

Table 5-I : DT based classification

Actual Class	Training Cases	Testing Cases	Predicted Class		% correct
			Non-fault	Fault	
Non-fault	220	30	30	0	100
Fault	105	35	4	31	89

Table 5-II summarizes the classification results for the HMM classifier. According to the simulation results all non-fault transients were classified correctly as non-faults and six percent of the fault transients were misclassified as non-faults. Furthermore, examination revealed that the majority of misclassified disturbances are the transients originating from the switching of very large loads.

Table 5-II : HMM based classification

Actual Class	Training Cases	Testing Cases	Predicted Class		% correct
			Non-fault	Fault	
Non-fault	220	30	30	0	100
Fault	105	35	2	33	94

The classification results obtained with the PNN classifier is summarized in Table 5-III. According to the simulation results both fault transients and non-fault transients were classified 100 percent correctly by the PNN classifier.

Table 5-III : PNN based classification

Actual Class	Training Cases	Testing Cases	Predicted Class		% correct
			Non-fault	Fault	
Non-fault	220	30	30	0	100
Fault	105	35	0	35	100

The initial investigations carried out using the 12-bus test system showed the capability of developing a recognition system using the proposed approach [68]. In order to investigate the applicability of the proposed method for actual scenarios further investigations were carried out using the actual transmission system used for the prototype tested in chapter 4 [69].

5.3.2 Actual transmission system

As shown in Figure 5-9 the classifier was located on bus 9 to measure the current on one of the transformers connecting buses 9 and 10. The transients generated using PSCAD/EMTDC simulations were used to train the classifier. For this study, a total of 1044 fault and non-fault transients were used for training the classifier.

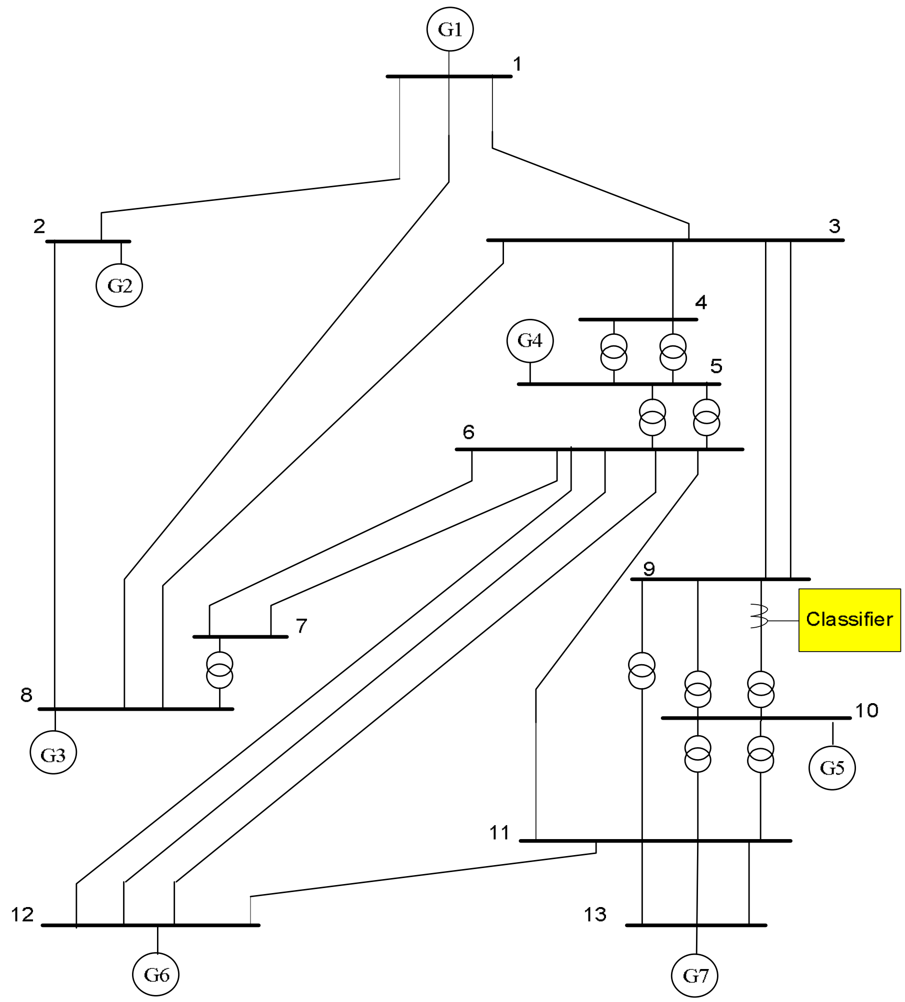

Figure 5-9 : Location of the transient classifier on 765/400/230kV transmission system

Validation of the Simulation Model

One of the recorded transient waveforms was used to fine tune the simulation model of the power system. Since the inputs for the proposed classifier are wavelet coefficients of the high frequency transients, it is important to ensure that the simulation is sufficiently accurate at the required frequencies. In order to verify the accuracy of the simulations at higher frequencies, the actual recorded transients were compared against the transients generated from the simulations. Figure 5-10 compares the wavelet coefficients of a recorded transient with the wavelet coefficients of the current signals obtained through simulating the same fault in PSCAD/EMTDC. The plots drawn with solid lines represent the transients corresponding to recorded signals while the plots drawn with broken lines represent the transients obtained from the simulated system. These results confirmed the fact that the simulation model is sufficiently accurate at the required frequency range.

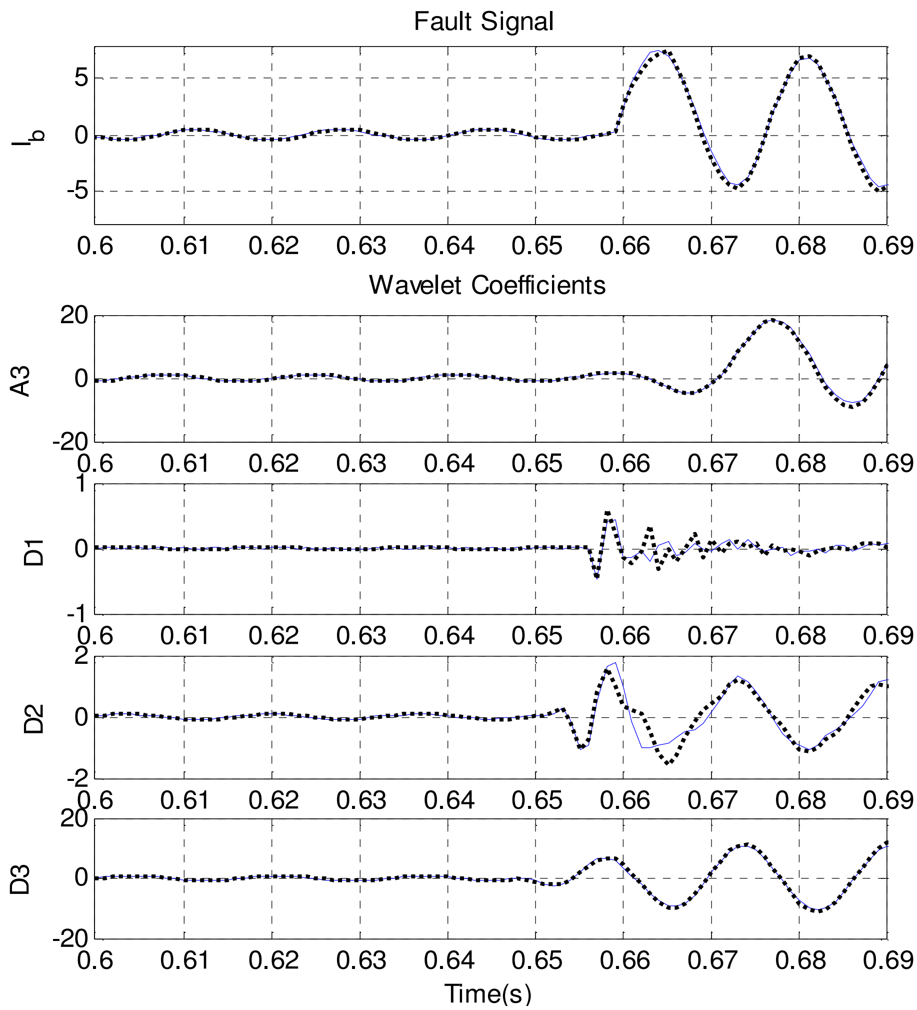

Figure 5-10 : Comparison of wavelet coefficients of the recorded and simulated current waveforms.

Classification Results

The classification results obtained for DT classifier is summarized in Table 5-IV. According to the simulation results, only 88% of the faults were correctly classified as faults whereas 94% of the non-faults were correctly classified as non-faults.

Table 5-IV: Classification results for DT

Actual Class	Number of events	Predicted Class		% correct
		Fault	Non-fault	
Faults	78	69	9	88
Non-faults	54	3	51	94

Table 5-V summarizes the classification results obtained for HMM classifier. According to these results, both classes have shown over 95% classification accuracies.

Table 5-V: Classification results for HMM

Actual Class	Number of events	Predicted Class		% correct
		Fault	Non-fault	
Faults	78	74	4	95
Non-faults	54	2	52	96

Table 5-VI shows the classification results obtained for PNN classifier. According to these results, the classifier shows close to 95 % overall accuracy in categorizing the faulty and non faulty disturbance.

Table 5-VI: Classification results for PNN

Actual Class	Number of events	Predicted Class		% correct
		Fault	Non-fault	
Faults	78	73	5	94
Non-faults	54	2	52	96

Effect of Noise

Simulations were carried out to investigate the effect of noise on the performance of the recognition algorithms. A uniformly distributed noise ranging form 30 dB to 60 dB was added into the current waveforms. The classifiers were re-trained with the noisy data and the classification accuracies were determined for the noisy testing data. The simulation results obtained are summarized in Table 5-VII. According to these results both HMM and PNN have shown a higher classification accuracy in comprison to that of DT classifier.

Table 5-VII: Overall classification accuracy with noisy data

Classifier	% correct
DT	85
HMM	91
PNN	90

Effect of Fault Location

Table 5-VIII: Classification result for disturbances originating close to the classifier

Classifier	No. of fault events in test set	No. of non-fault events in test set	% correct
DT	24	20	95
HMM	24	20	100
PNN	24	20	100

In this investigation, the effect of the location of transient event on the classification accuracy is analyzed. It is expected that transient events occurring at locations electrically close to the measurements point would be easier to recognize. In order to test this hypothesis, the classification accuracies for the transients originating in the region shown in Figure 5-11 were analyzed. The classification results obtained from all three classifiers for the events in this region are summarized in Table 5-VIII. According to these results both HMM and PNN classifiers showed 100% accuracy whereas, DT classifier showed only 95% accuracy.

The above results have shown that (i) the proposed feature set (wavelet energies) are satisfactory for classification of the transients and (ii) the PNN based method and HMM based methods are superior in distinguishing the fault transients form the non-fault transients compared to the DT classifier.

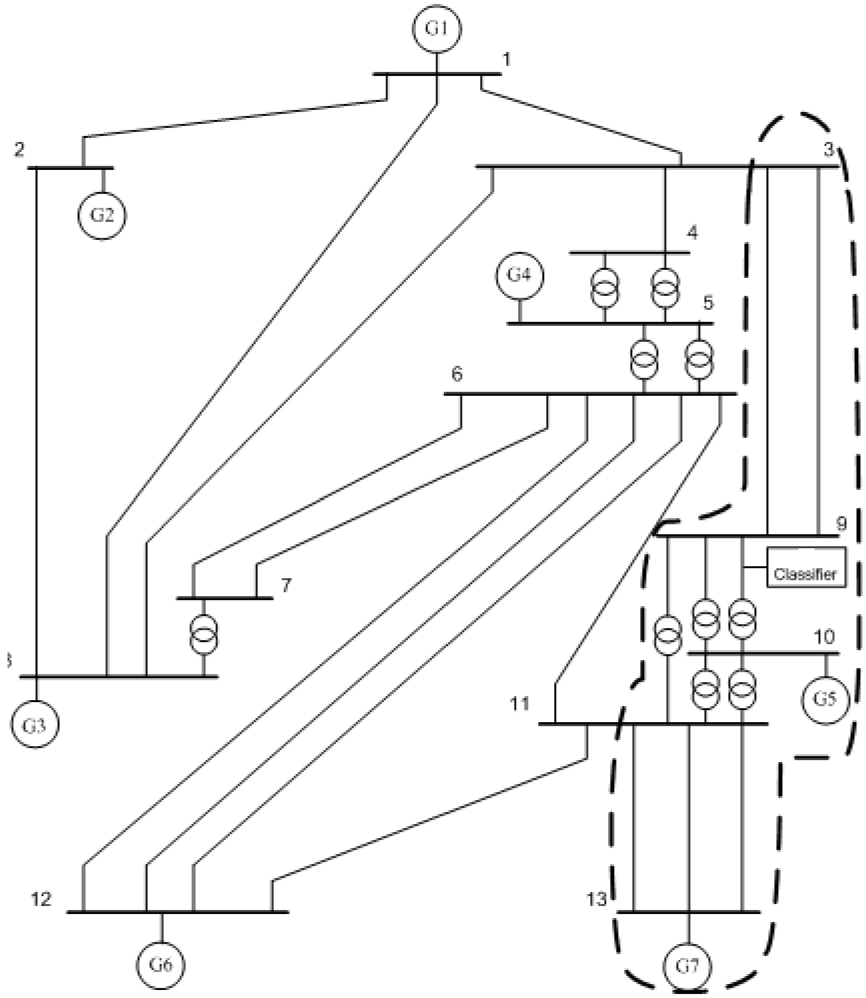

Figure 5-11 : Division of zones in transmission system

Although both PNN and HMM based classification schemes have shown encouraging results, the real-time implementation of PNN is challenging due to the large amount of computations involved in the classification algorithm depending on the size of training data set. On the other hand the HMM technique does not involve such a large amount of computations. Therefore the HMM based classifier was selected to be the most suitable method for prototype implementation for further testing.

5.4 Prototype Implementation

5.4.1 Structure

The structure of the HMM based fault recognition system is shown in Figure 5-12. In this thesis only one phase of the recognition system was implemented [70] to demonstrate the practicality.

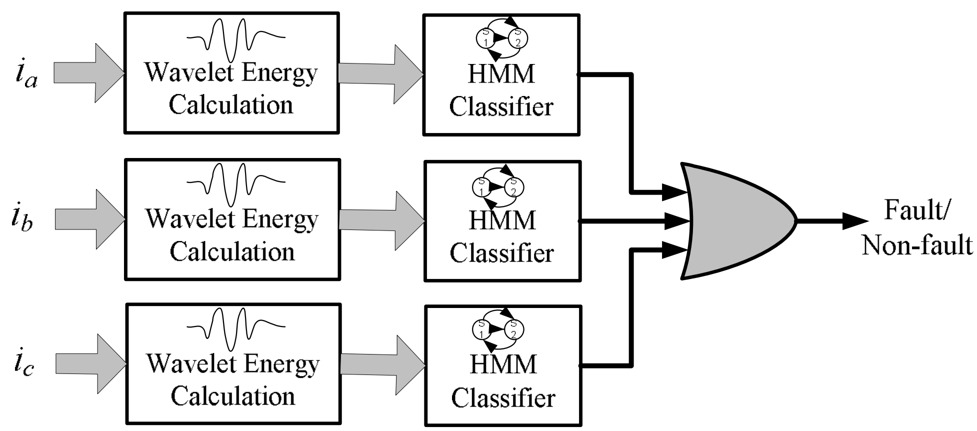

Figure 5-12 : Structure of fault recognition system

The real-time implementation of algorithms for transient recognition system (i.e. wavelet energy calculation and HMM classifier) is described below.

5.4.2 Wavelet Energy Calculation

In prototype implementation, the wavelet energies were calculated using (5.12) and (5.13). These equations were used to calculate the energies with less computational burden compared to the equations (5.1) and (5.2) used for off-line studies. The difference is due to the use of non-reconstructed approximation and detail wavelet coefficients, a_3 and d_i, in place of the reconstruction coefficients (CA_3 and CD_i) used in (5.1) and (5.2).

$$EA3 = \sum_{j=1}^{N3} \left| a_3(j) \right|^2 \tag{5.12}$$

$$EDi = \sum_{j=1}^{Ni} \left| d_i(j) \right|^2 ,i = 1,2,3 \tag{5.13}$$

Here, *EA3* is the energy of the approximated wavelet coefficients and *ED1*- *ED3* are the energies of the detail wavelet coefficients. When the Mallet algorithm is used for performing the discrete wavelet transform, non-reconstructed coefficients calculated at different levels have a different number of samples due to down sampling. On the other hand, reconstruction wavelet coefficients at all levels have the same number of samples within a given time window. Thus the lengths of the moving windows in terms of the number of sample points are denoted by *N1*, *N2* and *N3* in (5.13).

The implementation of the wavelet transform and the energy calculation algorithm is shown in Figure 5-13. The input signal is passed through the low pass and high pass filters implemented using the FIR module explained in Section 2.3.3. Since these filters need the past values of the input signals, *m* sampled values of the input signal (as well as the intermediate signals that goes in the filters) are stored in buffers, which are updated with the arrival of new values. The controller is used to select the appropriate input buffer and update corresponding output buffers.

The energy values; *EA3*, *ED1*, *ED2* and *ED3* were obtained through the amplification and direct summation of the squares of the decomposition wavelet coefficients stored in output buffers (sizes of *N1*-*N3*) as shown in Figure 5-13. The energy values determined during the disturbances were sent to the classification algorithm. In order to ensure the correct operation the classification system, the calculated wavelet energy values of different levels need to be properly aligned by time before inputting into the classification algorithm.

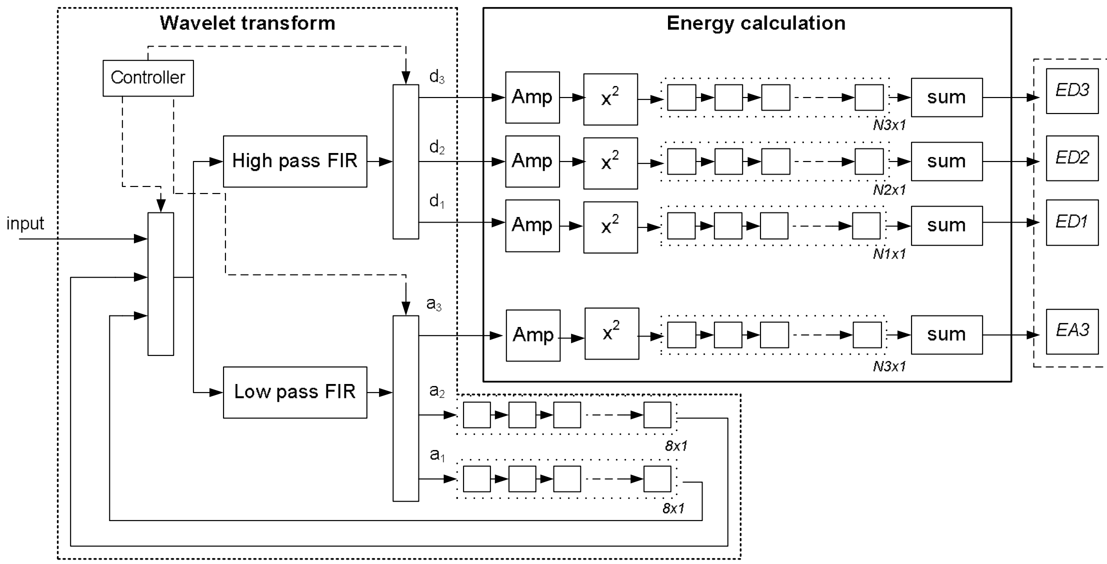

Figure 5-13 : Implementation of wavelet transform and wavelet energy calculation

5.4.3 HMM Classification

Parameters needed for two HMMs λ_F and λ_{NF} corresponding to faulty and non-faulty classes were estimated by the off-line training program found in [67] using the method explained in Section 5.2.2. In other words, the parameters a_{ij}, α_i, c_i^l, $\boldsymbol{\mu}_i^l$ and Σ_i^l corresponding to each HMM are determined for all i and l (i.e. $i = 1,2$ and $l = 1,2$). These parameters (estimated using the off-line program) were uploaded into the HMM classifier implemented on the hardware. When a new input vector consisting of wavelet energies (**E**=[*EA3*, *ED1*, *ED2,ED3*]) were presented to the classifier, the log likelihoods of the input vector belonging to each HMM (λ_F and λ_{NF}) were estimated. The results were then used to determine the most probable class using the classification criterion given by (5.10) explained in Section 5.2.2.

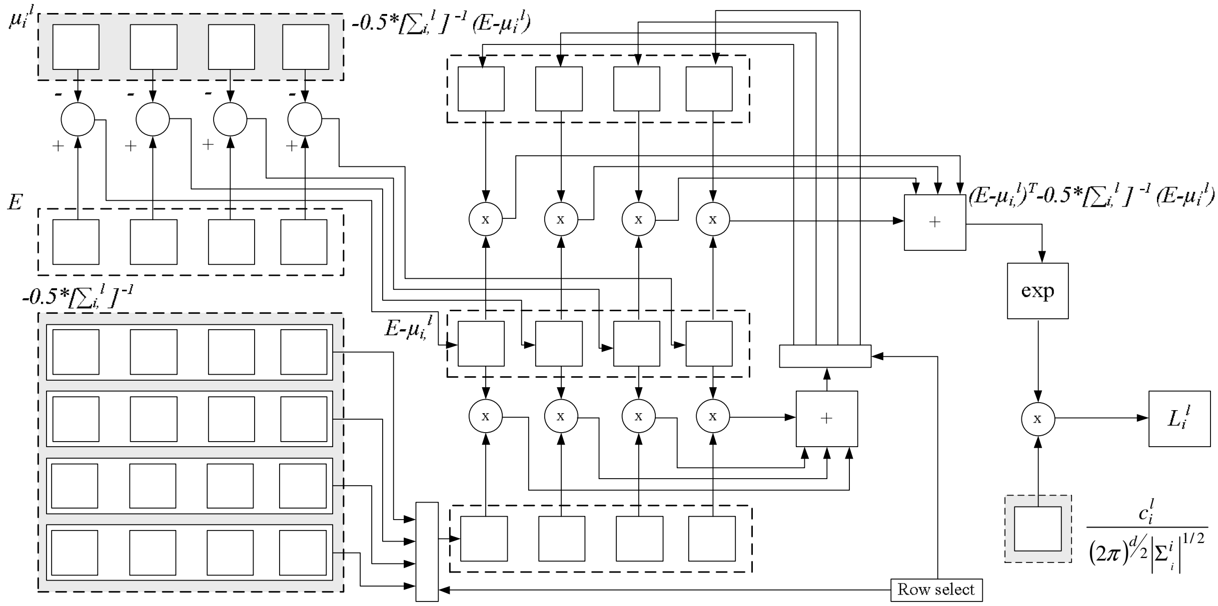

Figure 5-14 : Likelihood estimation

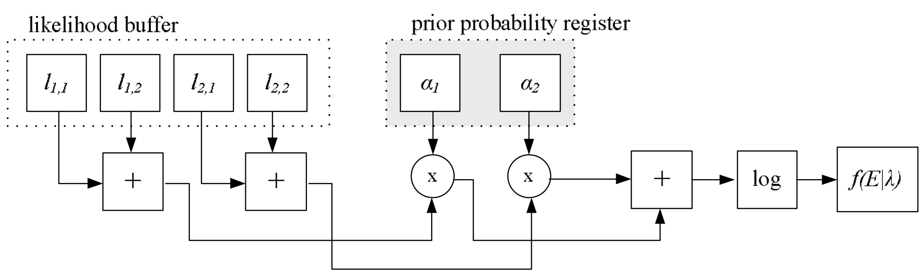

Figure 5-15 : Computation of log likelihood

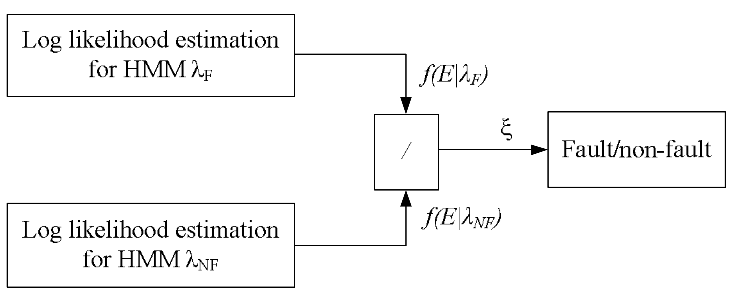

Figure 5-16 : Implementation of classification algorithm

The structure of the hardware module implemented for likelihood estimation described by (5.9) is shown in Figure 5-14. This module was repeatedly used to compute the likelihood parameters L_i^l (i = 1,2 and l = 1,2) for both HMMs using the parameters found during the training process. Then the log likelihood estimation given in (5.8) was implemented as shown in Figure 5-15. The estimated the log likelihoods for two HMMs are input to the module shown in Figure 5-16, which determines the classification criterion given in (5.10) to categorize the disturbance into the most probable class.

5.4.4 Digital Filtering

Simple low-pass R-C analog filters were used as the input side filter to band-limit the sampled signal to prevent the aliasing errors. The cut-off frequencies of the filters were set to half of the sampling frequency. These anti-aliasing filters only remove the high frequency component of the signal outside the sampling bandwidth, but they may also introduce errors into the high frequency components just inside the sampling bandwidth. This may significantly affects the magnitudes of the wavelet coefficients corresponding to the highest frequency band. In order overcome this problem, the highest frequency detailed wavelet coefficient was discarded. Thus the wavelet transform was performed up to level- 4, and the level-1 detail coefficients were discarded. The retained coefficients can be considered as wavelet coefficients of the first three levels, calculated at an effective sampling frequency that is equal to half of the original sampling frequency. Thus the actual sampling frequency used was two times the required value.

5.4.5 System Operation

The complete algorithm for the recognition system was implemented on the DSP hardware platform presented in chapter 4. It is capable of handling input/output (I/O) devices, wavelet energy calculation algorithm, transient detection algorithm and HMM classification algorithm. The transient detection was done by monitoring and comparing the wavelet energies with a threshold value. Figure 5-17 shows the system scheduler corresponding to the classifier implementation.

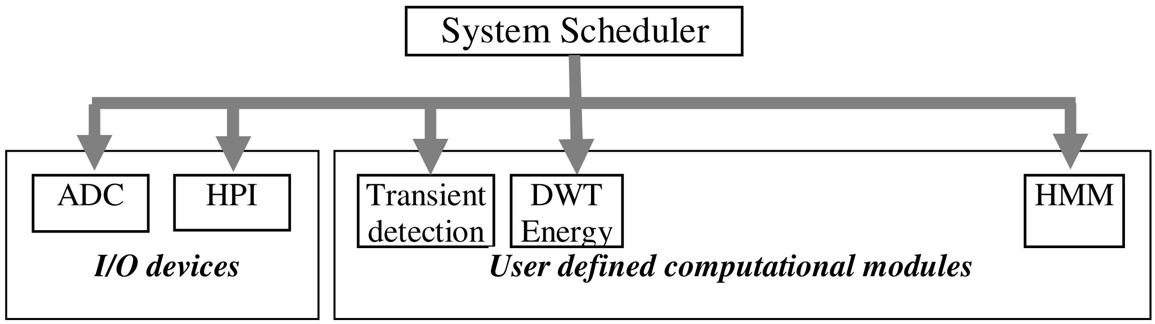

Figure 5-17 : System scheduler of the classifier

The operation of the DSP system for a sampling rate of 40 kHz is shown in Figure 5-17. The operating system was developed to measure the current, perform the DWT and calculate wavelet energies continuously. As shown in Figure 5-17 the ADC process is enabled at the beginning of each sampling period. The DWT energy is calculated at every second time step. The classification algorithm is enabled only when a transient is detected by the system. Thereafter the remaining processor time is fully used to run classification algorithm until the disturbance is categorized. The HPI signal is enabled at the end of the first ADC operation immediately followed by the completion of the classification algorithm. The operation is restarted again after a certain time period. The time delays, classifier operating time and waiting time shown here are used for illustration purposes only.

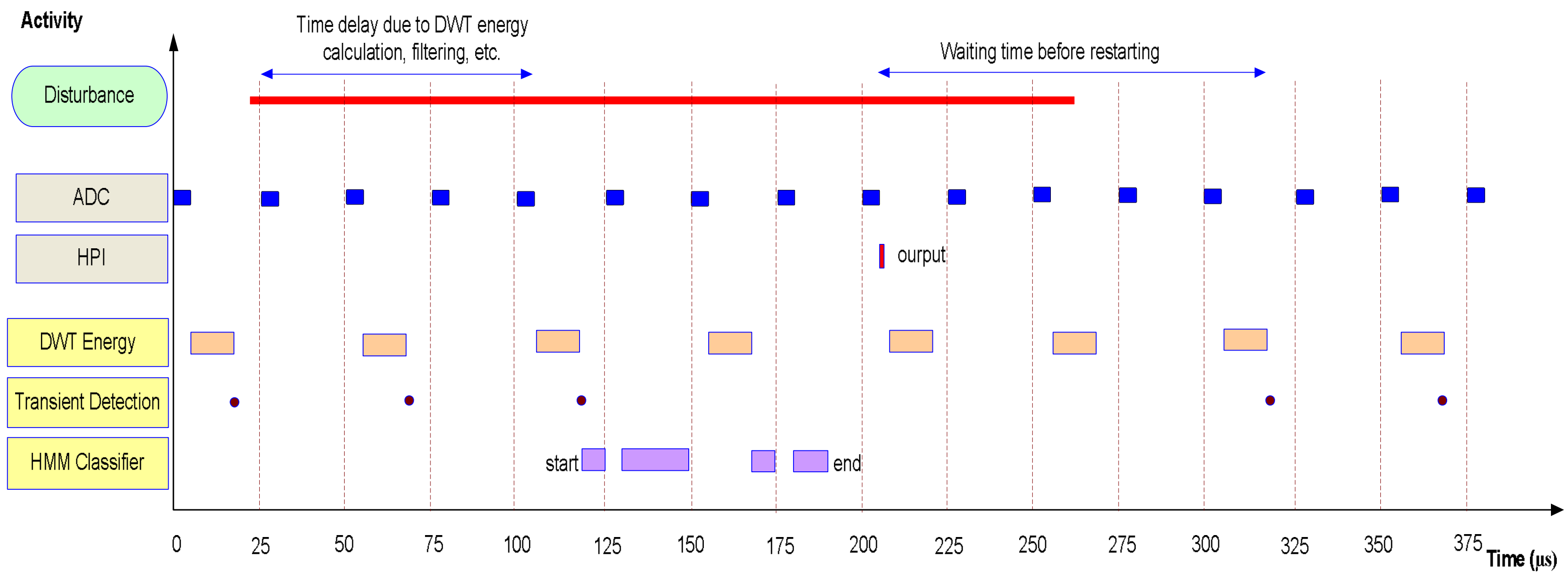

Figure 5-18 : Operation of the DSP system

5.5 Testing and Results

5.5.1 Test System

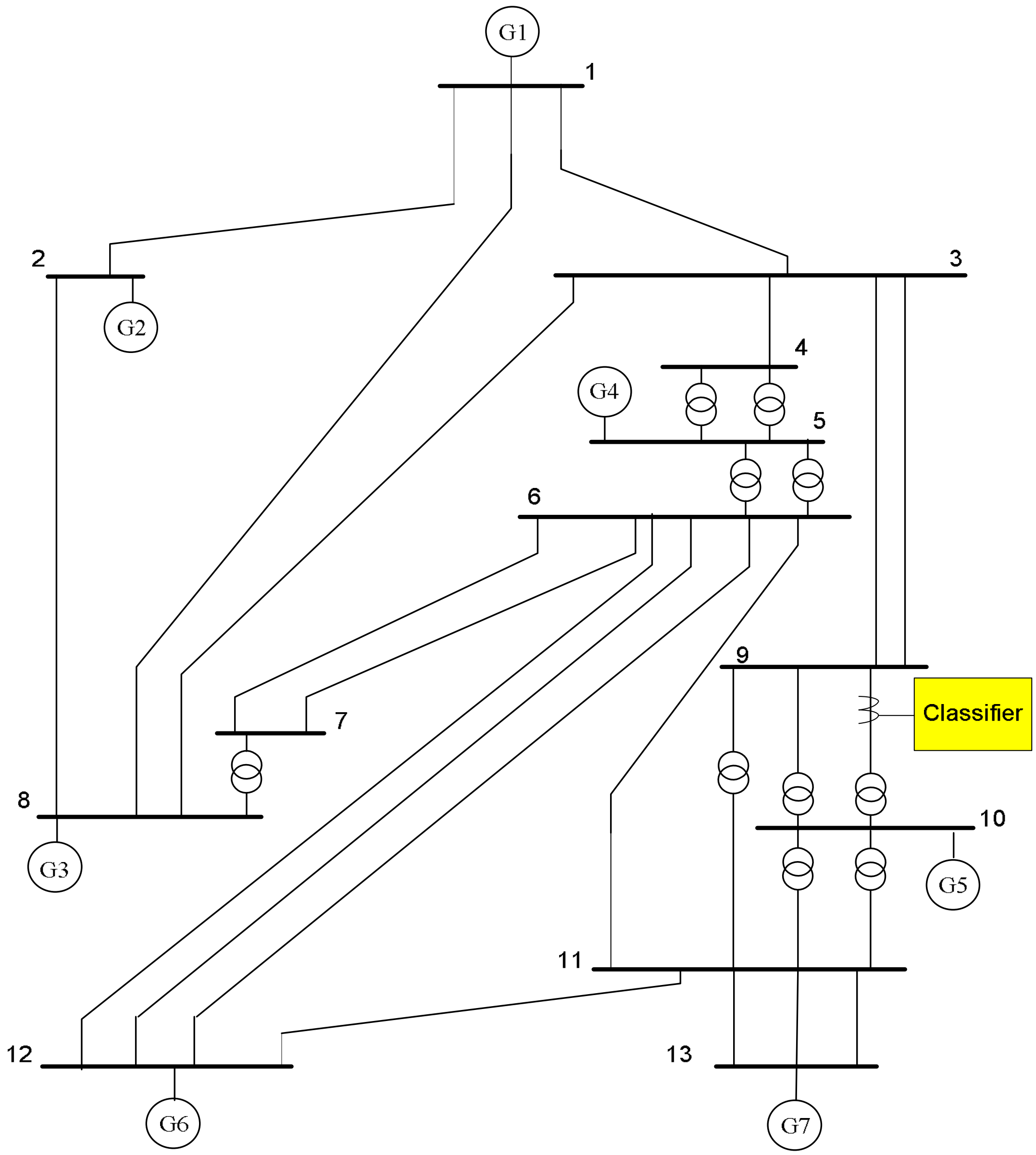

Figure 5-19 : Actual transmission system with classifier

In order to evaluate the performance of the classification system, investigations were carried out using the actual transmission system shown in Figure 5-19 simulated in

PSCAD/EMTDC. The location of the transient classifier was considered as bus 9. Three phase current signals were measured using the current transformers on the transmission line connecting buses 9 and 10. The recorded waveforms obtained using the simulations and actual fault recorders were played back using a waveform playback unit to verify the operation of the classifier.

5.5.2 Test Setup

Figure 5-20 shows the test interface of the hardware prototype. This is very similar to the test setup used in chapter 4. The RTP was used to playback the waveforms in real-time. The trip signal generated by the prototype was fed back to the RTP for recording purposes. The user interface for hardware prototype and RTP was provided using a personal computer. A digital oscilloscope was used to monitor the operation of the prototype. A sampling frequency of 20 kHz was used.

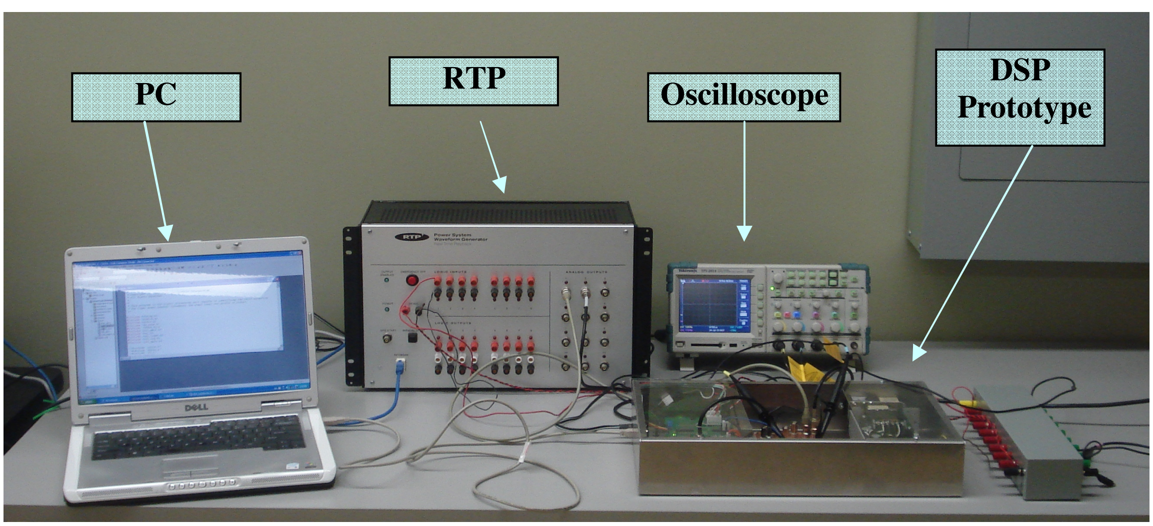

Figure 5-20 : Test setup

5.5.3 Validation

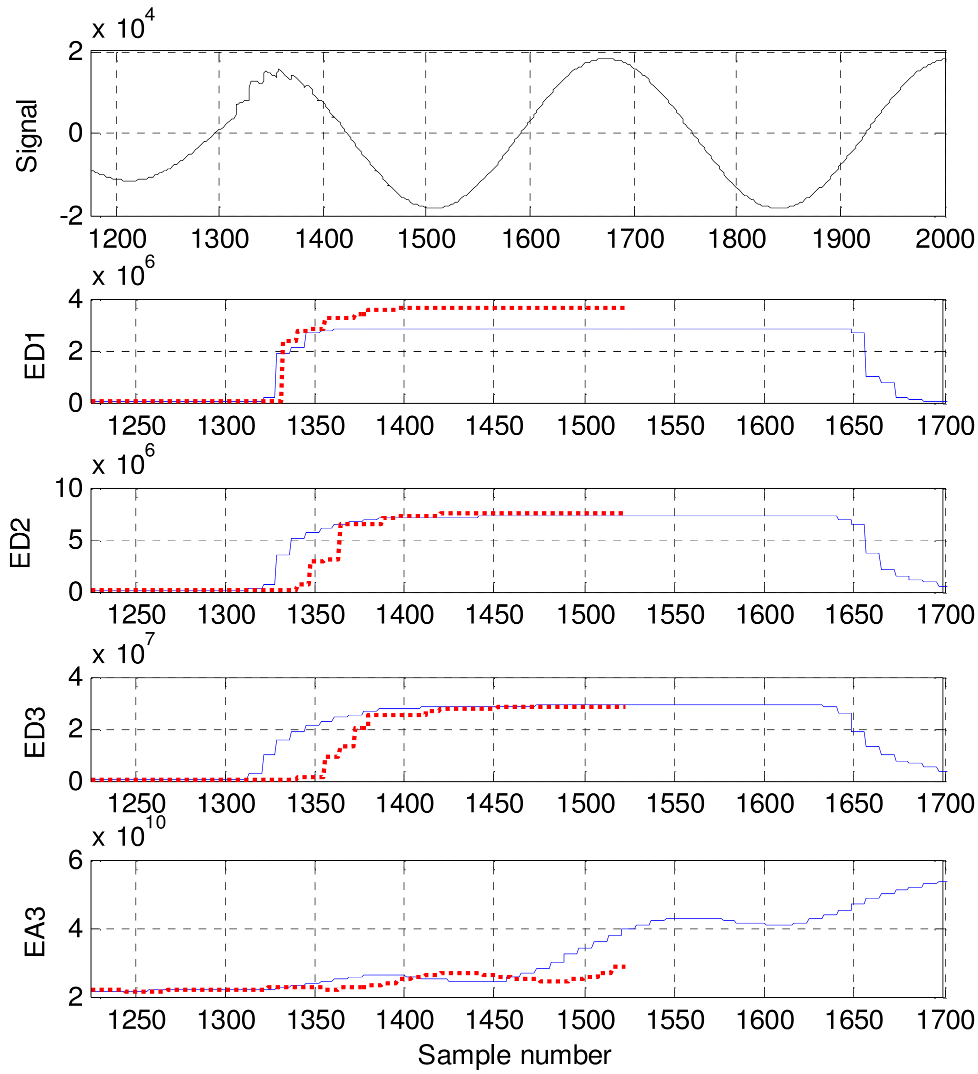

Figure 5-21 : Wavelet energies calculated using MATLAB simulation and DSP (blue continuous line – MATLAB calculations, red dotted line – DSP calculations)

In order to validate the real-time implementation of the wavelet energy calculation algorithm, the energy values calculated using the simulations were compared against the energy values obtained using the laboratory prototype. Figure 5-21 compares the energy values computed for a fault disturbance using a computer program implemented in MATLAB with those obtained from DSP for the same disturbance played back using RTP. The graphs show that the all the energy values except the level-1 match with each other, if the time shift observed in the case of DSP calculations is removed. These results confirm that the higher order energy values obtained from the simulation can be accurately obtained from real-time calculations.

5.5.4 Training and Testing Database

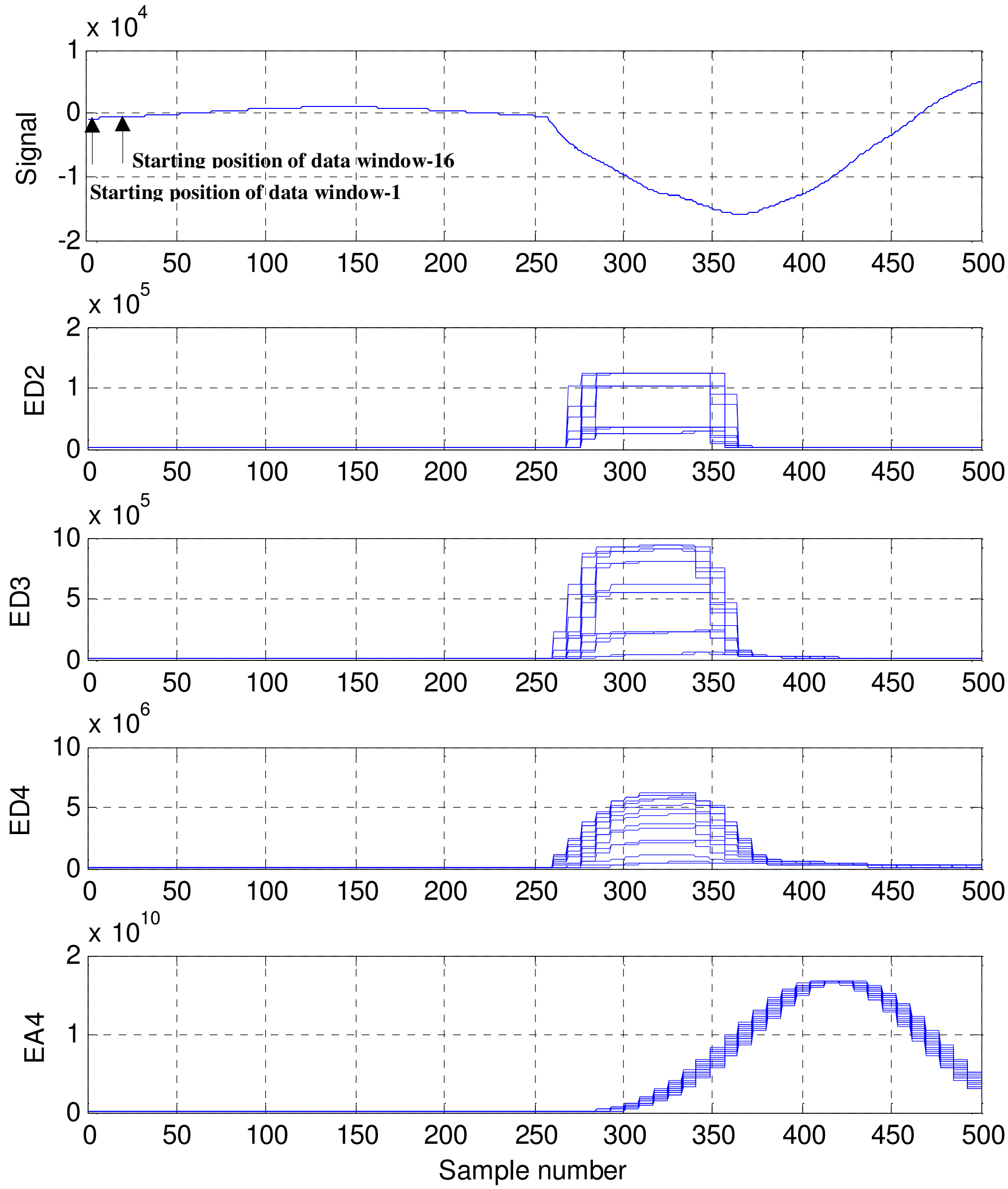

Figure 5-22 : Wavelet energy calculation starting at different positions on data steam

According to the 'Mallat filter bank implementation of DWT' the higher level coefficients are calculated after every second output of the preceding lower order coefficients (down sampling). Therefore changes in the starting position on the data stream can result in different set of DWT coefficient magnitudes; this ultimately results in different energy magnitudes. For example, Figure 5-22 shows the wavelet energies for a recorded disturbance. The different curves shown in the energy (EA4, ED2..ED4) plots are calculated with 16 different starting positions (initial position of the sliding data window) on the data stream. Thus a given input waveform can produce any combination of the wavelet energy waveforms shown in Figure 5-22, depending on the alignment of data windows with the samples. Therefore, in order to ensure the correct operation of the classification system, all possible energy values need to be included into the training database.

A total of 1,433 disturbances (1170 faults and 263 non-faults) were used to construct the training database. In this calculation all possible energy outputs corresponding to each disturbance was included. This resulted in a total of 22,928 data sets. This dataset was used to train the HMM classifier using an offline MATLAB program. The parameters obtained from the training are used in the real time classifier implemented on the DSP. Seventy disturbances (35 from each category) were used as the test database. In order to test the operation of the prototype, the test waveforms were played back using the RTP. The performance of classifier was investigated considering various practical scenarios such as measurement noise and CT saturation.

5.5.5 Operation of the Classifier

Figure 5-23 shows the operation of the classifier during a phase to ground fault recorded using the oscilloscope. The wavelet energies determined by the prototype scheme during the fault recorded by the DSP are also shown in Figure 5-24.

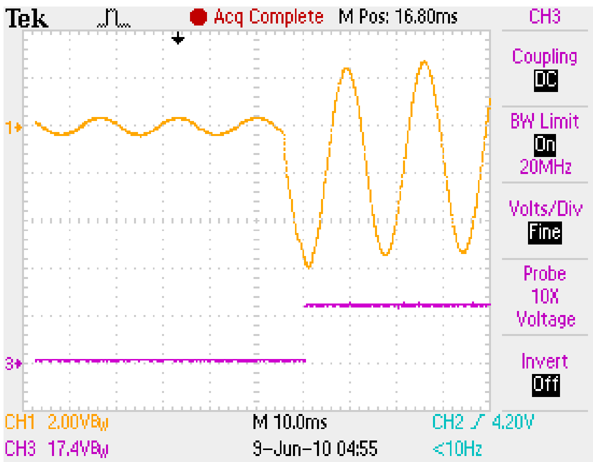

Figure 5-23 : Operation of the classifier during a phase to ground fault

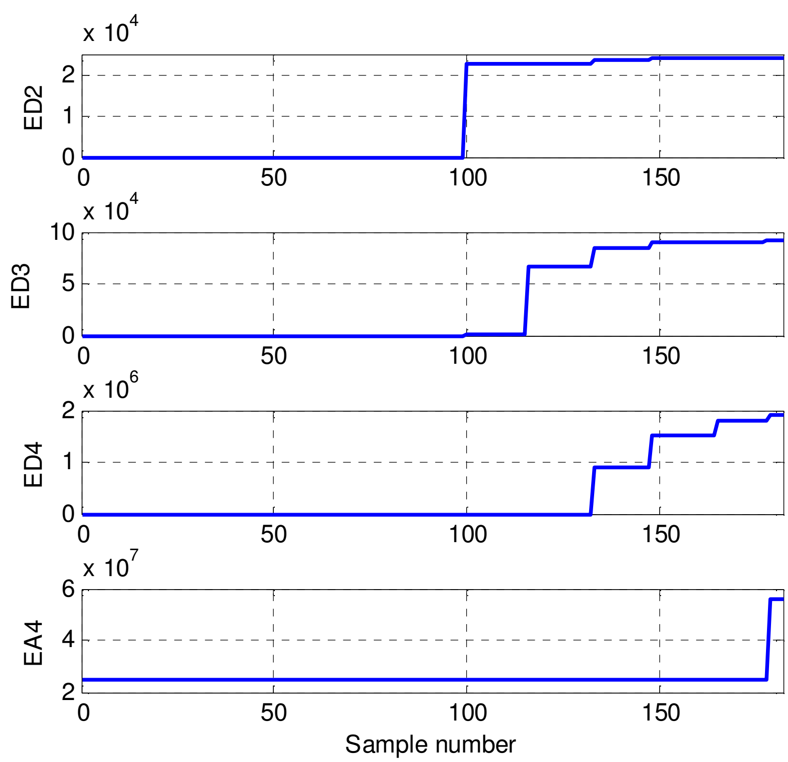

Figure 5-24 : Wavelet energies determined by the prototype during the fault

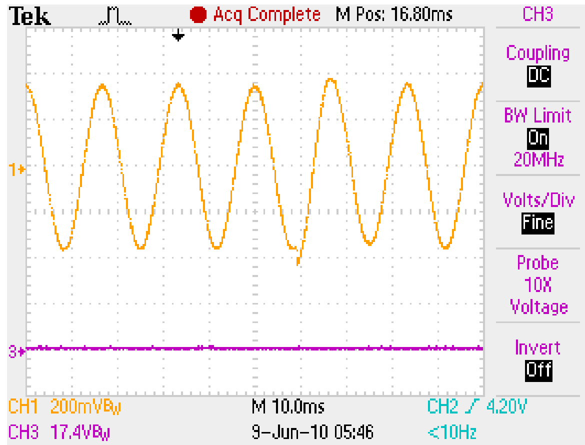

Figure 5-25 : Operation of the classifier during a switching disturbance

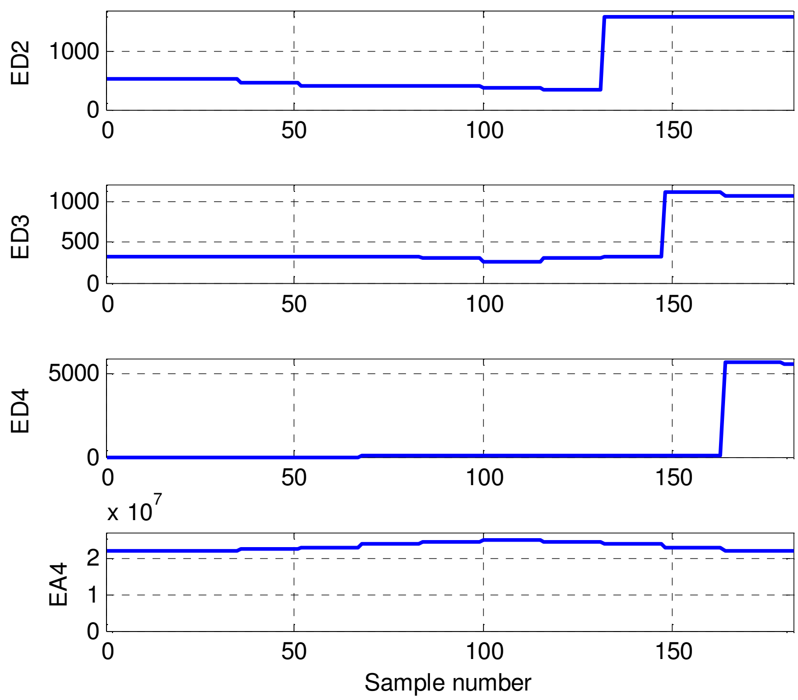

Figure 5-26: Wavelet energies determined by the prototype during the switching disturbance.

Figure 5-25 shows the operation of the classification system during a switching transient recorded using the oscilloscope. The wavelet energies determined by the prototype were recorded on the DSP and they are shown in Figure 5-26. These results show the correct operation of the hardware prototype during faulty and non-faulty conditions.

Table 5-IX: Classification results

Actual Class	Testing Cases	Predicted Class		% correct
		Fault	Non-fault	
Fault	35	31	4	88.6
Non-fault	35	0	35	100

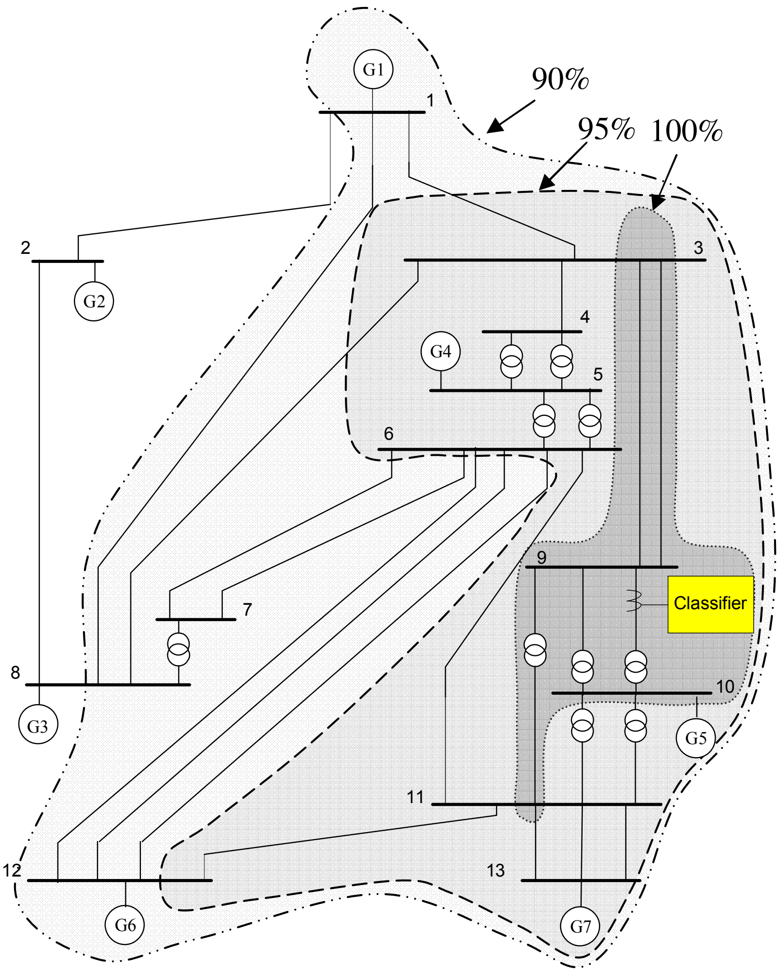

Figure 5-27 : Accuracy boundaries (100%, 95% and 90%)

In order to further investigate the performance of the hardware prototype, a number of fault and non-faulty disturbances were played back using the RTP. Table 5-IX summarizes the overall classification performance of the hardware prototype. According to the results obtained, all the non-fault transients were classified correctly; however, 4 out of 35 fault transients were misclassified as non-fault. Careful analysis showed that misclassified faults were those occurred at locations far from the location of the transient classifier. In order to illustrate the variation of classification accuracy with the location of a fault, accuracy boundaries were determined based on the test results. In Figure 5-27, these accuracy boundaries are superimposed on the network, and the diagram clearly shows that the classifier was able to correctly recognize all disturbances originating close to its location.

5.5.6 Operation during CT Saturation

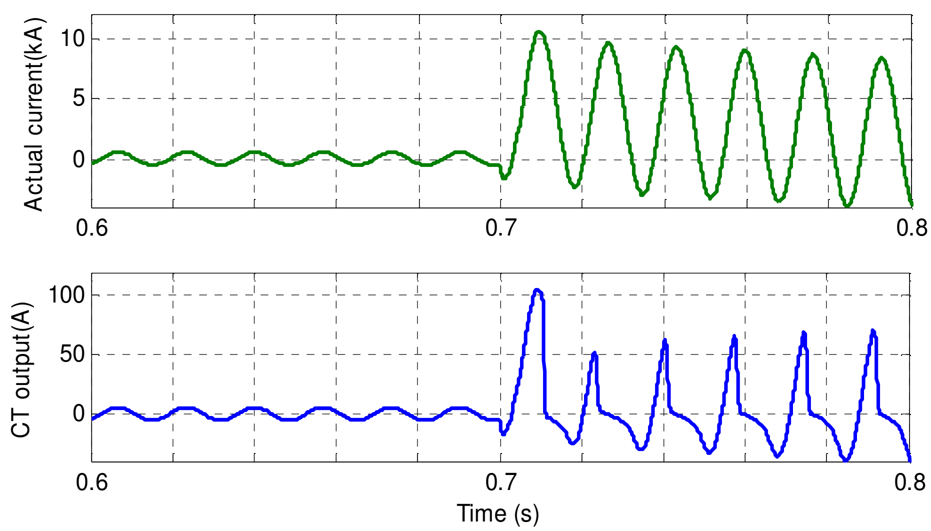

Figure 5-28 : Current waveforms during a CT saturation

The current transformer saturation is one of the major concerns that affect the operation of protection devices. In order to demonstrate the operation of this classification system during CT saturation, the CT on phase-A was intentionally saturated during a fault simulated on bus 9. Figure 2-28 shows the actual current signal and saturated current measurement. The operation of the classification system recorded using the oscilloscope is shown in Figure 5-29. It can be clearly seen from Figure 5-29 the transient classifier can recognize the fault using the initial transient which is observed well before the CT saturation occurs.

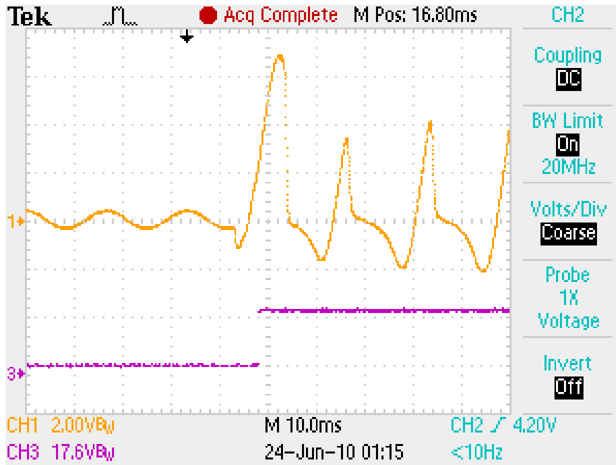

Figure 5-29 : Operation of the classifier during CT saturation

5.5.7 Verification Using Actual Transients

In order to verify the operation of the classification system during an actual transient, a recorded disturbance obtained from a fault recorder was played back using the RTP. Figure 5-30 shows the played back current waveform and the operation of the classifier recorded using the oscilloscope.

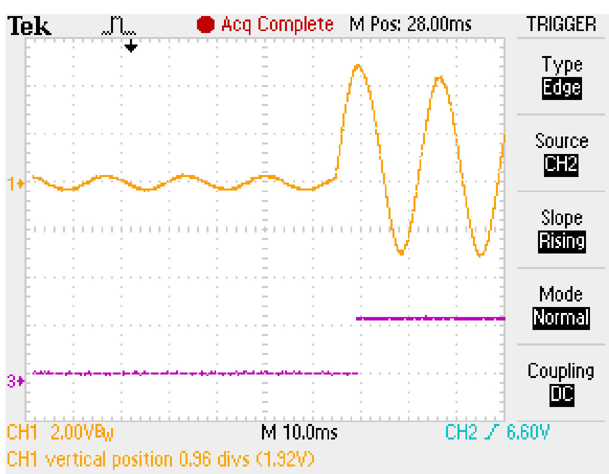

Figure 5-30 : Operation of the classifier during an actual transient

5.5.8 Effect of Measurement Noise

The use of high frequency sampling at 20 kHz can introduce noise into the measurements. In order to investigate the effect of noise, some noisy waveforms were played back using the RTP and the classification results are summarized in Table 5-X. The signal to noise ratios ranging from 30 dB to 60 dB was used. The faults simulated close to the classifier were selected for this study. According to the results presented in Table 5-X, all twenty faulty transients were correctly classified as faults whereas two out of twenty non-faulty transients were misclassified as faults.

Table 5-X: Classification result for classifier trained without noise

Actual Class	Testing Cases	Predicted Class	
		Fault	Non-fault
Fault	20	20	0
Non-fault	20	2	18

In order to make the recognition system more robust under noisy conditions, the classifier was re-trained using the wavelet energies determined under different noise levels. Table 5-XI shows classification results obtained using the classifier trained with the noisy data. These results show accurate operation of the classifier for both types of disturbances.

Table 5-XI: Classification result for classifier trained without noise

Actual Class	Testing Cases	Predicted Class	
		Fault	Non-fault
Fault	20	20	0
Non-fault	20	0	20

5.5.9 Effect of Changes in Network Configuration

Simulations were carried out to investigate the robustness of the proposed classification system to the changes in the network configuration. Both faulty and non-faulty events simulated for two different network configurations (the transmission line connecting buses 3-4 and the transformers connecting buses 4-5 were taken out) was tested using the previously trained classifier and the results are given in Table-5-XII. According to the results presented in Table-5-XII, the overall classification accuracy decreases for untrained network configurations. The majority of the misclassified events were originated from the nodes (buses 5 & 6) where the network configuration was changed. However the events inside the high accuracy region (shown in Figure 5-27) were properly classified.

Table 5-XII: Classification result for previously trained classifier

Actual Class	Testing Cases	Predicted Class	
		Fault	Non-fault
Fault	35	25	10
Non-fault	35	0	35

In order to make the classifier more robust under the changes in network configuration, the classifier was re-trained with a training dataset augmented with examples obtained with the altered network configurations. The classification results obtained using the modified classifier is presented in Table-5-XIII. These results show an improved performance after being re-trained with additional data.

Table 5-XIII: Classification result for modified classifier

Actual Class	Testing Cases	Predicted Class	
		Fault	Non-fault
Fault	35	32	3
Non-fault	35	0	35

5.5.10 Effect of Lightning Strokes

The effect of lighting strokes on the operation of the proposed technique was also investigated. The lightning transients were simulated assuming standard characteristic waveform [71]. The classifier was re-trained using a new training dataset that includes lightening transients. The lightning transients were categorized as non-faults. Offline testing showed that the trained classification system is capable of recognizing lightening strikes as non-faulty events.

Figure 5-31 shows the operation of the classification system during one of the lightning transients played back using the RTP. It should be noted that owing to bandwidth limitations in RTP, lightning transients cannot be played back with their entire frequency spectrum. However, since the input analog filters have a bandwidth of 0-10 kHz, the absence of these high frequency components in the played back signal would not make a significant effect on the classification performance. Also, further investigations have shown that, any fault resulting from and followed by a lightning stroke can be recognized as a fault using this system.

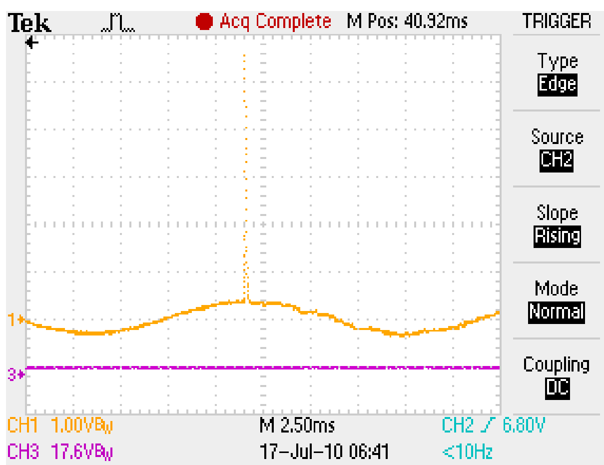

Figure 5-31: Operation of the classifier during a lightning transient

5.6 Modified Relay Arrangement

The transient classifier proposed in this chapter can be incorporated into the transient directional protection scheme proposed in chapter 3, as shown in Figure 5-32. The classification system uses one of the available three phase current signals as the input. Its output is sent to the decision making unit. The outputs of the decision making unit are supervised by the transient classifier so that trip signals are issued only when the transients are confirmed as originating from a fault.

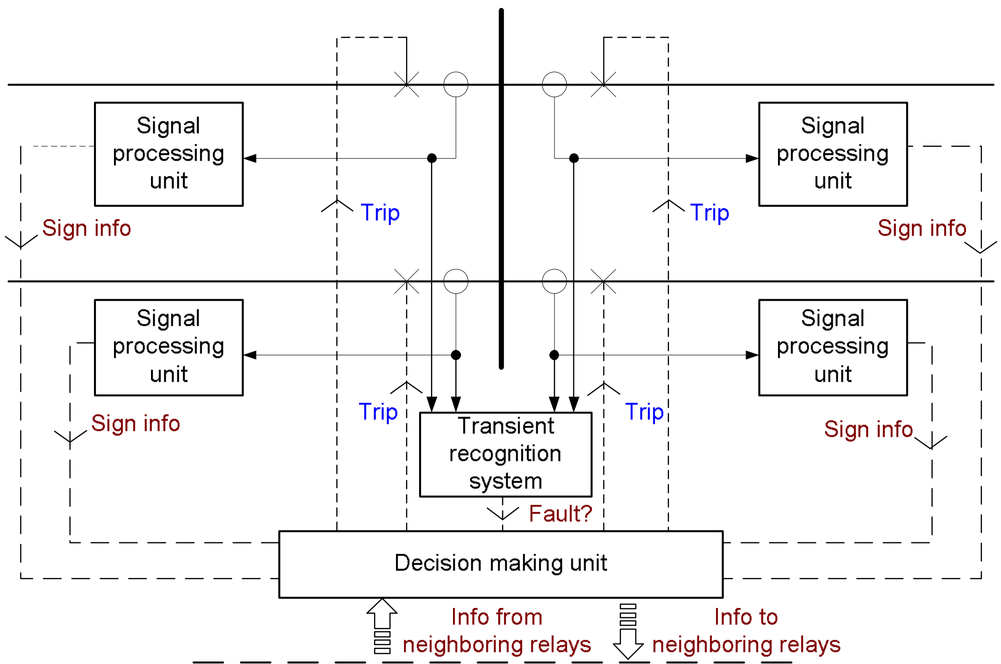

Figure 5-32: Modified arrangement of the relay agent with the transient classifier

5.7 Chapter Summary

In this chapter, a recognition system to distinguish transients originating from faults from those of non-faults was proposed. Applicability of three classification methods: Decision tree, Hidden Markov Model and Probabilistic Neural Network were investigated [68].

The energies calculated using the wavelet coefficients of current transients were used as the input features for the recognition system. Studies were carried out using two transmission system simulated in PSCAD/EMTDC. The results presented in this study showed the potential for implementing a fast and a reliable recognition system using the Hidden Markov Model technique.

A hardware prototype of the HMM transient classification system was implemented using a DSP platform. Investigations were carried out using an actual extra high voltage system simulated in an electromagnetic transient type simulation program. The performance of the hardware prototype was tested using the simulated and actual waveforms played back using a real-time signal playback unit under different scenarios such as measurement noise, current transformer saturation and lightning strokes. The results presented in this chapter have shown the capability of implementing a reliable fault recognition scheme using the proposed technique.

Chapter 6

Conclusions and Recommendations

6.1. Conclusions

In this thesis, a high speed transients based protection scheme for high voltage transmission networks was investigated. The investigation led to the following conclusions.

- Fault directions with respect to a busbar can be accurately determined by comparing the polarity of high frequency transients contained within the branch currents measured at the busbar. The wavelet transform can be successfully used to extract the high frequency transients to obtain the polarity components of the waveforms.
- A faulted section in a transmission system can be identified using the fault direction information determined at different nodes in the network. The information required to locate the faulted segment can be communicated only using logic signals, transmitted only to its neighbouring relays. The faulted segment identification can be achieved with simple logic using the exchanged

information. Information exchange can be achieved with simple telecommunication facilities similar to those used in transfer trip schemes.

- The high frequency transients originating from faults can be differentiated from those originating from the normal switching events using pattern recognition techniques. Energy associated with the wavelet coefficients of the currents are good features for transient classification. Investigations have shown that the hidden Markov model based classifier to be the most appropriate classification technique for this application.
- The proposed transient based protection scheme can be implemented on DSP based hardware. The modular implementation approach proposed in the thesis enabled development of the hardware prototypes of the signal processing unit and the transient classification system using a readily available DSP hardware platform.
- The tests conducted by playing back waveforms obtained from the simulations using a real time signal generator to verify the performance of the proposed protection scheme. The tests have shown that the protection scheme can correctly function under different practical scenarios such as current transformer saturation, changing fault impedance values, changing source to line impedance ratios, and different fault inception angles. The tests have also shown that increasing signal noise can affect the accuracy of fault transient recognition and fault direction identification.

- The results presented in this thesis clearly indicate the potential of developing a reliable transient based protection scheme for fast clearing of the faults in transmission systems using the proposed method.
- The bandwidth problem associated with measuring of high voltages using capacitive voltage transformers can be successfully circumvented by using only current signals for the proposed protection scheme.

The main contributions of the work presented in this report are as follows;

- Development of the transient directional protection methodology for a high voltage transmission system using wavelet coefficients of the current transients.
- Development of a modular approach that makes the implementation of the protection scheme more practical.
- Implementation of the EMT type simulation models required to investigate the performance of the proposed protection scheme, including many custom models.
- Design of a suitable hardware platform for implementing the protection algorithms, and implementation of the hardware prototype of the transient directional protection scheme.
- Development of an instrumentation setup and conduct of extensive verification test using recorded waveforms.
- Development of a fault recognition system to block the operation of the transient based relays due to transients not related to a fault.
- Implementation of the fault recognition algorithms on hardware and testing the prototype using recorded waveforms.

These contributions have led to the following publications;

Journal papers

- N. Perera and A.D. Rajapakse “Series compensated double circuit transmission line protection using directions of current transients”, *IEEE Trans. on Power Del.* (Under review).
- N. Perera and A.D. Rajapakse “Design and hardware implementation of a modular transient directional protection scheme using current signals”, *IET Generation, Transmission and Distribution*, vol.6, no. 6, 2012, pp.554 - 562.
- N. Perera and A.D. Rajapakse “Development and hardware implementation of a fault recognition system”, *IEEE Trans. on Power Del.,* vol. 27, no. 1, Jan. 2012.
- N. Perera and A.D. Rajapakse “Recognition of fault transients using a probabilistic neural-network classifier”, *IEEE Trans. on Power Del.*, vol. 26, no. 1, Jan. 2011.

Conference papers

- N. Perera, A.D. Rajapakse and D. Muthumuni, “Wavelet based transient directional method for busbar protection”, *International Conference on Power Systems Transients (IPST)*, Delft, The Netherlands, Jun. 2011.
- N. Perera, A.D. Rajapakse, and A.M. Gole, "Real-time implementation of wavelet transform for transient type protection applications", *IEEE EPEC 2010*, Halifax, NS, Canada, Aug. 2010.
- N. Perera, A.D. Rajapakse, D. Muthumuni and R. Jayasinghe, "On-line probabilistic neural network classifier in EMTP environment for fault

classification", *International Conference on Power Systems Transients (IPST)*, Kyoto, Japan, Jun. 2009.

- N. Perera and A.D. Rajapakse, "Power system transient classification for protection relaying", *13th IEEE International Conference on Harmonics and Quality of Power (ICHQP)*, Wollongong, New South Wales, Australia., pp. 1-6, - Oct. 2008.

6.2. Recommendations for Future Work

As an extension of this thesis, further research is recommended in the following areas;

- Applicability of the proposed faulty segment identification method needs to be further investigated for complex transmission systems that include power electronic elements such as thyristor-controlled series capacitors (TCSC), thyristor-controlled series reactor (TCSR), etc..
- The proposed fault direction identification fails to identify fault directions, if there are only two lines connected to a particular busbar. As explained in Chapter-3, Section 3.4.4, this is not a significant disadvantage because the faults in such situations can be cleared from remote ends without interrupting additional loads. Nevertheless, finding a method to determine the directions when only two branches are connected to a node has benefits such as simplification of logic and reduced communication delays.
- Transients observed on open branches or branches with very light loads tend to have lower magnitudes. This sometimes makes it difficult to accurately determine

the fault directions. This issue need to be further investigated to find a suitable solution.

- In this thesis, a pattern recognition method (developed based on the hidden Markov model classification technique) was proposed to discard non-faulty transients from faulty transients. Although the results showed a good classification accuracy, further research is required to validate the robustness of the classifier under different events such as temporary faults, auto-reclosure operations, etc..

Appendix - I

IEC 61850 Architecture

This is a standard for substation automation. The standard aims to promote the interoperability and integration of automation devices from different suppliers [29], [43]. The standard defines data representations and facilitates digital communication, i.e. the use of station LAN, for transferring signals including circuit breaker trip signals. This significantly lowers the cost of installation, maintenance and configuration of protection and control equipment (intelligent electronics devices - IEDs) in comparison to the traditional wire connections between the devices. Figure 6-1 shows the concept in a very simplified manner. Simple descriptions of the various terms are also provided.

Merging Unit

Merging unit has the task of converting the analog signals to sampled values that can be transmitted to intelligent electronic devices (IEDs).

Intelligent Electronic Device (IED)

An Intelligent Electronic Device (IED) is a microprocessor-based controller such as a circuit breaker, a protection relay, etc..

Process Bus

The process bus transfers the sampled values of voltages/currents and status signals such as circuit breaker status, etc. between IEDs. The IEDs in substation can use this information.

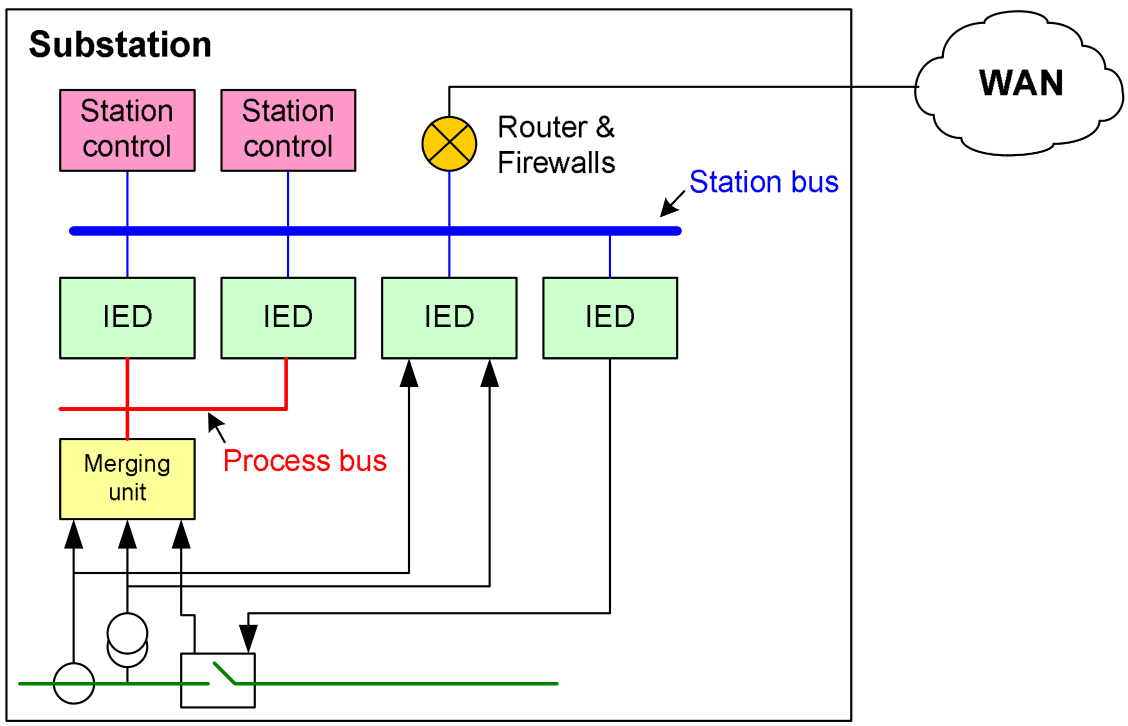

Figure 6-1: IEC 61850 structure

Station Bus

Station bus facilitates high speed pear to pear messaging and multicasting. Layered mapping (TCP/IP) is used for data acquisition and control.

GOOSE Messaging

Generic Object Oriented Substation Events (GOOSE) is a control model mechanism in which any format of data (status, value) is grouped into a data set and transmitted within a time period of 4 milliseconds.

The following mechanisms are used to assure specified transmission speed and reliability;

- GOOSE data is directly embedded into Ethernet data packets and works on publisher-subscriber mechanism on multicast or broadcast MAC addresses.
- GOOSE uses Virtual LAN and priority tagging to have separate virtual network within the same physical network and sets appropriate message priority level.
- The same GOOSE message is retransmitted with varying and increasing retransmission intervals. A new event occurring within any GOOSE dataset element will result in the existing GOOSE retransmission message being stopped. A state number within the GOOSE protocol identifies whether a GOOSE messages is a new message or a retransmitted message.

GSSE Messaging

Generic Substation State Events (GSSE) is an event transfer mechanism. Only Status data can be exchanged through GSSE and it uses a status list (string of bits) rather than the dataset used in GOOSE. GSSE message is transmitted over MMS based stack (base stack without using TCP/IP).

Appendix - II

System Parameters

Table 6-I: Branch Data [45]

Line	Voltage (kV)	Length (km)	R(pu)	X(pu)	B(pu)	Rating (MVA)
1-2	230	100	0.01144	0.09111	0.18261	250
1-6	230	300	0.03356	0.26656	0.55477	250
2-5	230	300	0.03356	0.26656	0.55477	250
3-4 (1)	230	100	0.01144	0.09111	0.18261	250
3-4 (2)	230	100	0.01144	0.09111	0.18261	250
4-5	230	300	0.03356	0.26656	0.55477	250
4-6	230	300	0.03356	0.26656	0.55477	250
7-8	345	600	0.01595	0.17214	3.28530	500

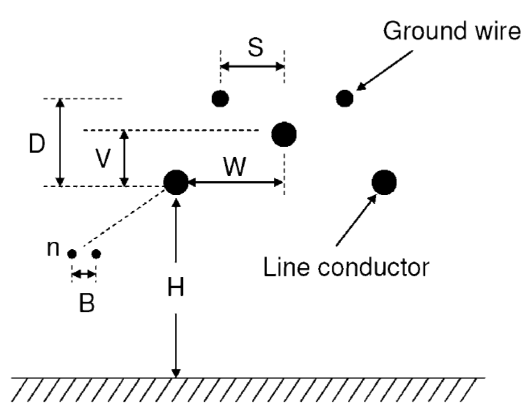

Figure 6-2 : Transmission line structure [45]

Table 6-II : Configuration of the transmission line [45]

Voltage (kV)	230	345
Structure	3H6	2H6
H (m)	14.4	17.5
V (m)	1.22	3.51
W (m)	5.49	7.93
sag	5.94	7.25
N (Conds/bundle)	1	2
B (m)	0.4572	0.4572
Conductor type	954ACSR 54/7	795ACSR 26/19
DC resistance (ohms/km)	0.0587	0.0683
Ground wires	2	2
S (m)	3.05	4.65
D (m)	3.81	5.00
Ground resistively (ohm*m)	100	100
Sag of GW (m)	4.45	7.25

Table 6-III : Bus Data [45]

Bus	Nominal voltage (kV)	Specified voltage (kV)	Load (MVA)	Shunt (MVAr)	Generation (MW)
1	230				
2	230		280+j200		
3	230		320+j240		
4	230		320+j240	160	
5	230		100+j60	80	
6	230		440+j300	180	
7	345				
8	345				
9	22	1.04			
10	22	1.02			500
11	22	1.01			200
12	22	1.02			300

Appendix - III

DSP Platform

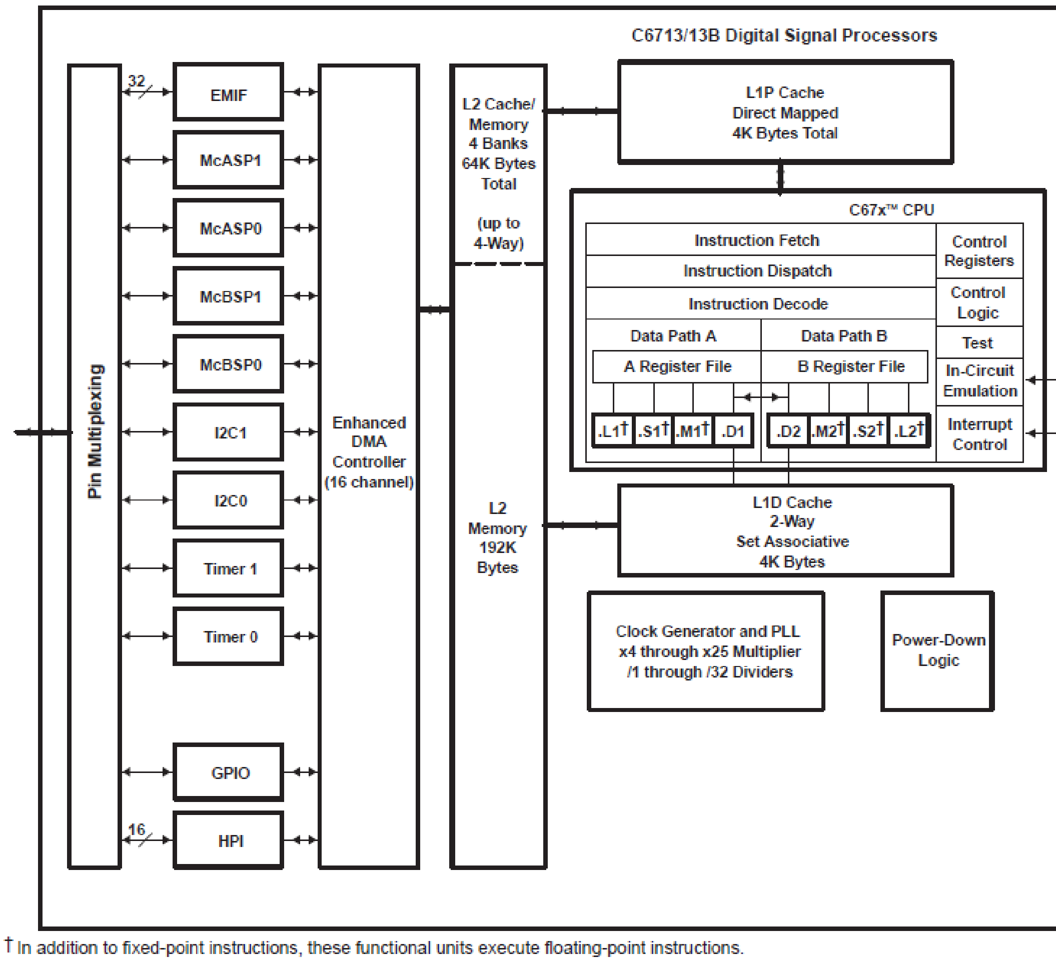

Figure 6-3 : Functional blocks of TMS320C6713 DSP [49]

ADS8364M EVM

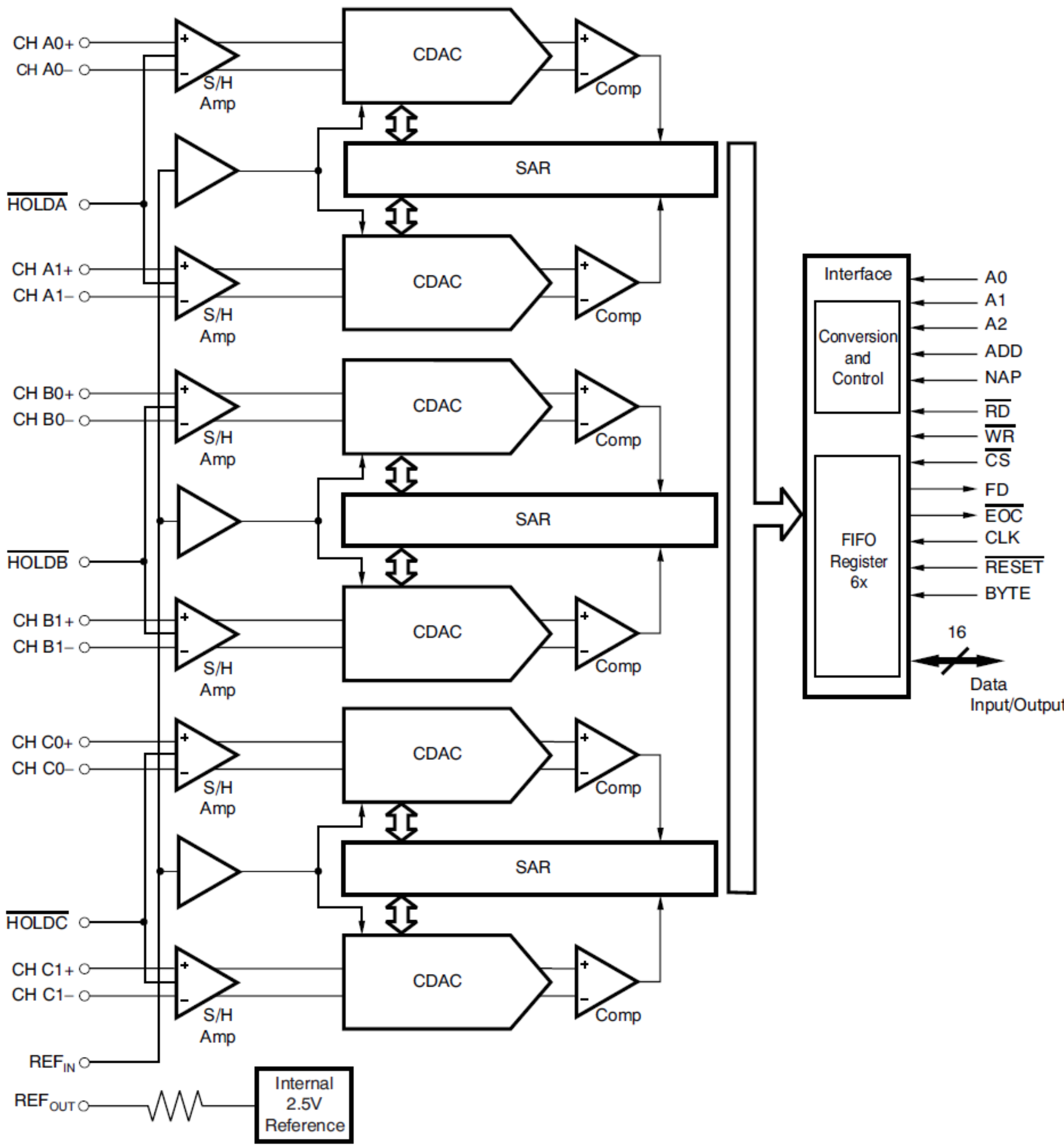

Figure 6-4 : Functional blocks of ADS8364 [50]

5/6K Interface Board

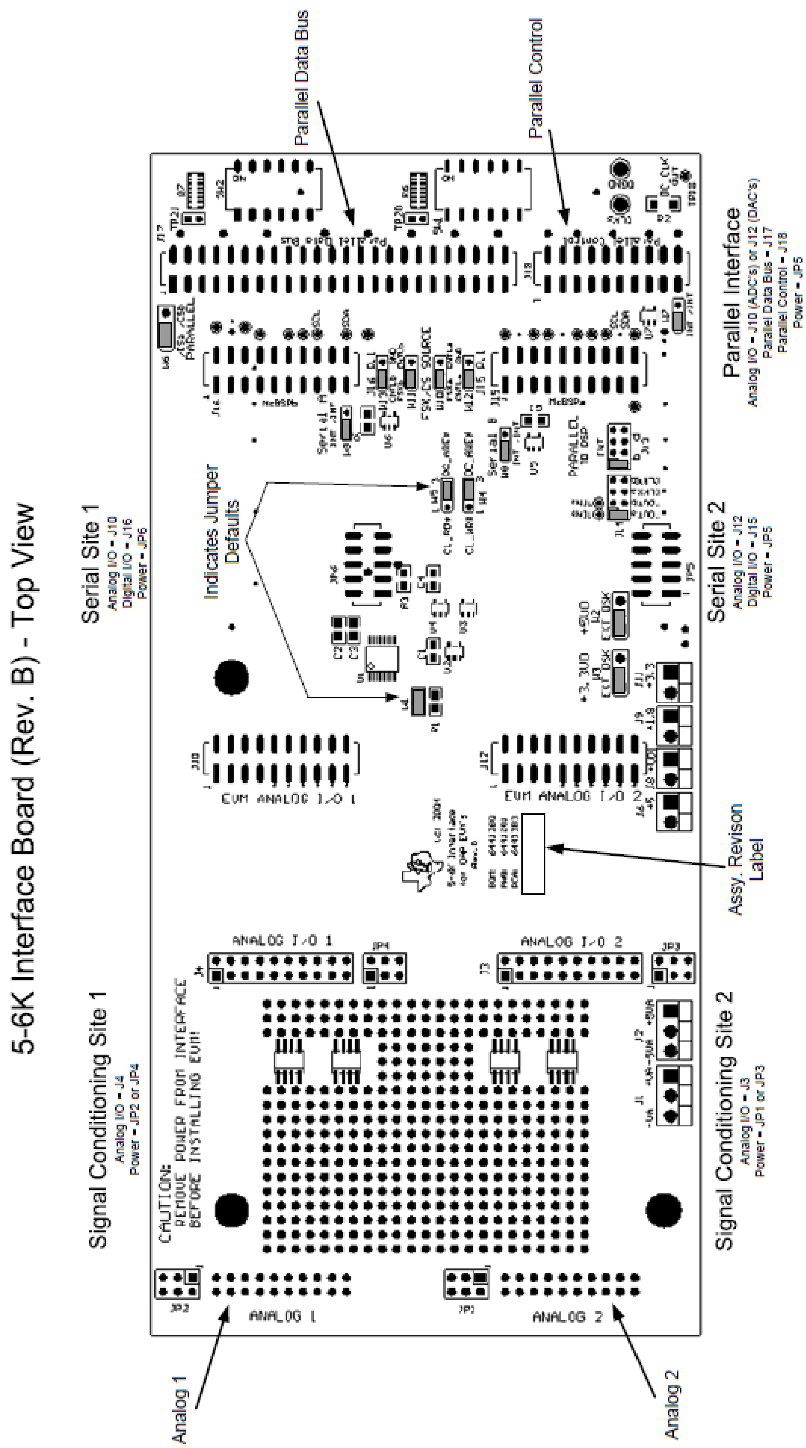

Figure 6-5 : 5/6K interface board [51]

Signal Conditioning Unit

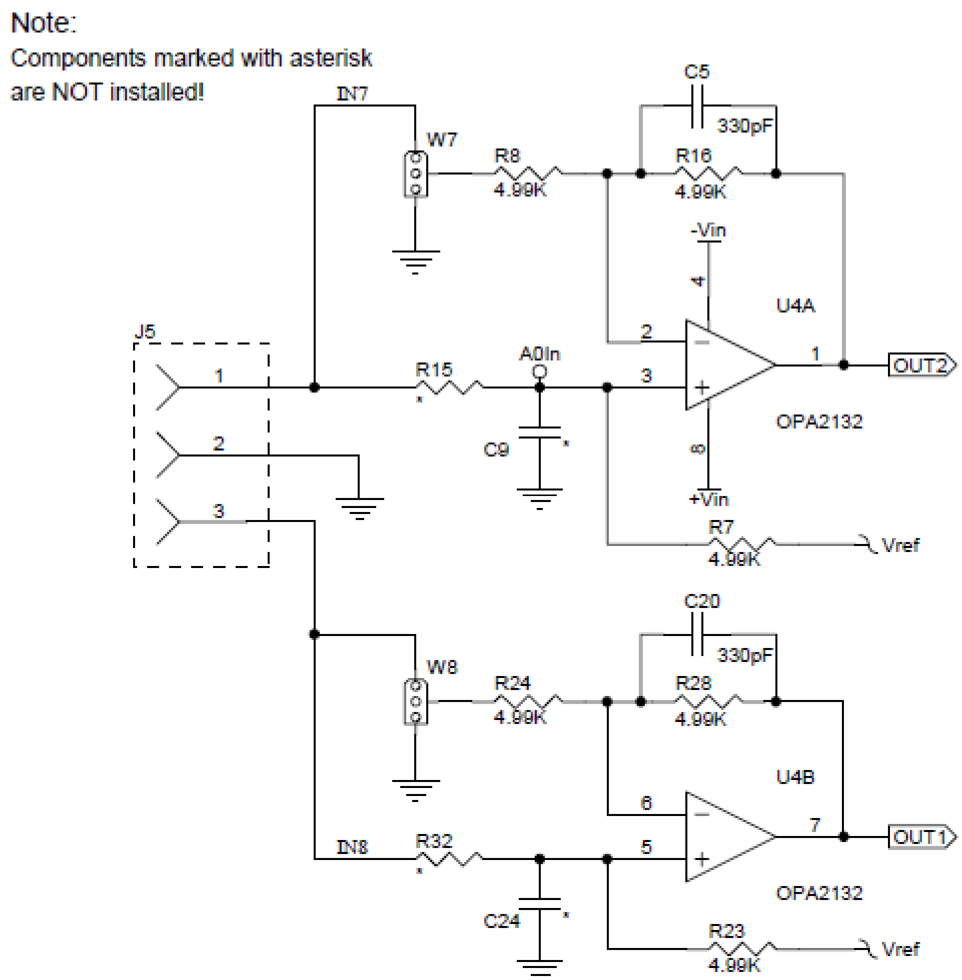

Figure 6-6 : Channel configuration of signal conditioning unit [52]

Specification of Power Supply

Table 6-IV : Specifications of Power Supply [72]

Family	AC DC Converters
Series	International Linear
Voltage - Output	5V, ±12 ~ ±15V
Number of Outputs	3
Power (Watts)	22W
Applications	Commercial
Power Supply Type	Linear, Regulated (Open Frame)
Voltage - Input	100, 120, 240VAC
Mounting Type	Chassis Mount
1st Output	5 VDC @ 2A
2nd Output	12 ~ 15 VDC @ 400mA
3rd Output	-12 ~ -15 VDC @ 400mA

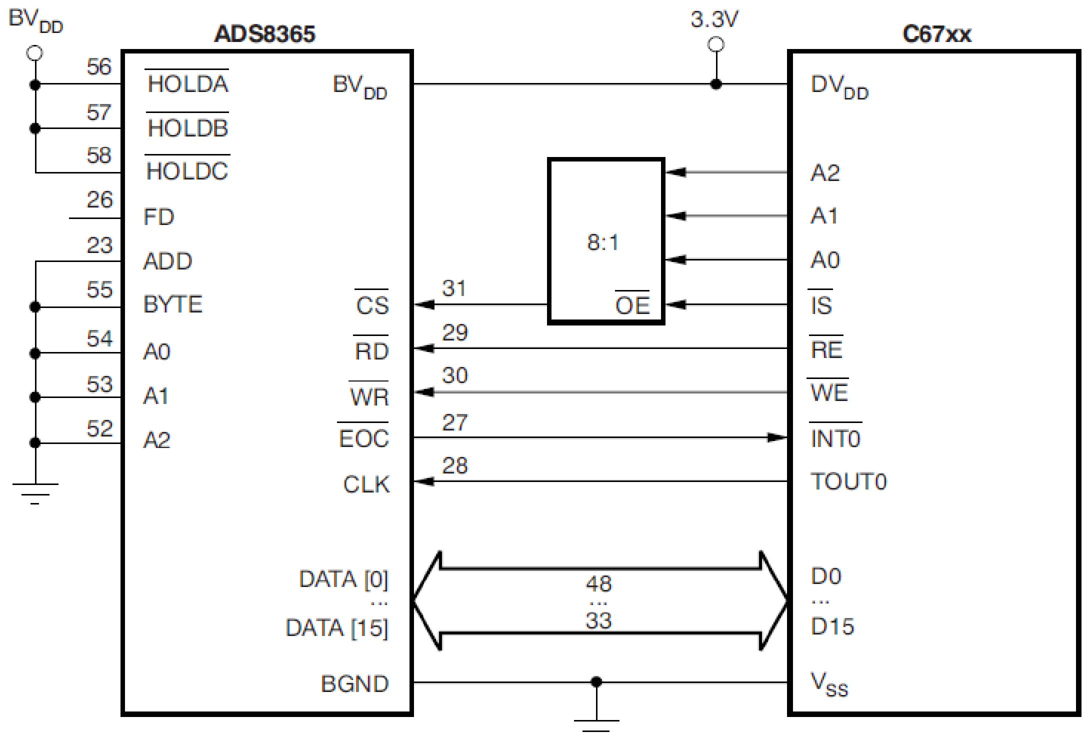

Figure 6-7 : Typical C67xx Connection (Software Control) [73]

Appendix - IV

Prototype Validation

In order to validate the accuracies of the hardware platform, algorithm for wavelet transform was implemented and compared against off-line calculations in MATAB [55].

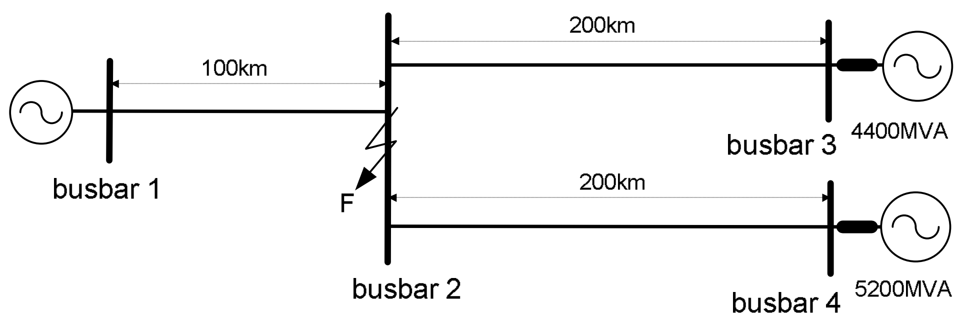

Figure 6-8 : Test network

The 230 kV, transmission network shown in Figure 6-8 was used to generate the transient waveforms required for testing. Specifications of the network are given in the Appendix. A fault was applied at busbar 2 and the measured current at busbar 2 on the transmission line connecting busbars 1 and 2 (Figure 6-8) was recorded and transferred to the RTP. This signal was played back to the DSP based wavelet analyzer via the RTP. Figure 6-9 shows the hardware setup for prototype validation. A photograph of the test setup is shown in Figure 6-10.

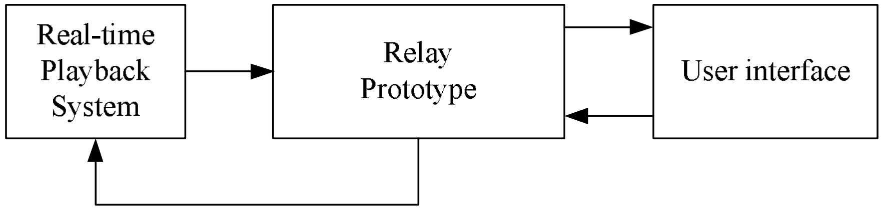

Figure 6-9 : Test setup for prototype validation

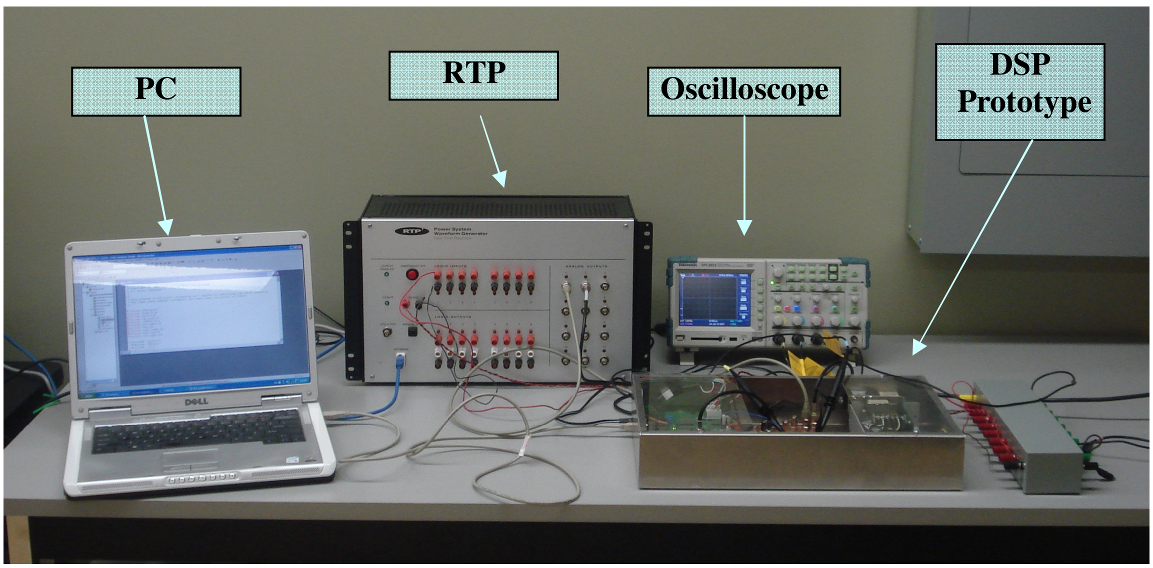

Figure 6-10 : Test setup

Figure 6-11 shows the sampled waveforms and its wavelet decompositions calculated in real-time using a 'Db4' mother wavelet using a sampling frequency of 40 kHz. The detailed wavelet decompositions from level 1 to 3 are named as *cD1*, *cD2* and *cD3* and level 3 approximated decomposition is named as *cA3*. The decompositions calculated using MATLAB wavelet tool box are shown using thin lines, and the decompositions calculated using real-time system are shown in thick dotted lines.

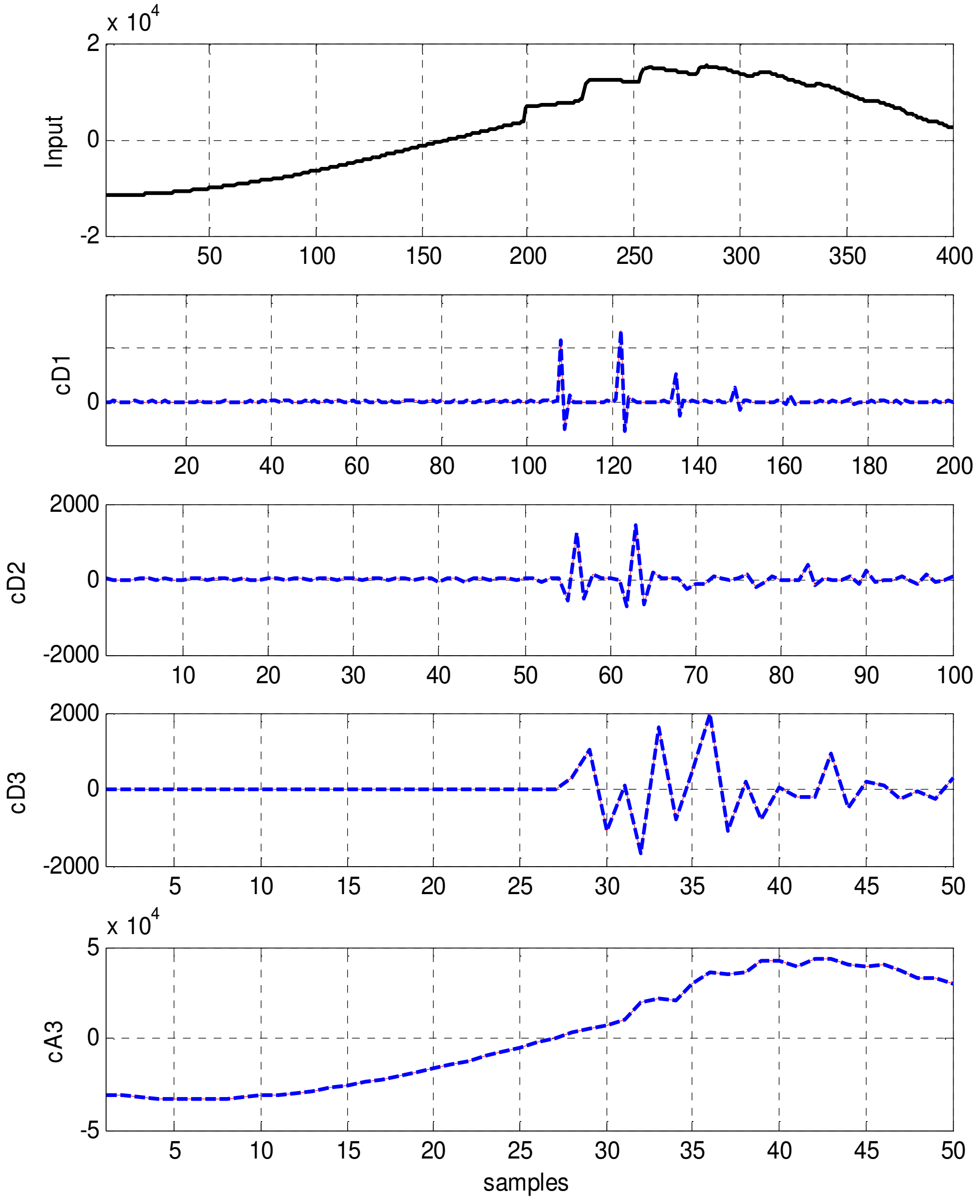

Figure 6-11 : Wavelet decompositions calculated for a fault

Bibliography

[1] *IEEE Guide for protective relay applications to transmission lines*, IEEE Std C37.113-1999, 2000.

[2] P.Kundur, “Power system stability and control”, McGraw-Hill, Inc., 1994.

[3] V. Pathirana, and P. G. Mclaren, “A hybrid algorithm for high speed transmission line protection”, *IEEE Trans. Power Delivery*, vol. 20, no. 4, pp. 2971–2983, Oct. 2005.

[4] H. W. Dommel, and J. M. Michels, “High speed relaying using traveling wave transient analysis”, *IEEE PES Winter Power Meeting*, New York, pp.1-7, Jan.1978.

[5] R. A. Hedding and F. Mekic, “Advanced multi-terminal line current differential relaying and applications”, *Protective Relay*, pp.102-109, 2007.

[6] B.Li, W.Chang, J. He, and Z.Q. Bo, “Special problems in current differential protection based on Bergeron model,” *Asia-Pacific Power and Energy Engineering Conference*, pp. 1 - 4, 2009.

[7] A. Abur, and F. Magnago, “Fault location using wavelets”, *IEEE Trans. Power Delivery*, vol. 13, no. 4, pp. 1475–1480, Oct. 1988.

[8] A. A. Girgis and R. G. Brown, “Application of Kalman filtering in computer relaying”, *IEEE Trans. on Power Apparatus and Systems*, vol. PAS-100, no.7, pp .3387-3397, Jul. 1981.

[9] M. Chamia, and S. Liberman, “Ultra high speed relay for EHV/UHV transmission lines - Development, design and application”, *IEEE Trans. on Power Apparatus and Systems*, vol. PAS-97, no. 6, pp.2104-2116, Nov. 1978.

[10] T. Takagi et al, “Fault protection based on travelling wave theory - Part. 1: Theory”, *Summer Power Meeting*, Mexico, Jul. 1977.

[11] T. Takagi et al, “Fault protection based on traveling wave theory Part II: Sensitivity

analysis and laboratory test", *Winter Power Meeting*, New York, Jan. 1978.

[12] A.T. Johns, "New ultra-high-speed directional comparison technique for the protection of EHV transmission lines," *IEE Proceedings*, vol. 127, no.4, pp.228-239, Jul. 1980.

[13] M. Vitins, "A correlation method for transmission line protection," *IEEE Trans. on Power Apparatus and Systems*, vol.97, no.5, pp. 1607-1617. Sep. 1978.

[14] P. A. Crossly, and P. G. Mclaren, "Distance protection based on traveling waves," *IEEE Power App. Systems*, vol.102, no. 9, pp. 2971–2983, Sep. 1983.

[15] H.Y. Li, P.A. Crossley and N. Jenkins, "Transient directional protection for distribution feeders with embedded generations", *PSSC*, Sevilla, Jun. 2002.

[16] C.Y. Evrenosoglu, and A. Abur, "Traveling wave based fault location for teed circuits," *IEEE Trans. Power Delivery*, vol.20, no. 2, pp. 1115- 1121, Apr.2005.

[17] N. Perera, A.D. Rajapakse and T. Buchholzer, "Isolation of faults in distribution networks with distributed generators", *IEEE Trans. on Power Delivery*, vol. 23, no. 4, pp. 2347 - 2355, Oct. 2008.

[18] S. Mishra, C.N. Bhende, and B.K. Panigrahi, "Detection and classification of power quality disturbances using S-Transform and probabilistic neural network", *IEEE Trans. on Power Delivery*, vol. 23, no. 1, pp. 280 – 287, Jan. 2008.

[19] Y Sheng, and S.M Rovnyak, "Decision tree-based methodology for high impedance fault detection", *IEEE Trans. on Power Delivery*, vol. 19, no. 2, pp.533-536, April 2004.

[20] M. F. Othman and H. A. Amari, "Online fault detection for power system using wavelet and PNN", *2nd IEEE Int. Conf. Power and Energy*, Johor Baharu, Malaysia, Dec. 1–3, pp.1644–1648, 2008.

[21] K. M. Silva, B. A. Souza, and N. S. D. Brito, "Fault detection and classification in transmission lines based on wavelet transform and ANN", *IEEE Trans. Power Del.*, vol. 21, no. 4, pp. 2058–2063, Oct. 2006.

[22] M. Kezunovic and I. Rikalo, "Detect and classify transmission line faults using neural nets", *IEEE Comput. Appl. Power*, vol. 9, no. 4, pp. 42–47, Oct. 1996.

[23] C.M. Liaw, and Y.M. Lin, "Random slope PWM inverter using existing system background noise: analysis, design and implementation", *Electric Power Applications, IEE Proceedings*, vol.147, no.1, pp.45-54, Jan 2000.

[24] *IEEE Recommended practice for monitoring electric power quality*, IEEE Std. 1159-1995, 1995.

[25] D.C. Robertson et al, "Wavelets and electromagnetic power system transients", *IEEE Trans. on Power Delivery*, vol. 11, no. 2, Apr. 1996.

[26] R. Wain et al, "An overview of FPGAs and FPGA programming; Initial experiences at Daresbury", no. 2, *Computational Science and Engineering Department*, *CCLRC Daresbury Laboratory*, Daresbury, Warrington, Cheshire, UK, Nov 2006.

[27] ML50x Reconfigurable platform with RT-XSG toolbox support from Opal-RT Technologies, User Guide, Montréal, Opal-RT Technologies Inc, Québec, Canada, 2007.

[28] R. Moxley, and K Fodero, "High-speed distribution protection made easy: communications-assisted protection schemes for distribution applications", *58th Annual Conference for Protective Relay Engineers*, pp.18- 26, Apr. 2005.

[29] IEC 61850-90-1 Communication between Substations, Technical Report, *IEC TC* 57, 2009.

[30] J. A. B. Faria, and J. B. Mendez, "Modal analysis of un-transposed bilateral three-phase lines. A perturbation approach," *IEEE Power Engineering Society Summer Meeting 1996*, Denver, USA, July 1996, pp. 983- 993.

[31] C.R Paul, "Analysis of Multi-conductor Transmission lines", Wiley Inter Science 1994.

[32] J.R. Lucas, High Voltage Engineering, Department of Electrical Engineering, University of Moratuwa, Sri Lanka, 2001.

[33] L. V. Bewley, “Travelling waves on transmission systems”, New York: Wiley, 1951.

[34] E. Clarke, “Circuit analysis of AC power systems”, New York: Wiley, pp. 81, vol. 1, 1950.

[35] J.A.B. Faria, and J.H. Briceno, “On the modal analysis of asymmetrical three-phase transmission lines using standard transformation matrices”, *IEEE Transactions on Power Delivery*, vol.12, no.4, pp.1760-1765, Oct 1997.

[36] C. H. Lee, Y. J. Wang, and W.L. Huang, “A literature survey of wavelets in power engineering applications”, Proc. of Science Council, vol. 24, no.4, pp. 249-258, 2000.

[37] D.C. Robertson et al, “Wavelets and Electromagnetic Power System Transients”, *IEEE Trans. on Power Delivery*, vol. 11, no. 2, Apr. 1996.

[38] Hd. O. Mota, F. H. Vasconcelos, and R. M. da Silva, “Real-time wavelet transform algorithms for the processing of continuous streams of data”, *IEEE International Workshop on Intelligent Signal Processing*, pp.346 – 351, 2005.

[39] C. H. Lee, Y. J. Wang, and W.L. Huang, “A literature survey of wavelets in power engineering applications”, *Proc. of Science Council, ROC (A)*, vol. 24, no.4, pp. 249-258, 2000.

[40] SEL-421 Relay, Protection and Automation System, Instruction Manual, Schweitzer Engineering Laboratories Inc., 2011.

[41] H. J. A. Ferrer and E. O. Schweitzer, Modern Solutions for Protection, Control and Monitoring of Electric Power Systems, Schweitzer Engineering Laboratories Inc., 2010.

[42] Protection, Monitoring and Control Terminals for Sub-transmission and Transmission Networks, ABB, 2004.

[43] IEC 61850 in MiCOM Relays, Interoperability for advanced protection and control, AREVA T&D, AREVA.

[44] N. Perera and A.D. Rajapakse “Design and hardware implementation of a modular transient directional protection scheme using current signals”, *IET Generation, Transmission and Distribution* - (Accepted, Feb. 2012).

[45] S. Jiang, U. D. Annakkage, and A. M. Gole, “A platform for validation of FACTS models”, *IEEE Trans. on Power Delivery*, vol. 21, no. 1, pp.484 – 491, Jan. 2006.

[46] J. R. Lucas, “Representation of Magnetization curves over a wide region using a non–integer power series”, *International Journal of Electrical Engineering Education*, Manchester U.K, vol. 25, pp. 335-340, Oct. 1988.

[47] N. Perera, A.D. Rajapakse, and R. Jayasinghe, “On-line discrete wavelet transform in EMTP environment and applications in protection relaying”, *International Conference on Power Systems Transients (IPST),* Jun. 2007.

[48] H.A. Darwish et al, "Close Accord on DWT Performance and Real-Time Implementation for protection applications," *IEEE Trans. Power Delivery*, vol.25, no.4, pp.2174-2183, Oct. 2010.

[49] TMS320C6713 Floating-point digital signal processor, *Texas Instrument*, Nov. 2005.

[50] ADS8364/65MEVM User's Guide, *Texas Instrument,* Sep. 2006.

[51] 5–6K Interface board, User's Guide, *Texas Instrument*, Mar. 2009.

[52] DAP signal conditioning board, Data acquisition, Digital/Analog converters, *Texas Instrument*, Jun. 2003.

[53] TMS320C6000 EMIF to TMS320C6000 Host Port Interface, Code Composer Studio getting started guide, *Texas Instrument*, May 2001.

[54] Using the CMSIS DSP library in CCS for Stellaris, Texas Instrument, Feb. 2012.

[55] N. Perera, A.D. Rajapakse, and A.M. Gole, “Real-time implementation of discrete wavelet transform for transient type protection applications”, *4th Annual Electrical Power and Energy Conference (EPEC 2010)*, Halifax, Canada, Aug.25-27, 2010.

[56] R. Bracewell, “The Fourier transform and its applications”, New York: McGraw-Hill, 1965.

[57] Power system waveform generator: Real time playback, Operations manual, Version 3.3, *Manitoba HVDC Research Centre Inc.*, Winnipeg, Manitoba, Canada.

[58] S. M. Rovnyak et al, “Decision trees for real time transient stability prediction”, *IEEE Trans. on Power Systems*, vol. 9, no. 3, pp.1417-1426, Aug 1994.

[59] A.M Youssef et al, “Disturbance classification utilizing dynamic time warping classifier”, *IEEE Trans. on Power Delivery*, vol. 19, no. 1, pp. 272 - 278, Jan. 2004.

[60] D. F. Specht, "Probabilistic Neural networks for classification, mapping, or associative memory", *IEEE Conference on Neural Networks*, San Diego, vol. 1, pp.525-532, July 1988.

[61] A. Goh, “Probabilistic neural network for evaluating seismic liquefaction potential,” *Canadian Geotechnical Journal*, vol. 39, no. 1, pp. 219-232, Feb. 2002.

[62] T. K. Abdel-Galil et al, “Disturbance classification using hidden Markov models and vector quantization”, *IEEE Trans. on Power Delivery*, vol. 20, no. 3, Jul. 2005.

[63] J. Chung et al, “Power disturbance classifier using a rule-based method and wavelet packet-based Hidden Markov Model*”, IEEE Trans. on Power Delivery*, vol. 17, no. 1, pp. 233-241, Jan. 2002.

[64] L. R. Rabiner, “A tutorial on hidden Markov models and selected applications in speech recognition,” *IEEE Proc.*, vol. 77, pp. 257–286, Feb.1989.

[65] E, Parzen, "On estimation of a probability density function and mode", Annals of Mathematical Statistics, vol. 33, pp. 1065–1076, 1962.

[66] CART- Classification and Regression Trees, San Diego, CA: Salford Systems, 1997. Available: http://www.salford-systems.com.

[67] K. Murphy, Hidden Markov model toolbox for Matlab, 1998. Available: http://www.cs.ubc.ca/~murphyk/Software/HMM/hmm.html.

[68] N. Perera and A.D. Rajapakse, “Power system transient classification for protection relaying”, *13th IEEE International Conference on Harmonics and Quality of Power (ICHQP)*, Wollongong, New South Wales, Australia., pp.1-6, Oct. 2008.

[69] N. Perera and A.D. Rajapakse “Recognition of fault transients using a probabilistic neural-network classifier”, *IEEE Trans. on Power Delivery*, vol. 26, no. 1, Jan. 2011.

[70] N. Perera and A.D. Rajapakse "Development and hardware implementation of a fault recognition system", *IEEE Trans. on Power Delivery*, vol. 27, no. 1, Jan. 2012.

[71] Lightning and surge protection - basic principles, *MTL Surge Technologies*, Power Court, Luton, Bedfordshire, England.

[72] International liner series installation instructions, *SL Power Electronics Cooperation*, Ventura, CA, 2009.

[73] Software control of the ADS8364, Application report, Data acquisition applications, *Texas Instrument*, Aug. 2002.